DROSOPHILA AS A MODEL SYSTEM TO STUDY NEUROPSYCHIATRIC AND NEUROLOGICAL DISORDERS

By

Jenny Aguilar

Dissertation

Submitted to the Faculty of the

Graduate School of Vanderbilt University

in partial fulfillment of the requirements

for the degree of

DOCTOR OF PHILOSOPHY

in

Pharmacology

May 31, 2020

Nashville, Tennessee

Approved:

Brad Grueter, Ph.D.
Eugenia Gurevich, Ph.D.
Kevin Currie, Ph.D.
Hassane Mchaourab, Ph.D.
Qi Zhang, Ph.D.
Aurelio Galli, Ph.D.

Para mis padres,

Mercedes y Oscar.

Los pilares de mi vida.

Sus sacrificios, pacienca, amor y apoyo me hacen ser quien soy hoy.

ACKNOWLEDGEMENTS

Foremost, I would like to thank my adviser, Dr. Aurelio Galli. Aurelio has motivated and challenged me to think “bigger” than I imagined. I would also like to acknowledge the members of my thesis committee: Drs. Brad Grueter, Eugenia Gurevich, Kevin Currie, Hassane Mchaourab and Qi Zhang. Their diverse insights were invaluable in shaping my work. I am thankful for the incredible support I have received from the Pharmacology Department, and specifically, from Dr. Christine Konradi and Karen Gieg for being wonderful personal mentors through the highs and lows of graduate school. I am deeply grateful to Drs. Roger Chalkey and Linda Sealy for their efforts to promote diversity and inclusion at Vanderbilt University and advocacy of my career.

I would also like to thank a series of inspiring scientists who devoted themselves to my training and encouraged my career: Dr. Patric K. Stanton, who welcomed me into his lab at New York Medical College as a high school student; Drs. Carolyn Tyler and Lisa Boulanger, who mentored me as an undergraduate at Princeton University; and Drs. Zachary Freyberg and Johnathan Javitch for whom I worked as a research assistant at Columbia University.

I would also like to thank the members of the Galli and Matthies Labs for their day-to-day camaraderie and commiseration. I am fortunate to have done great science alongside Dr. Heiner Matthies, Dr. Danielle Zanella, Dr. Aparna Shekar and Samuel Mabry. A special thanks to Heiner who has always been a great source of knowledge, encouragement and wisdom.

Finally, I would like to thank my family, friends and partner for their endless encouragement and support: my parents, for everything they do; Giselle Saltos and her family, for being my home away from home; Tania Montesdeoca, for being a source of inspiration and strength; the Secret Bagel Society (Dr. Bethany Dale, Katie Rothmel, Monica Bomber and Victoria Ng), for every coffee date, text and call; and my partner, Bradley Nelson, for every hour spent in and outside the lab supporting my science. This journey has taken a village and I am fortunate that mine stood by me and gave me strength when I needed it. ¡Si se puede!

TABLE OF CONTENTS

LIST OF FIGURES

Figure **Page**

LIST OF ABBREVIATIONS

5-HT	Serotonin
α-Synuclein	Alpha-synuclein
AADC	L-amino acid decarboxylase
AC	Adenylyl cyclase
ADE	Anomalous dopamine efflux
ADHD	Attention-deficit hyperactivity disorder
AMPH	Amphetamine
ANOVA	Analysis of variance
ASD	Autism spectrum disorder
BH4	Tetrahydrobiopterin
CaMKII	Ca^{2+}/calmodulin-dependent protein kinase II
cAMP	Cyclic adenosine monophosphate
CHO	Chinese hamster ovary
CNS	Central nervous system
COMT	Catechol-o-methyltransferase
DA	Dopamine
DAG	Diacylglycerol
DARPP-32	32-kDa DA and cAMP-regulated phosphoprotein
DAT	Dopamine transporter
dDAT	*Drosophila melanogaster* dopamine transporter
DEER	Double electron electron resonance
DR	Dopamine receptor
EL	Extracellular loop
EP	Adrenaline/Epinephrine

EPR	Electron paramagnetic resonance
ER	Endoplasmic reticulum
ERK	Extracellular signal-regulated kinase
Flot 1	Flotillin-1
FRET	Fluorescence energy transfer
Gβγ	G-protein beta gamma
GFP	Green fluorescent protein
GPCR	G-protein coupled receptors
GIRK	G protein-coupled inwardly-rectifying potassium channel
GRK	G-protein coupled receptor kinase
GTP	Guanosine triphosphate
hDAT	Human dopamine transporter
HEK	Human embryonic kidney
HVA	Homovanillic acid
IF	Inward-facing open
IL	Intracellular loop
IP_3	Inositol trisphosphate
IP_3R	Inositol trisphosphate receptor
IO	Inward-facing occluded
L-DOPA	L-dihyroxyphenylalanine
LeuT	Leucine transporter
KO	Knock-out
MAO	Monoamine oxidase
MD	Molecular dynamics
MDPV	3,4-Methylenedioxypyrovalerone
NE	Nonadrenaline/Norepinephrine

NAc	Nucleus accumbens
NSS	Neurotransmitter:sodium symporters
OF	Outward-facing open
OO	Outward-facing occluded
PD	Parkinson's disease
PICK1	Protein interacting with C-kinase 1
PIP_2	Phosphatidylinositol (4,5)-bisphosphate
PKA	cAMP-dependent protein kinase/Protein kinase A
PKC	Protein kinase C
PLC	Phospholipase C
PNS	Peripheral nervous system
PP1	Protein phosphatase 1
SERT	Serotonin transporter
SLC6	Solute carrier 6
STX1A	Syntaxin 1A
Rin	Ras-like GTPase
TH	Tyrosine hydroxylase
TI	Tuberoinfundibular
TMD	Transmembrane domain
VMAT	Vesicular monoamine transporter
VTA	Ventral tegmental area
WT	Wild-type

CHAPTER I

INTRODUCTION

Elements of this chapter are derived from: Aguilar JI *et al*. Neuronal Depolarization Drives Increased Dopamine Synaptic Vesicle Loading via VGLUT. *Neuron*. 2017

The Origin of Dopamine

The cathecolamine neurotransmitter dopamine (3-4-dihydroxyphenylethylamine; DA) was first synthesized in 1910 by George Barger and James Ewens. In its early days, DA was largely accepted as a mere metabolic intermediate for nonadrenaline (norepinephrine, NE) and adrenaline (epinephrine, EP) (1). It was not until the 1950's, through the works of Holtz, Blaschko and Hornykiewicz, among others, that DA became recognized as its own signaling molecule able to regulate bodily functions independent of NE and EP (1, 2). Specifically, Hornykiewicz, confirming Blascho's earlier work, showed that DA, unlike EP, had a vasopressor effect that could be modulated pharmacologically. Shortly thereafter, Kathleen Montagu (3) and Arvid Carlsson (4) independently identified DA in the brain of various animals, setting the stage for the investigation of DA's role in the brain. The development of various techniques including the colorimetric iodine assay by von Euler and Hamberg, fluorescence histochemical method by Falk and Hillarp, and microdialysis by Brito, Delgado and Ungerstedt propelled the study of DAergic pathways as well as DA's physiological and behavioral effects in the 1960's and 1970's (5). These investigations laid the foundation for the field of neurochemistry, and neuroscience more broadly.

Dopamine Circuitry in the Central Nervous System

Today, DA is well known to regulate several biological functions in both the peripheral (PNS) and central nervous systems (CNS). Peripheral DA is synthesized mainly by neuronal,

adrenal medulla and neuroendocrine cells (6). Here, DA acts as both an autocrine and paracrine messenger regulating blood pressure, ventilation, and gastrointestinal motility, among others (7-10). In the central nervous system, DA plays key roles in voluntary movement, motivation, reward, and cognition as well as in the pathophysiology associated with various neurological and neuropsychiatric disorders. DAergic innervation of the brain is classified into four major pathways: tuberoinfundibular (TI), mesocortical, mesolimbic and nigrostriatal, as illustrated in **Fig. 1**. In a simplified view, DA neurons originating in the dorsomedial arcuate nucleus of the hypothalmus that project to the pituitary gland comprise the TI pathway and regulate hypophyseal activities (*green*). DA neurons originating in the ventral tegmental area (VTA) that project to limbic areas (nucleus accumbens (NAc), hippocampus and amygdala) comprise the mesolimbic pathway and regulate reward (*magenta*). DA neurons originating in the VTA that project to the prefrontal cortex comprise the mesocortical pathway and regulate cognition (*blue*). DA neurons originating in the substantia nigra that project to the dorsal striatum comprise the nigrostriatal pathway and regulate motor activity (*red*).

Dopamine Neurotransmission

DA neurotransmission in the CNS relies on the coordination of various factors including DA (1) synthesis, (2) vesicular packing, (3) localization and release, (4) pre- and post-synaptic signaling, and (5) degradation and clearance. The classical pathway for catecholamine biosynthesis, including DA biosynthesis, was independently proposed by Blaschko and Holtz in 1939 (1, 2). This process occurs presynaptically in the cytosol of catecholaminergic neurons (**Fig. 2**). Foremost, the rate-limiting enzyme tyrosine hydroxylase (TH) catalyzes the conversion of dietary L-tyrosine (*green circle)* to L-dihyroxyphenylalanine (L-DOPA) (*red circle*). Next, L-DOPA is decarboxylated to DA (*blue circle*) by L-amino acid decarboxylase (AADC). Thereafter, DA can be converted further to NE by DA-hydroxylase and NE can be subsequently converted to EP by phenylethanolamine N-methyltransferase.

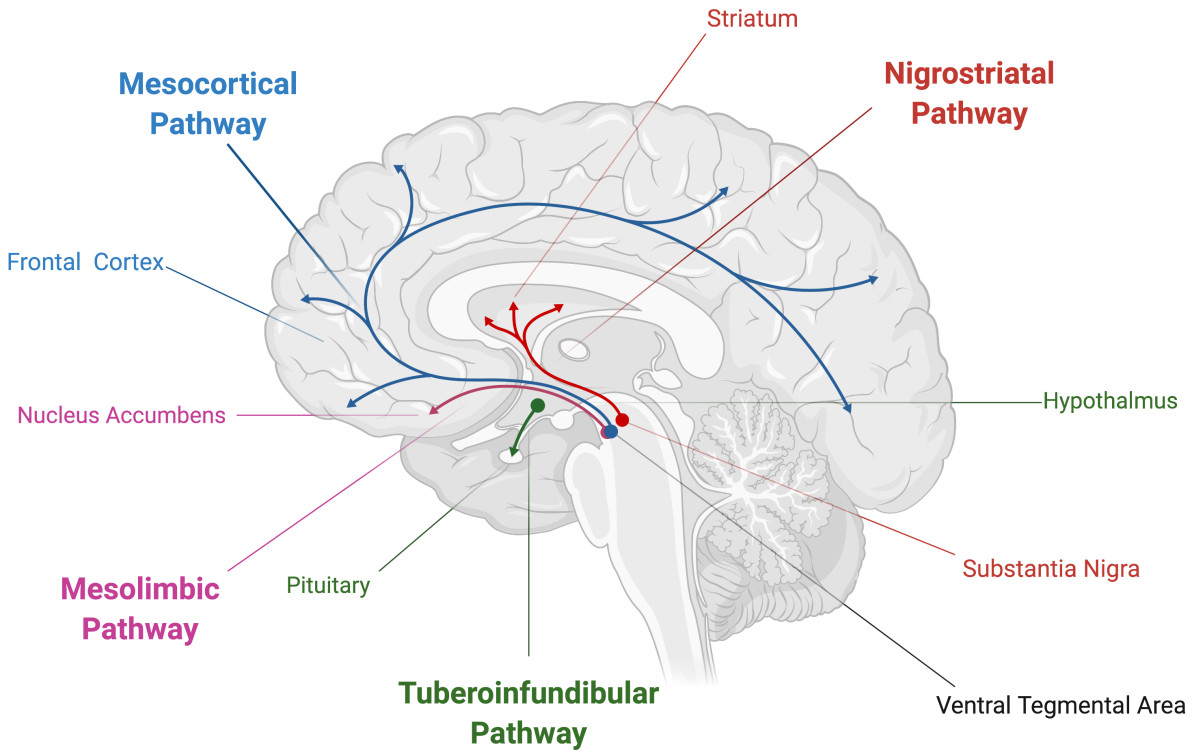

Figure 1: Dopaminergic pathways in the human CNS

Illustration of a sagittal section of the human brain highlighting the four major DAergic pathways.

Reference: Created with Biorender.com

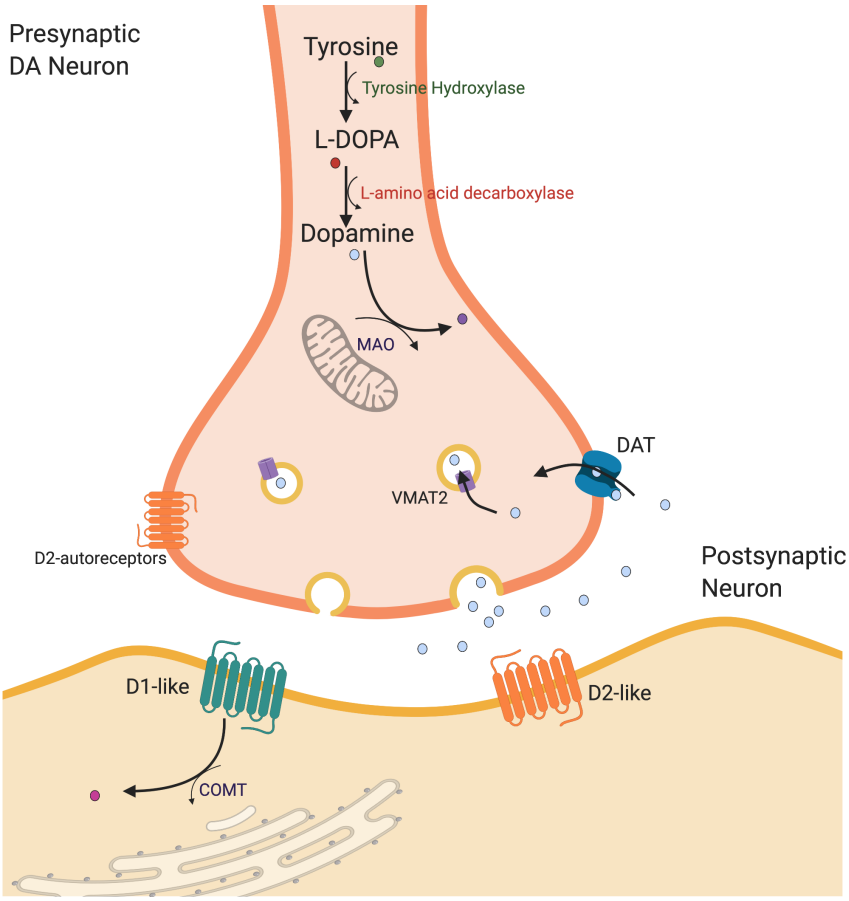

Figure 2: Dopamine at the Synapse

Illustration of DA neuron synapsing onto a postsynaptic neuron. Highlighted are pathways for (a) DA synthesis, (b) packaging via the vesicular monoamine transporter 2 (VMAT2), (c) signaling via D1-like receptors and D2-like receptors, (d) recycling via the dopamine transporter (DAT) and (e) degradation via monoamine oxidase (MAO) and catechol-O-methyltransferase (COMT) enzymes.

Reference: Created with Biorender.com

TH activity undergoes long-term regulation of gene expression and short-term regulation of enzyme activity, where the latter closely modulates catecholamine levels (11, 12). TH activity is directly dependent on the availability of (1) tetrahydrobiopterin (BH4), a cofactor which is synthesized from guanosine triphosphate (GTP), (2) molecular oxygen (O_2), and (3) ferric iron (Fe^{2+}). Catecholamines compete with BH4 to reversibly bind Fe^{2+} at the TH catalytic site (12), whereby high levels of catecholamines inhibit TH activity. Catecholamines also irreversibly bind Fe^{2+} at the TH catalytic site to decrease enzyme activity (11). Thus, TH functions as a local sensor for intracellular catecholamine concentrations. TH is subject to further regulation by site-specific phosphorylation at three sites (Ser 19, Ser 31 and Ser 40) by various kinases including cyclic adenosine monophosphate (cAMP)-dependent protein kinase (PKA), protein kinase C (PKC) and Ca^{2+}/calmodulin-dependent protein kinase II (CaMKII). Of these sites, phosphorylation at Ser 40, mainly by PKA, has the most significant increase on TH activity and subsequently, catecholamine synthesis (11). Phosphorylation of Ser 31 also increases TH activity (albeit to a lesser extent relative to Ser 40 phosphorylation) by increasing the affinity of TH for BH4 (11, 12). Although Ser 19 phosphorylation does not directly affect TH activity, Ser 19 phosphorylation can facilitate Ser 40 phosphorylation (11). Kinase activity in DA neurons is primarily driven by increases in intracellular calcium (Ca^{2+}) that occur via the excitation and depolarization of the presynaptic neuron as well as activation of G-protein coupled receptors (GPCRs). Importantly, high extracellular DA levels activate DA autoreceptors (**Fig. 2**, *orange*), which as part of a negative feedback loop suppress neuronal activity and inhibit cAMP-PKA signaling pathways, ultimately limiting TH activity (13). In this way, TH activity and subsequently, DA synthesis are tightly regulated by both extracellular and intracellular DA levels.

Once synthesized, cytoplasmic DA (**Fig. 2**, *blue*) is concentrated into synaptic vesicles via the vesicular monoamine transporter 2 (VMAT2) (**Fig. 2,** *purple*). VMAT2 activity regulates the concentration of DA in the cytosol and in synaptic vesicles, subsequently, modulating the scale of extracellular DA release (14). Synaptic vesicles accumulate and retain neurotransmitter cargo,

including DA by manipulating the electrochemical gradient ($\Delta\mu_{H}^{+}$) across the vesicle membrane that is generated by the vacuolar-type H^{+}-ATPase (V-ATPase). $\Delta\mu_{H}^{+}$ is comprised of the chemical H^{+} gradient (ΔpH) and electrical potential (Δψ), where $\Delta\mu_{H}^{+}$ = ΔpH + Δψ (15-17). Vesicular neurotransmitter transporters depending on their substrates rely to different extents on ΔpH and Δψ to fill synaptic vesicles (16, 18). In the case of VMAT2, two luminal H^{+} are exchanged for every charged entering DA molecule. This exchange results in a greater deficit in ΔpH (-2) compared with Δψ (-1) and in turn, a greater dependence on ΔpH for VMAT2-mediated DA loading (18). Importantly, the interplay between H^{+}-exchanging vesicle transporters, such as VMAT2 and the V-ATPase, dynamically modulates ΔpH and in turn, quantal size (the number of molecules released during a quantal event) (16, 17, 19-21). In addition, changes in the expression or activity of synaptic vesicle transporters and/or the cytosolic environment, which alter ΔpH also alter the scale of DA release. To this end, studies showed that overexpression of VMAT2 in cultured neurons increases quantal size (15). Further, recent studies showed that neuronal activity by driving ΔpH can significantly increase DA content in synaptic vesicles (“stores") in striatal slices (22). In contrast, knockout of VMAT2 expression in mice depletes intracellular monoamine stores, eliminates exocytic release and results in neonatal death (18, 23, 24).

VMAT2 also sequesters DA from the cytoplasm and protects neurons against cytosolic DA toxicity. DA oxidation, which results in the production of free radicals can injure cells and promote neurodegeneration (18, 25). By sequestering DA from the cytoplasm, VMAT2 also regulates mitochondrial enzyme monoamine oxidase (MAO)-dependent DA metabolism (to be discussed in detail in the following sections). MAOs limit DA oxidation by metabolizing cytosolic DA. In the absence of VMAT2, MAO activity is thought to aberrantly increase resulting in enhanced DA degradation (18). Together, these data highlight the essential role of VMAT2-mediated DA synaptic vesicle loading in regulating DA quantal size and DA-induced toxicity; regulation which is particularly relevant during periods of high burst firing that likely result in DA accumulation (26).

Following vesicular packing, DA is released into the synaptic space in response to neuronal activity that elicits the fusion of DA-containing vesicles with the plasma membrane. DA neurons undergo two distinct firing patterns: tonic versus phasic, to differentiate behaviorally relevant information (27) (for detailed review on this topic refer to Bromberg-Martin et al., 2010). Briefly, tonic activity consists of population-, low-frequency (3 - 5 Hz) firing that establishes steady, baseline levels of extracellular DA (28). These slow changes in DA levels are thought to regulate motivation (29). On the contrary, phasic activity consists of burst-, high-frequency (20 Hz or greater) firing that generates greater, transient increases in extracellular DA (30). It is widely thought that these fast changes in DA levels encode reward prediction errors (RPEs) defined as the difference between a reward that is received and the reward that is predicted to be received (29). RPEs are key to evaluating future rewards, making choices that maximize those reward, and ultimately, learning (29). Importantly, recent studies have begun to expand on this dogma as both phasic and tonic release have been found to regulate motivation and motivated behaviors (29). Of note, amphetamine (AMPH)-like molecules can also elicit DA release (15, 31), the details of which will be discussed in following chapters. Together, these forms of activity-dependent and independent DA release modulate extracellular DA concentrations that determine downstream signaling.

Extracellular DA can signal via five subtypes of DA receptors (DR) (DA 1 Receptor (D1R), D2R, D3R, D4R and D5R) to activate or inhibit specific downstream signaling pathways. These receptors are widely and differentially expressed throughout the forebrain and are distributed pre, post- and extra-synaptically (32, 33). DRs belong to the GPCR superfamily and signal through both G protein-dependent and -independent mechanisms. They are broadly divided into two classes: D1-like (D1R and D5R) and D2-like (D2R, D3R, D4R). D1-like receptors, located predominantly postsynaptically, typically couple to $G\alpha_{s/olf}$ proteins to stimulate the production of second messenger cAMP through the activation of the enzyme adenylyl cyclase (AC) (**Fig. 3**). cAMP activates PKA promoting the phosphorylation of several downstream substrates that work

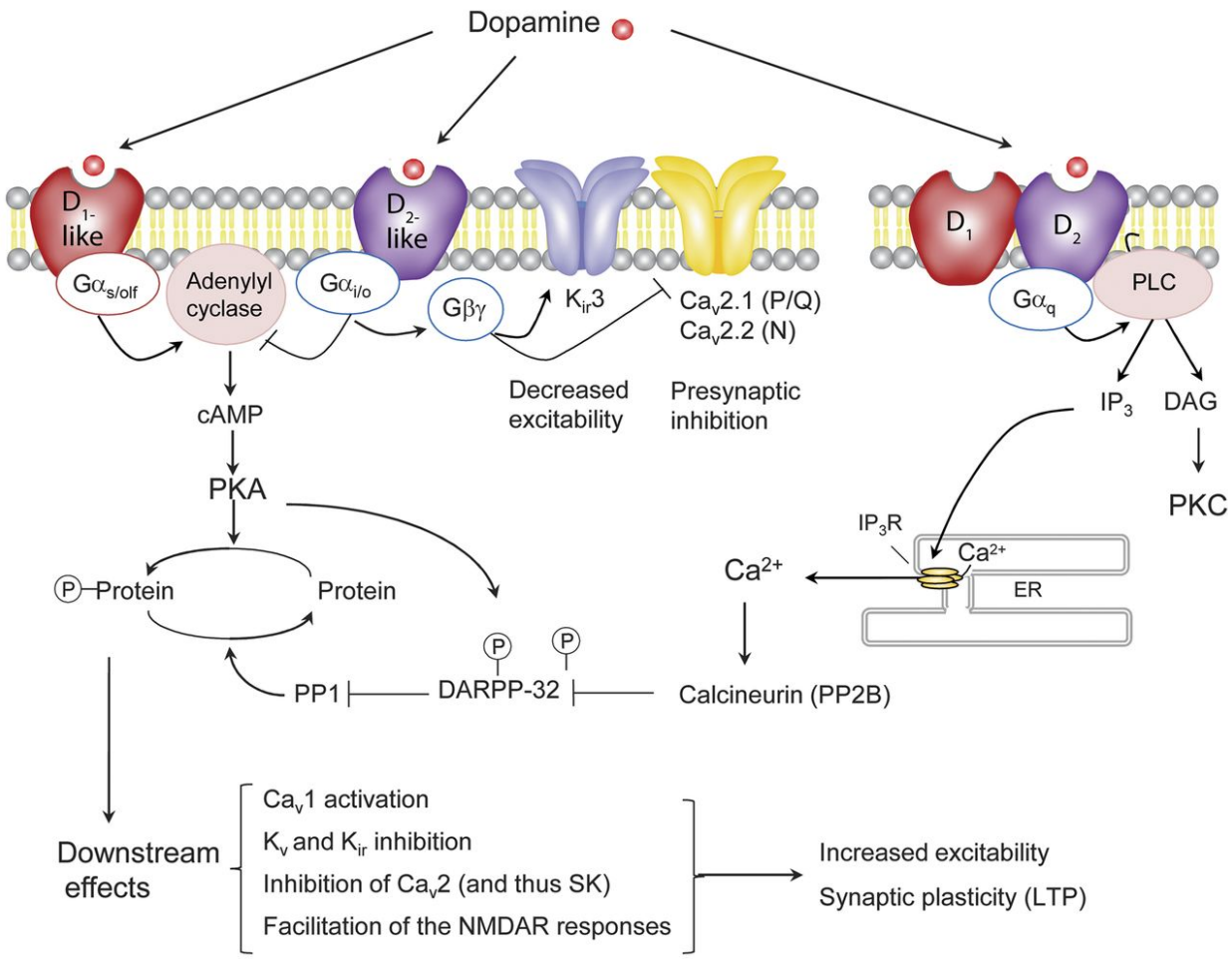

Figure 3: DA signaling mechanisms and downstream effectors

DA receptors are G-protein coupled receptors (GPCRs) that are classified into D1-like receptors (D1R and D5R) and D2-like receptors (D2R, D3R and D4R). D1-like receptors are coupled to Gαs, stimulate adenylyl cyclase (AC) activity, increase the production of cAMP and activate PKA to increase neuronal excitability. In contrast, D2-like receptors are coupled to $G\alpha_{i/o,}$ inhibit AC and decrease cAMP production to decrease neuronal excitability and neurotransmitter release.

Reference: Savica R, Benarroch EE. Dopamine receptor signaling in the forebrain: recent insights and clinical implications. Neurology. 2014;83(8):758-6

together to increase neuronal excitability and firing (33). Among PKA substrates, 32-kDa DA and cAMP-regulated phosphoprotein (DARPP-32) once phosphorylated amplifies PKA-mediated signaling by inhibiting protein phosphatase 1 (PP1). D2- like receptors, distributed both post- and pre-synaptically, typically couple to $G\alpha_{i/o}$ proteins to suppress the production of cAMP through the inhibition of AC. D2-like receptors can also signal via their G-protein beta gamma (Gβγ) subunit to inhibit Ca^{+} channel activity and decrease neuronal excitability (33). Interestingly, due to the differences in DA affinity between D1-like and D2-like receptors, these receptor classes are thought to have differential roles in responding to tonic versus phasic firing (27). D2-like receptors have 10- to 100-fold higher DA affinity relative to D1-like receptors *in vitro* (32, 34). As such, D2-like receptors are thought to preferentially detect changes in lower levels of DA associated with tonic DA release. On the contrary, D1-like receptors are thought to preferentially detect changes associated with transient, high changes in DA levels typically associated with phasic DA release. Although this hypothesis has the potential to couple specific types of presynaptic DA release to postsynaptic signaling mechanism, whether this differential pattern of activation occurs *in vivo* remains unclear.

Presynaptic D2-like receptors (predominantly D2R and to a lesser extent D3R) function mainly as autoreceptors to regulate extracellular DA levels as part of a dynamic negative feedback system (35). Specifically, D2Rs are known regulate the rate of neuronal firing (36), DA synthesis (13), DA uptake (37), and vesicular neurotransmitter release (32, 33). D2Rs are susceptible to alternative splicing where D2S (short form) is thought to act primarily as a presynaptic autoreceptor, while D2L (long form) is thought to act primarily as a postsynaptic receptor (32). Interestingly, presynaptic D2Rs can complex with D1Rs to form D1R-D2R heterodimers that couple to $G\alpha_{q/11}$ proteins, directly linking DA to Ca^{2+} signaling in the brain (38). Phospholipase C (PLC) activation by $G\alpha_{q/11}$ leads to the production of inositol trisphosphate (IP_3) and diacylglycerol (DAG). In turn, IP_3 binds to its receptor (IP_3R) to trigger Ca^{2+} release from the endoplasmic reticulum (ER), while diacylglycerol (DAG) activates protein kinase C (PKC) (**Fig 3**). Of note,

various other DA receptor homodimers and heterodimers have been observed, each of which have distinct receptor pharmacology as well as downstream signaling (39).

DA signaling is terminated on the postsynaptic terminal by G-protein coupled receptor kinases (GRKs) and multifunctional adaptor proteins β-arrestins and on the presynaptic terminal by DA transporter (DAT)-mediated uptake of DA, to be discussed in more detail in the next chapter. Additionally, DA is subject to oxidation or further degradation by MAO or catechol-O-methyltransferase (COMT) to its major metabolite homovanillic acid (HVA) (**Fig. 2**). Although the acidic synaptic vesicle lumen inhibits DA oxidation, once in non-acidic environment (i.e. cytoplasm or extracellular space) DA is subject to spontaneous, metal-catalyzed or enzyme-catalyzed oxidation (40). MAOs isozymes (A or B) are outer membrane-bound mitochondrial enzymes localized predominantly in presynaptic neurons, which catalyze the oxidative deamination of various amines, hormones and monoamine neurotransmitters, including DA (41). By degrading free, cytosolic DA, MAOs are thought prevent neuronal oxidative stress that results from DA oxidation. However, recent studies have also suggested that MAO-mediated degradation itself can contribute to oxidative stress through the accumulation of hydrogen peroxide, a major byproduct of MAO-mediated degradation (41). This MAO-induced oxidative damage is to underlie various neuropsychiatric and neurological disorders (12). Although these findings are highly contended (26), as MAO inhibitors can have parkinsonian-like deficits, they do highlight the importance of cytosolic DA homeostasis and MAOs role in this process. Less is known about COMTs isozymes (membrane-bound or soluble), however, higher levels have been identified in non-neuronal cells with lower levels in postsynaptic neurons (42). COMT catalyzes the O-methylation of catecholamine neurotransmitters, catecholestrogens and dietary polyphenols. MAO and COMT work together, often synergistically to catalyze the degradation of DA and to maintain DA levels.

The Dopamine Transporter: Structure, Function and Regulation

The DAT is a perisynaptic membrane protein critical to DA neurotransmission (43). Upon vesicular release, the DAT mediates the active, high-affinity re-uptake of DA from the synapse to the presynaptic bouton; thereby, regulating (1) the concentration and persistence of extracellular DA and consequently, the intensity and duration of DA signaling, and (2) the concentration of intracellular DA available for recycling, and consequently, DA storage and release (44). Altered DA neurotransmission is linked to multiple neurological and neuropsychiatric disorders, including Parkinson's disease (PD), (45, 46), attention deficit hyperactive disorder (ADHD) (47), mood disorders (48), schizophrenia (49), and autism spectrum disorder (ASD) (50-52). Growing evidence implicates DAT dysfunction in many of these disorders, as will be discussed later in this chapter. In addition, the DAT is a primary target for various psychostimulants, including cocaine and AMPH as well as therapeutic agents, including Ritalin (methylphenidate) and Wellbutrin (bupropion), whose actions on the DAT will also be explored later in this chapter (53).

Structure

The DAT is a member of solute carrier 6 (SLC6) transporter family, which are secondary active co-transporters that utilize the Na^+ gradient generated by the Na^+/K^+ ATPase to transport substrates against their concentration gradients (43, 54). In particular, the DAT also requires the co-transport of Cl^-, where one Cl^- and two Na^+ ions are co-transported per molecule of substrate (43). Thus, substrate translocation across the plasma membrane is electrogenic, resulting in two net positive charges per transport cycle that produce a measurable inward current (55-57).

The *SLC6A3* gene, localized to chromosome 5p15.3, encodes the human DAT (hDAT), whose full-length cDNA was first cloned in the early 1990's (54). According to hydropathicity analysis, this 620-amino acid protein consists of 12 transmembrane domains (TMDs), 6 extracellular loops (EL), 5 intracellular loops (IL), a large EL containing glycosylation sites located between TMD 3 and TMD 4, and cytoplasmic N- and C-termini (43, 54), as shown in **Fig 4**.

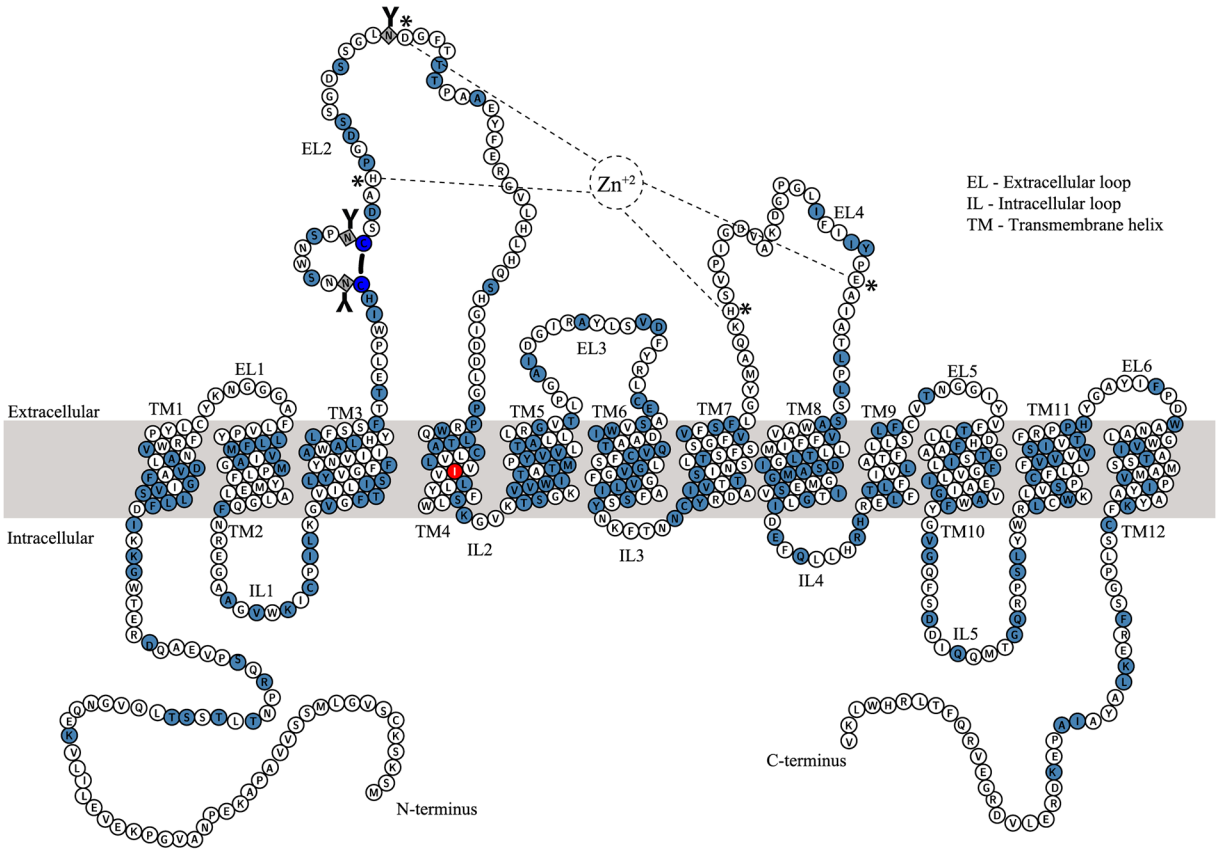

Figure 4: Topographical representation of the dopamine transporter

The predicted membrane topology illustrated was based on a thermostable mutant of the hDAT (Ile at position 287 mutated to Tyr, highlighted in *red*). Residues comprising the Zn+ binding sites are highlighted (*) as well as those that undergo N-linked glycosylation (Y). In addition, a disulfide bond between two proximal cysteines (*indigo*) is demarcated with a *black dash*.

Reference: Navratna V, Tosh DK, Jacobson KA, Gouaux E (2018) Thermostabilization and purification of the human dopamine transporter (hDAT) in an inhibitor and allosteric ligand bound conformation. PLoS ONE 13(7): e0200085

Homology models of hDAT derived from crystal structures of other SLC6 transporters, such as that the *Drosophila melanogaster* DAT (dDAT) (58, 59), serotonin transporter (SERT) (60) and the bacterial homolog leucine transporter (LeuT) (61) have provided key insights about the structure of hDAT (which has not yet been crystallized). The protein core of the hDAT follows a 5 x 5 architecture, where TMDs 1-5 are related to TMDs 6-10 by a pseudo-two-fold axis of symmetry along the plasma membrane. TMDs 11 and 12, located on the periphery, are thought to play important regulatory functions, but be less critical to substrate translocation (61). Based on LeuT and dDAT crystal structures, the substrate (S1 and S2), Na^+ (Na1 and Na2) and Cl^- binding sites are located in the center of the protein approximately halfway across the membrane bilayer (58, 61, 62), as illustrated in **Fig. 5**. Notably, the S1 site, formed by residues on TMDs 1, 3, 6 and 8, is predicted to have an allosteric effect on the S2 site, where ligand occupancy at one site affects binding at the other site (62). The N- and C-termini are relatively unstructured and flexible structures that play key regulatory roles in the hDAT through a host of interactions with innate lipids of the bilayer (63, 64), ILs (64-67) and cytoplasmic proteins (68-72). The N-terminus is subject to extensive phosphorylation and ubiquitination that modulates the expression and transport capacity of the DAT (53). The N-terminus is also critical to various protein-protein and protein-lipid interactions, including those with D2R (73, 74), Syntaxin 1A (STX1A) (52, 69, 75) and phosphatidylinositol (4, 5)-bisphosphate (PIP_2) (63, 64). The C-terminus is subject to S-palmitoylation and also interacts with various proteins, such as CAMKII (68, 76), the small ras-like GTPase Rin1 (77) and $G\beta\gamma$ (53, 71, 72, 78). The relevance of these post-translational modifications, binding partner interactions and DATs localization to membrane rafts will be discussed in detail later in this chapter.

Function: Mechanisms of Translocation

Transport via the DAT is thought to occur via an alternating access mechanism, wherein the central binding site (S1) is accessible either to the extracellular space through various “outward-facing conformations” or to the intracellular space through various “inward-facing”

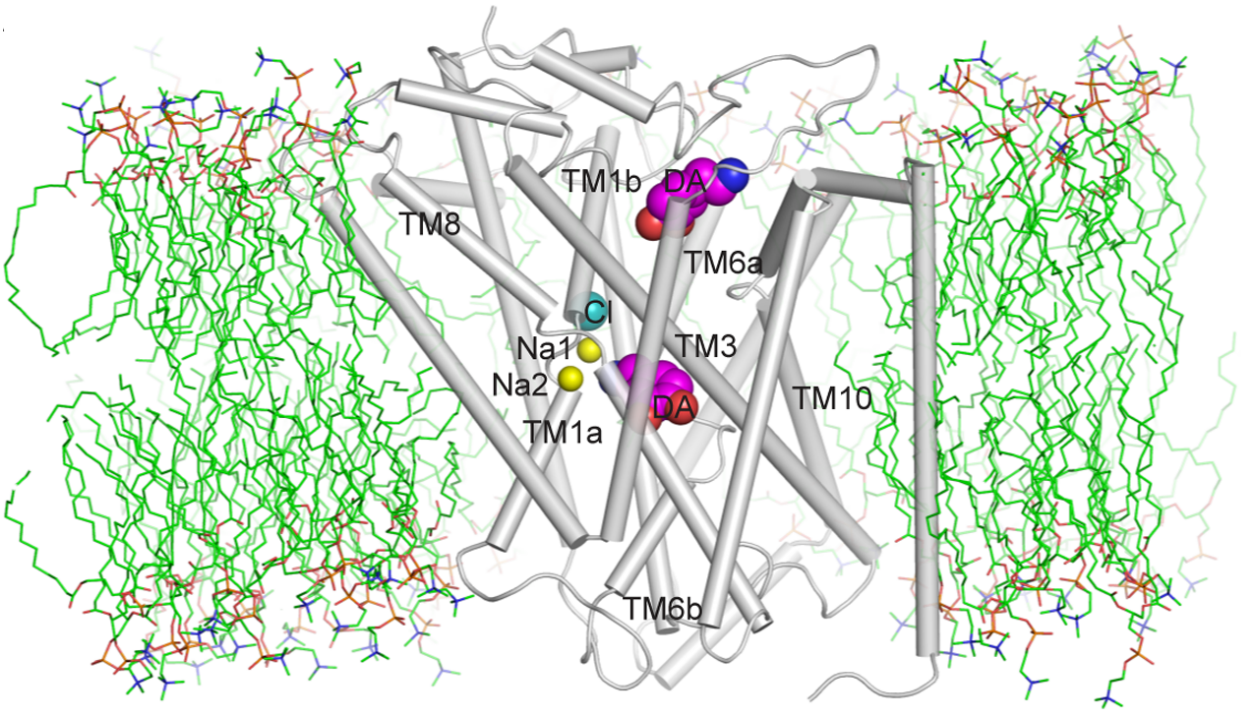

Figure 5: The substrate binding sites of the DAT

Homology model of DAT in the occluded-state immersed in a lipid bilayer. Highlighted are two Na+ ions (*yellow spheres*), one Cl- (*cyan sphere*) binding site and one dopamine (DA) molecule in the S1 site and another in the S2 site. DA in the S1 site interacts with TMDs 1, 3, 6 and 8. DA in the S2 site interacts predominantly with TMDs 1, 3 and 10 and EL2 and 4. Modeling is based on a LeuT template (PDB ID: 2a65).

Reference: Shan J, Javitch JA, Shi L, Weinstein H (2011) The Substrate-Driven Transition to an Inward-Facing Conformation in the Functional Mechanism of the Dopamine Transporter. PLoS ONE 6(1): e16350

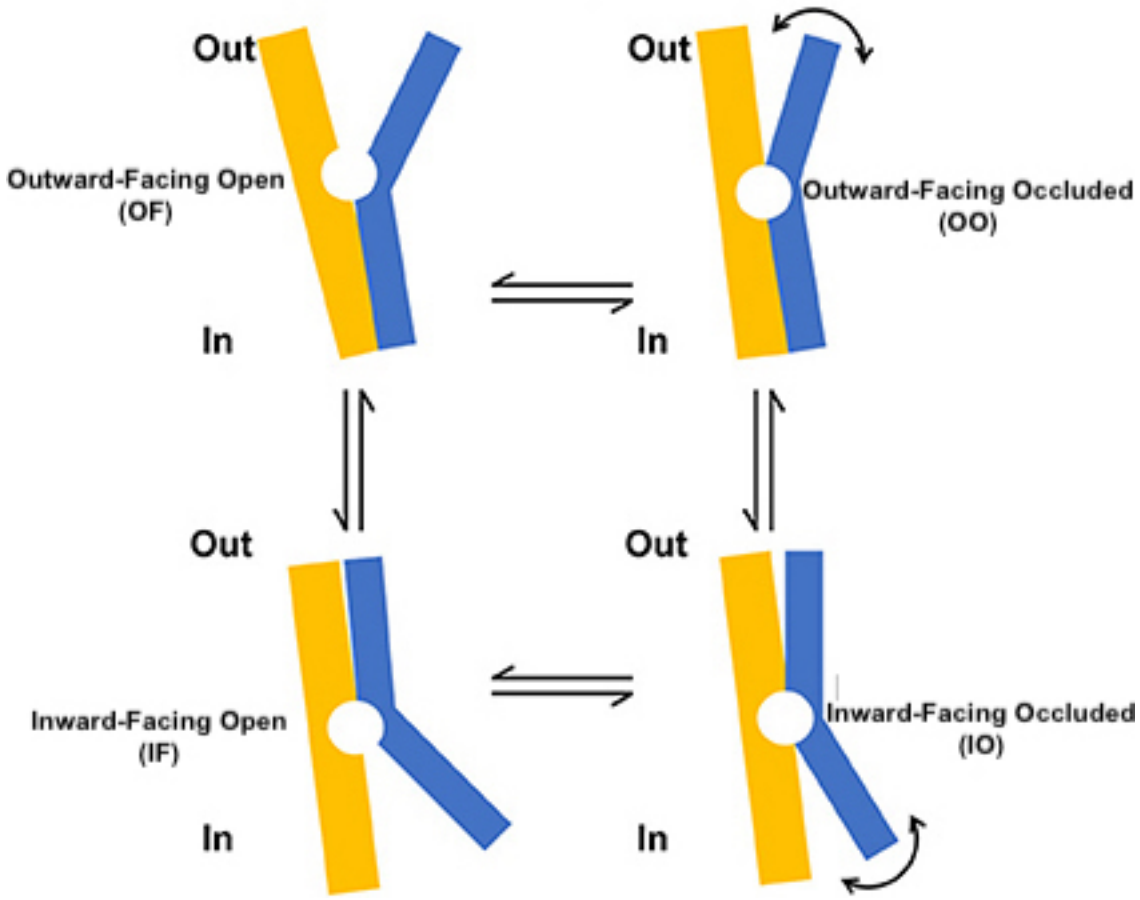

Figure 6: Alternating access mechanism of substrate transport

Schematic of the alternating access mechanism employed by various Neurotransmitter:Sodium Symporters (NSSs), including the SERT, NET, and DAT for substrate transport. The transport cycle samples multiple conformational states of which the OF, OO, IF and IO are highlighted.

Figured adapted from: Joseph D, Pidathala S, Mallela AK and Penmatsa A (2019) Structure and Gating Dynamics of Na^{+}/Cl^{-} Coupled Neurotransmitter Transporters. Front. Mol. Biosci. 6:80

conformations, as shown in **Fig. 6** (79-81)**.** Key to this alternating mechanism is a dynamic network of interactions facing the extracellular space ("extracellular gate") and the intracellular space ("intracellular gate"), which occlude the central binding site from the external or internal environment, respectively (62, 82, 83). As part of this mechanism, substrate binds the outward-facing open (OF) conformation of the transporter after which the transporter undergoes a series of conformational rearrangements to assume an inward-facing open (IF) conformation. These conformational rearrangements transport substrate from the extracellular environment, through the permeation pathway and into the cytoplasm. Upon completion of the transport cycle, the transporter resets itself to an OF conformation. The kinetic capacity of the DAT is thought to be regulated by the rate of these conformational changes. Further, according to this model the DAT exists in constant dynamic equilibrium between these conformations, where conformational changes are driven by numerous factors, including the localization of the DAT on the plasma membrane, presence of lipids on the plasma membrane, and the availability of substrate or ions on both the extracellular and intracellular faces of the transporter (84).

Crystal structures of various SLC6 transporters, which are also thought to move substrates according to alternating access mechanism, have contributed to the development of this model. For example, the LeuT has been resolved in three of the conformations shown above (**Fig. 6):** OF (79), outward-facing occluded (OO) (61) and IF (79) conformations. The human SERT, the only human SLC6 transporter to be crystallized, has been resolved in an inhibitor-bound OF conformation (58, 60). Similarly, dDAT has been resolved in a substrate-bound OF conformation (58, 59). To date, there is no crystal structure available for the hDAT. Despite the limited crystal structures available, numerous other techniques including electron paramagnetic resonance (EPR), fluorescence energy transfer (FRET), molecular dynamic (MD) simulations and electrophysiology (amperometry and whole-cell patch-clamp recordings) have been used to study substrate/ion translocation through SLC6 transporters. Interestingly, these strategies showed that the DAT confers leak currents in the absence of substrate (55). In addition, these strategies

revealed that the DAT adopts a channel-like mode during substrate translocation characterized by uncoupled ion conductances (50, 85-88). To date, the physiological relevance of this channel-like mode of the DAT remains unclear; however, its potential contribution to disease will be explored in more detail in the following chapter.

Regulation: Post-translational modifications

Molecular regulation of the DAT occurs via site-specific modifications and through various interactions with other proteins or plasma membrane elements. These regulatory mechanisms are often overlapping, as specific post-translational modifications can influence protein-protein interactions or transporter localization with the plasma membrane, and vice versa.

The DAT is subject to at least four types of post-translational modifications including glycosylation, phosphorylation, palmitoylation, ubiquitination (89). DAT phosphorylation is stimulated by various cellular states and substrates, including AMPH. Multiple kinases have been implicated in this process, including PKC, CAMKII and extracellular signal-regulated protein kinase (ERK). This section will focus on PKC, as this signaling molecule acts as a downstream effector for many post-translational mechanisms. The action of other kinases, specifically as they correspond to psychostimulant action will be discussed in more detail in the following sections. PKC activation stimulates DAT phosphorylation (mainly at Ser 7), induces DAT internalization and impairs DA uptake (89-91). DAT internalization occurs for acute (rapid trafficking to and from the surface) or prolonged (lysosomal degradation) periods (90, 92-96) in a dynamin-dependent manner. PKC-stimulated DAT internalization has been observed in various cell types, in primary neurons and striatal slices (90). This process is thought to require Ras-like GTPase, Rin, which binds to the DAT C-terminus, and Flotillin-1 (Flot 1), which retains DAT in lipid microdomains (53, 77). Of note, neutralizing substitutions at the DAT N-terminus (Ser7 to Ala) or truncation of phosphorylation sites (Δ1-22) do not impair internalization of the transporter (90, 97). Together, these data suggest that N-terminal phosphorylation of the DAT is not necessary for PKC-

stimulated DAT internalization. PKC activation has also been shown to intricately regulate AMPH action, as will be discussed in the following sections.

The hDAT contains five potential sites: Cys 6, 135, 342, 523, 581 for S-palmitoylation, as shown in **Figure 4**. Of these sites, a neutralizing substitution of Cys 581 reduces transporter palmitoylation by more than 60% (98). Palmitoylation of the DAT increases DA transport (Vmax), without affecting DAT expression or DA affinity (Km) (98). In addition, palmitoylation and PKC-mediated phosphorylation of the DAT appear to be inversely associated, where conditions that reduce DAT palmitoylation enhance PKC-stimulated DAT phosphorylation and vice versa (91, 98). Indeed, sustained suppression of palmitoylation increases DAT degradation likely through a PKC-dependent mechanism (99). Thus, in addition to regulating transporter capacity, palmitoylation also likely opposes DAT turnover and PKC-mediated DAT regulation (89, 98, 99).

One of four major sites: Lys19, 27, and 35 and 63 (100, 101) on the N-terminus of the DAT can be ubiquitinated. N-terminal ubiquitylation of the DAT targets the transporter for rapid internalization from the cell surface and subsequent lysosomal degradation. Ubiquitinated DAT is sorted away from the constitutive recycling pathway and into a late endocytic pathway via PKC-dependent mechanisms (101). To date, two ubiquitin ligases: Nedd4-2 and parkin have been identified to act on the DAT (89). Interestingly, parkin is thought to be neuroprotective, where mutations in parkin have been associated with early-onset PD (102).

N-linked glycosylation of the DAT occurs at three sites: Asn 181, 188 and 205 (demarcated by Y) on EL2, as shown in **Fig. 4**. Glycosylation of the DAT stabilizes the transporter on the plasma membrane and in turn, increases DA transport capacity (Vmax) (103, 104). Although glycosylation is not necessary for the surface expression of the DAT, partially glycosylated or non-glycosylated transporters are preferentially internalized. The effects of glycosylation on DAT transporter affinity is less clear (103, 104). Importantly, glycosylation of the DAT varies within brain regions and cell types, and may regulate DAT surface stability *in vivo* (105). Recent studies suggest that DAT glycosylation also correlates with vulnerability to degeneration in specific

neuronal populations (106). Together, these studies link DAT surface stability with neurodegeneration, and highlight, this mechanism as a potential therapeutic target.

Regulation: Protein-protein interactions

DAT localization and function are further regulated through the transporter's association with various proteins, as shown in **Fig. 7**. The trafficking of the DAT to and from the plasma membrane and its specific localization away from the synaptic area to the perisynaptic area requires numerous scaffolding proteins (104, 107). The C-terminus of the DAT contains a PDZ domain, a protein interaction motif common to scaffolding proteins, which plays a critical role in DAT localization (108). DAT knock-in mice with disrupted PDZ domain binding sequences display a ~90% decrease in DAT levels in striatal terminals of DA neurons and behavioral anomalies that resemble DAT knockout (KO) mice (108). Protein interacting with C-kinase 1 (PICK1) is the only PDZ domain binding protein known to interact with the DAT and regulate surface expression (107, 109). To date the mechanism of this regulation remains elusive, as studies have demonstrated PICK1 both facilitates and inhibits DAT surface expression (101, 102). Recent studies show that PICK1 KO mice have increased strital DA content and TH levels, despite normal DAT surface expression (110). These findings suggest that PICK1 regulates DA homeostasis through DAT-dependent and independent mechanisms.

Various other proteins bind the DAT C-terminus, although the functional relevance of these interactions has not been as well studied. For example, alpha-synuclein (α-synuclein) directly couples to the C-terminus of the DAT at the plasma membrane (111), where AMPH exposure potentiates DAT/α-Synuclein interactions (111) and parkin disrupts these interactions (112). Of note, various studies have yielded opposing findings on whether α-synuclein promotes or inhibits DAT expression as well as activity (111-113).

DAT has also been shown to form complexes with DRs. D2Rs, most likely presynaptic D2Rs, interact with the DAT N-terminus to facilitate DAT surface expression, consequently enhancing DA clearance (74) (114). Disrupting this interaction *in vivo* results in hyperlocomotion

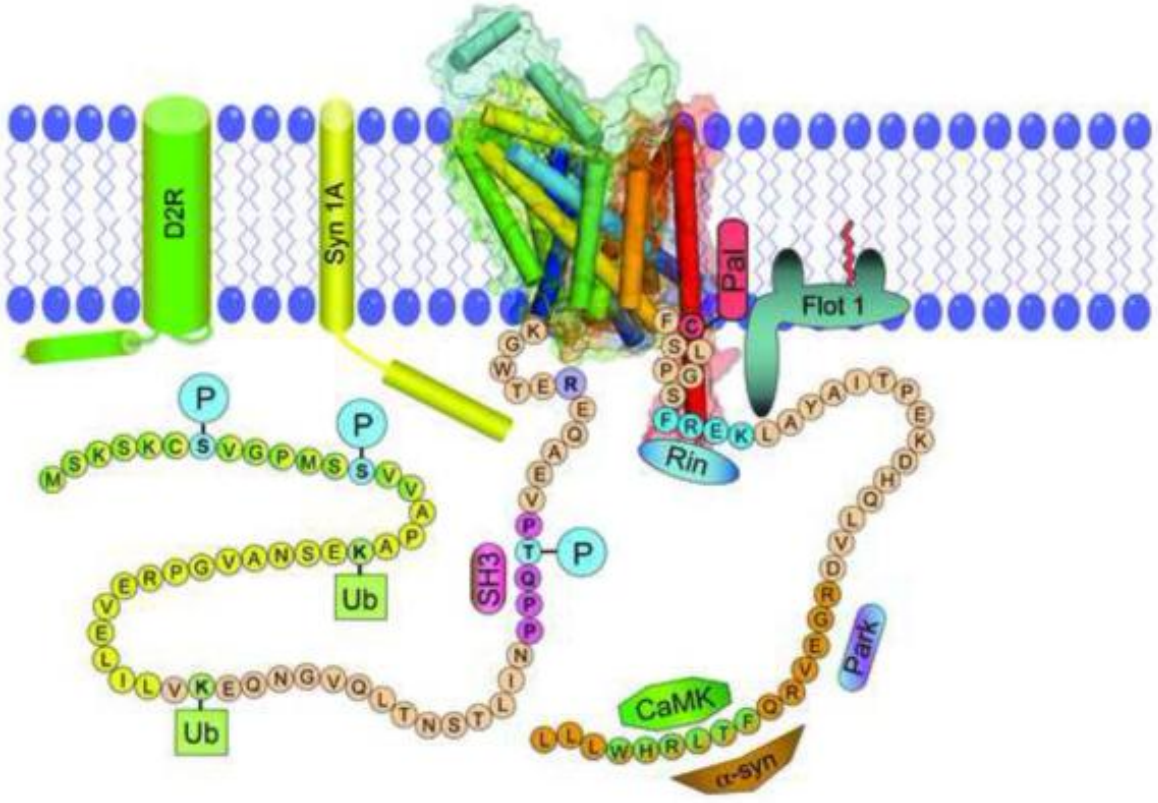

Figure 7: Regulatory elements of the dopamine transporter

Illustrated is a rat DAT based on LeuT crystal structure. Various post-translational modifications are highlighted: phosphorylation (*cyan sphere*, P) at Ser 7, 14 and Thr53; ubiquitylation (light green square, Ub) at Lys19 and Lys35 and palmitoylation (*pink*, Pal) at Cys580. Binding/interactions motifs are demarcated as follows: Src homology domain epitope (*mauve*, SH3), PKC endocytosis motif (*blue*, FREK), and Syntaxin 1A (STX1A, *yellow*), D2 DA receptor (D2R, *neon green*), Ras-like GTPase, Rin 1 (Rin, *blue*) and Calcium-Calmodulin-Dependent Protein Kinase (CaMK, *green*). Binding proteins α-synuclein (α-Syn, *orange*) and Parkin (Park, *dark blue-lavender*) and Flotillin 1 (Flot 1, *olive green*) are also shown.

Reference: Vaughan RA, Foster JD. Mechanisms of dopamine transporter regulation in normal and disease states. Trends Pharmacol Sci. 2013;34(9):489-96.

in mice, and suggests impaired DA uptake (74). Thus, in addition to D2Rs function as autoreceptors in negative feedback regulation of DA synthesis, release, uptake (13, 32, 33, 36, 37), D2Rs more directly regulate extracellular DA levels via their interaction with the DAT.

Aside from interacting with other proteins, DAT monomers also associate with each other to form dimers or higher order oligomers (104, 115, 116). Oligomerization of the transporter is thought to occur through interfaces at TMD 2, 4 and 6 (104, 115). Although the *in vivo* functional relevance of these complexes remains unclear, its postulated that oligomerization regulates DAT expression and function (104). To this end, some oligomers containing loss-of-function DAT mutants have been found to inhibit wild-type (WT) DAT activity without inhibiting expression of WT DAT, while others impair WT DAT activity by inhibiting surface expression of WT DAT (104). Curiously, while some substrates, namely AMPH and cocaine, promote the dissociation of DAT oligomers (117), others, such as methamphetamine (METH), promote the association of DAT oligomers (118). Thus, further studies are necessary to determine whether oligomerization regulates DAT surface stability as well as DAT function *in vivo*.

Regulation: Membrane microdomains

Under basal conditions, DAT moves between plasma membrane lipid raft and non-raft microdomains (94, 119). Although these findings are highly contended, it is thought that lipid raft microdomains are enriched with sphingolipids and cholesterol, where cholesterol directly interacts with the DAT to promote specific DAT conformations and regulate DAT function (119, 120). Flot 1 is thought to be essential for DAT localization to lipid rafts. In addition, as mentioned previously, Flot-1 is required for PKC-stimulated DAT internalization (121). PCK-stimulated DAT internalization requires Rin, where DAT/Rin interactions were shown to occur primarily in lipid raft microdomains (77). In contrast, constitutive DAT internalization is thought to occur in non-raft microdomains (77). Notably, Flot 1 is important for AMPH action in both *Drosophila (122)* and mice (123), as will be discussed below.

Finally, it is important to note that many of regulatory mechanisms discussed have been studied in heterologous expression systems which present with various limitations, including potential differences across cell lines, varied expression vectors, and protein overexpression; all factors that may reveal interactions not relevant *in vivo*. In addition, studies with whole-animal KO as opposed to brain-region or cell-specific knockdown are often difficult to interpret due to potential compensatory and/or developmental changes. Nonetheless, studies on these regulatory mechanisms of the DAT, whether *in vitro, in vivo* or *in silico* are essential as the DAT plays a pivotal role in maintaining DAergic tone.

Psychostimulant Action on the Dopamine Transporter

Psychostimulants increase extracellular DA levels in limbic regions of the brain, where this increase in DA is associated with their rewarding and reinforcing effects. However, unlike cocaine's well-characterized inhibition of DA uptake, the precise molecular mechanisms that underlie AMPH action remain unclear. Although this chapter will focus on AMPH's actions on the DAergic system, and the DAT specifically, it is important to note that AMPH has many off-target effects on the serotonergic and noradrenergic systems (124-127).

AMPH, as a substrate for the DAT, competes for the substrate-binding site, thereby, reducing DA uptake and increasing synaptic DA levels (128), as diagramed in **Fig. 8.** In addition, AMPH induces the reverse transport of DA (DA efflux) through the DAT to enhance further extracellular DA levels (129-131). AMPH relies on the tandem action of both DAT and VMAT to first concentrate AMPH in the cytoplasm and then in the synaptic vesicle lumen (19). AMPH translocation through the DAT elicits an inward current and is Na^+-dependent (57, 88). Once in the cytoplasm, AMPH is transported into synaptic vesicles through VMAT-mediated substrate:H^+ antiport, which alkalinizes the synaptic vesicle lumen. For every AMPH molecule that enters the synaptic vesicle, one proton exists; a process that ultimately collapses the pH gradient and redistributes DA to the cytoplasm (19). Here, DAT mediates the reverse transport of DA, from the

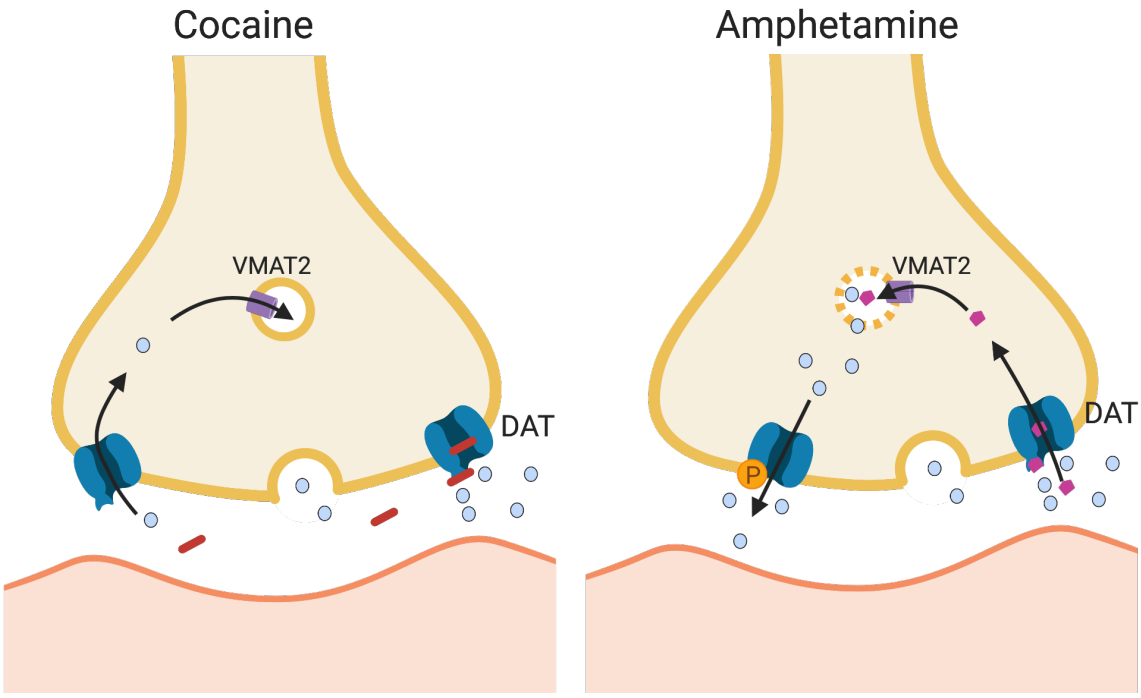

Figure 8: Psychostimulant action at the dopamine transporter

Actions of cocaine and AMPH result in increased DAergic signaling at DA receptors on the postsynaptic neuron. Left: Cocaine acts as a high-affinity antagonist of the DAT that competitively binds to the transporter to prevent substrate reuptake into the presynaptic neuron. Right: AMPH acts as a substrate of the DAT, and undergoes competitive reuptake into the presynaptic neuron. In addition, AMPH carries out multiple actions on the VMAT, DAT and DA metabolizing enzymes which results in DAT-mediated DA efflux. AMPH-mediated elevation of DA at the synaptic cleft is activity-independent.

Reference: Created with Biorender.com

cytosol to the extracellular space, through a process that is independent of vesicular release (132). Of note, at very high concentrations (>100 μM AMPH) studies speculate that AMPH acts independent of transporters via lipophilic diffusion; a theory termed the weak base hypothesis. This theory postulates that AMPH accumulates into synaptic vesicles due to its weak base properties and collapses the vesicular pH gradient by becoming protonated (133-135). To date, it is unclear whether this mode of action is physiologically relevant given the high AMPH concentrations required.

The DAT was first proposed to efflux DA through facilitated exchange diffusion. Facilitated exchange diffusion hypothesized the import of AMPH through the DAT induced the export of DA to the extracellular space (136). Since, various studies have challenged this hypothesis (137). Foremost, studies showed increasing intracellular Na^+ was sufficient to drive DA efflux even in absence of AMPH (57). Further, studies showed extracellular Na^+ influx was sufficient to trigger DA efflux through the DAT (56, 138, 139). Finally, DA efflux was shown to occur in rapid bursts through a channel-like mode of the DAT that doesn't reflect the kinetics of facilitated exchange diffusion (85). Although these findings do not rule out the possibility that DA efflux can occur via facilitated exchange diffusion, they suggest that others mechanisms are more likely at play.

AMPH's ability to promote DAT reverse transport is now known to be regulated by various signaling cascades as well as the direct interaction of the DAT with proteins, lipids, and other plasma membrane entities. Foremost, AMPH stimulates N-terminal phosphorylation of the DAT (140), which is necessary for DA efflux (141). Truncation of the distal N-terminus (Δ1-22) or neutralizing substitutions at Ser 2, 4, 7, 12, 13 (hDAT S/A) impairs DA efflux by approximately 80% without altering DA uptake (141). Moreover, *Drosophila* expressing hDAT S/A are not sensitive to the psychomotor effects of AMPH (142). Together, these data highlight the essential and selective role for DAT phosphorylation in AMPH-induced DA efflux and behaviors.

Various kinases have been shown to phosphorylate the DAT N-terminus in response to AMPH. Specifically, the DAT N-terminus contains putative phosphorylation sites for PKC and

CAMKIIα. AMPH increases striatal PKC activity (143, 144) in a Ca^{2+} dependent manner (145). Further, PKC activation leads to N-terminal phosphorylation in rat striatal tissue (96). Consistent with the pivotal role of N-terminal phosphorylation in DA efflux, PCK inhibition or downregulation decreases AMPH-induced DA efflux (146, 147) and hyperlocomotion in rats (148). Studies on PKC isoforms, implicate PKCβ in mediating AMPH action, including DA efflux and psychomotor activity (70, 149).

CaMKIIα interacts with the DAT C-terminus to promote N-terminal phosphorylation of the DAT (68). Inhibiting DAT/CaMKIIα interactions *in vitro*, *ex vivo* or in various mouse models *in vivo* significantly decrease DA efflux (68, 150). It is thought that CAMKII activation occurs through the elevation of intracellular Ca^{2+}. Indeed, AMPH increases intracellular Ca^{2+}, where Ca^{2+} chelation inhibits AMPH-induced DA efflux and voltage-dependent AMPH-induced DAT currents (151). Recent studies suggest that extracellular Ca^{2+} may also contribute to AMPH action. AMPH-induced DAT currents can activate various voltage-gated Ca^{2+} channels that elevate intracellular Ca^{2+} levels (152). In this way, intracellular Ca^{2+} levels critically regulate AMPH action, working upstream of both PKCβ and CAMKIIα activity.

In addition, a growing body of evidence suggests that aside from kinases, other proteins and lipids regulate AMPH action through direct interactions with the DAT, including Syntaxin 1A (STX1A) (52, 69, 153), G protein βγ subunits (Gβγ) (71, 72) and phosphatidylinositol (4,5)-bisphosphate (PIP_2) (63). PIP_2 binds the DAT N-terminus to promote N-terminal phosphorylation (63, 64), facilitating the interaction between IL3 and the phosphorylated N-terminus (64). The interactions of PIP_2 with the N-terminus as well as that of the N-terminus with IL3 are critical to AMPH-associated behaviors (63, 64), as will be discussed in Chapter 3.

Syntaxin 1A (STX1A) also plays a central role in AMPH action. STX1A interacts with the DAT N-terminus to promote AMPH-induced DA efflux (69). DAT/STX1A interactions require CaMKIIα activity and are potentiated by AMPH, suggesting that AMPH activation of CaMKIIα supports DAT/STX1A association (69). Significantly, STX1A itself can be phosphorylated, a

modification which affects its interaction with other proteins (154, 155). Indeed, inhibiting STX1 phosphorylation pharmacologically or via neutralizing substitutions at Ser14 (52) reduces DAT/STX1 interactions. Our understanding of how STX1A/DAT regulate DA efflux, is further complicated by findings showing that STX1A also modifies DAT cell surface expression (153), and that PIP_2 can module DAT/STX1A association (155). From these findings its evident that STX1/DAT and PIP_2/DAT associations as well as N-terminal phosphorylation of the DAT are highly interrelated and work concomininantly (and perhaps together) to promote DA efflux.

To date, although it's clear that AMPH-like substances induce DAT-mediated DA efflux, the physiological role of DA efflux remains unclear. Interestingly, various disease-associated hDAT variants display anomalous DA efflux (ADE), characterized by a constitutive DA leak through the DAT (156). Thus, studies on the AMPH-induced DA efflux may shed light on the mechanisms that underlie ADE, and more broadly, how DA dysregulation contributes to neuropsychiatric disease.

Of note, AMPH also regulates DAT trafficking by enhancing DAT surface expression acutely and promoting DAT internalization in the long-term (157, 158). Although the mechanisms that regulate these processes remain unclear and will not be discussed, these findings highlight that AMPH stimulates high extracellular DA via multiple, overlapping mechanisms. DAT internalization in response to AMPH limits DAT surface expression thereby sustaining high extracellular DA levels that result from DA efflux and competitive-inhibition at the DAT.

The Dopamine Transporter in Human Disease

Many genetic studies on neuropsychiatric disorders have focused on the DAT due to is essential role in regulating DA neurotransmission and because it is the target for various therapeutic drugs, including methylphenidate (Ritalin), AMPHs (Adderall) and bupropion (Wellbutrin). These studies have associated common variants in the *SLC6A3* gene, which encodes hDAT with increased risk for neuropsychiatric and neurological disease (159-161). In addition, recent studies have identified rare variants in the *SLC6A3* gene, which are associated

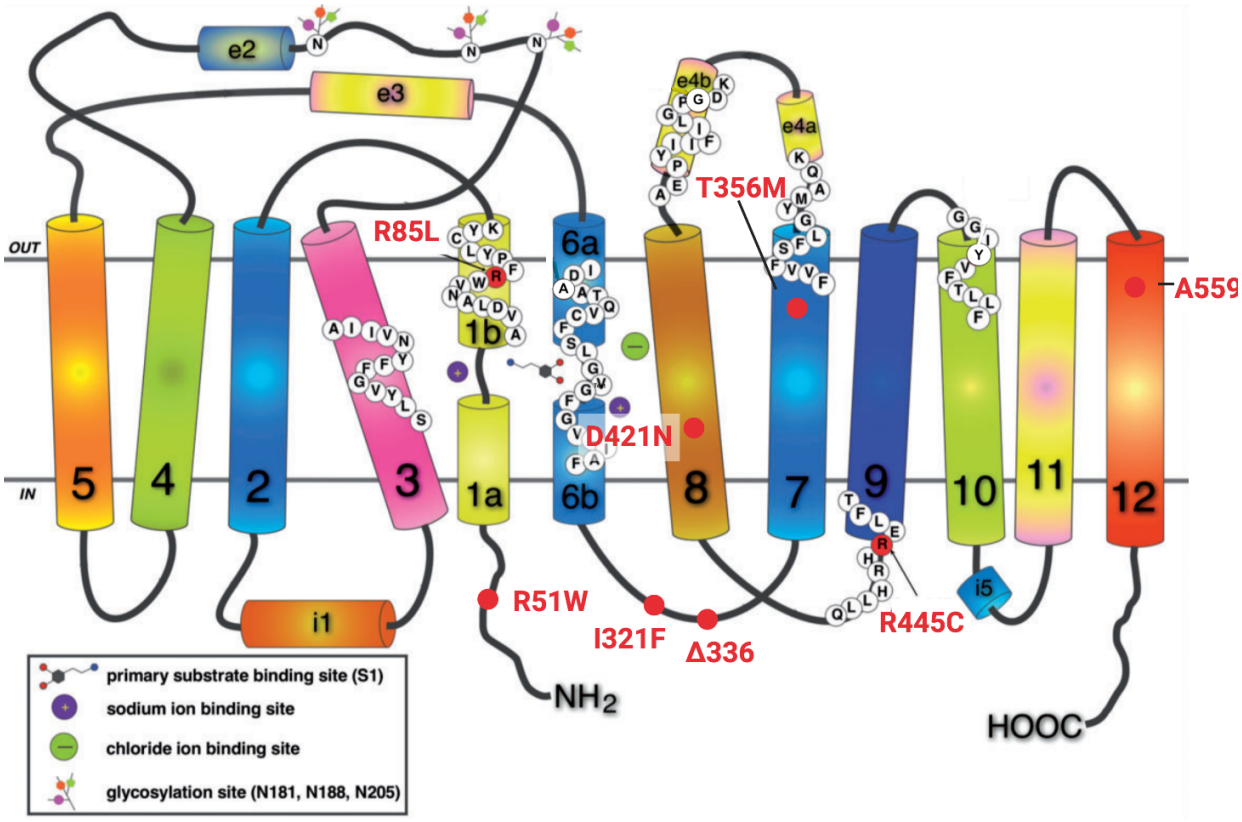

Figure 9: Rare disease-associated variants in the dopamine transporter

Schematic representation of the dopamine transporter highlighting specific rare variants.

Figure adapted from: Ng J, Zhen J, Meyer E, et al. Dopamine transporter deficiency syndrome: phenotypic spectrum from infancy to adulthood. *Brain*. 2014;137(Pt 4):1107–1119

with Dopamine Transporter Deficiency Syndrome (DTDS) (162, 163), early-onset PD (164), ASD (50-52, 165-167), ADHD (164, 168) and bipolar disorder (169) disorders. Rare variants have proven to be critical in the elucidation of the molecular mechanisms underlying complex diseases. This chapter will briefly discuss (1) A559V, T356M, Δ336, R51W, as they pertain to ASD and (2) D421N, I312F and R445C, as they pertain to PD or parkinsonian-like symptoms (**Fig. 9**).

ASD

ASD is a neuropsychiatric disorder depicted by impairments across two core domains: (1) social communication and interaction and (2) patterns of restricted and repetitive behaviors, interests, or activities (170). ASD-associated hDAT variants are located throughout functionally relevant sites on the transporter: A559V is found near the beginning of TMD 12, T356M is located near the substrate and ion-binding sites on TMD 7, Δ336 is located in IL3 proximal to the intracellular gate and R51W is located on the N-terminus. Common to these ASD-associated variants is the impaired or altered ability of the DAT to respond to AMPH in a coordinated manner.

The hDAT A559V variant has been identified in two unrelated patients with ASD (50), a patient with bipolar disorder (169) and in two siblings with attention deficit hyperactivity disorder (ADHD) (156, 168, 171). Heterologous expression of hDAT A559V showed normal DAT expression, surface trafficking, DA uptake and DA affinity (156). Notably, hDAT A559V cells displayed ADE blocked upon the application of methylphenidate, AMPH and cocaine (50, 156). ADE is characterized by a constitutive leak in DA efflux via the DAT, which is commonly revealed by cocaine or other DAT substrates. These substrates block the DAT and the constitutive DA leak, which in turn decreases the amperometric signal**.** ADE in hDAT A559V cells was shown to result from D2R-autoreceptor activation of CaMKII, a kinase known to phosphorylate the N-terminus of the hDAT (86). Consistently, the N-terminus of hDAT A559V was found to be hyperphosphorylated. Neutralizing substitutions at N-terminal serines (Ser 2, 4, 7, 12, 13; hDAT A559V S/A) in the hDAT A5599V background abolished ADE in cells (86). Studies in a murine model showed that DAT A559V elevated

extracellular DA levels, altered D2R function, blunted AMPH-evoked DA release, and blunted AMPH-induced locomotion (172). Interestingly, changes in DA neurotransmission were reversible by D2R antagonism.

T356M was the first *de novo* hDAT variant identified in a patient diagnosed with ASD (51). EPR studies in the bacterial homolog LeuT suggested that T356M biased the transporter in an OF conformation termed “efflux-willing”. Consistently, hDAT T356M cells conferred cocaine-sensitive ADE, similar to the molecular phenotype observed in hDAT A559V. In addition, hDAT T356M cells displayed reductions in DA uptake and AMPH-induced DA efflux that were not associated changes in hDAT surface expression. *Drosophila* expressing hDAT T356M displayed hyperlocomotion, likely a result of increased extracellular DA levels. Recent studies in mice homozygous for T356M showed that this variant impaired striatal DA neurotransmission and promoted behaviors commonly associated with ASD (altered social interactions and repetitive behaviors) as well as behaviors associated with ADHD (i.e. hyperactivity), a common comorbidity of ASD (166). Together, the findings from hDAT variants A559V and T356M suggest that ADE may underlie DA dysfunction observed in ASD.

The R51W variant was identified through exome sequencing of patients diagnosed with ASD (52). In a heterologous expression system, hDAT R51W significantly reduced DA efflux compared with hDAT WT, but did not alter DA uptake. Further, impairments in DA efflux were associated with weakened DAT/STX1 interactions. In *Drosophila*, hDAT R51W supported normal basal locomotion, but reduced sensitivity to the psychomotor effects of AMPH.

ΔN336, a rare in-frame deletion at the conserved residue Asn 336, was identified in a single ASD family. Crystallographic and EPR studies on LeuT as well as MD simulations suggested that ΔN336 compromised the structural integrity of hDAT and in turn, transport capacity. Specifically, this variant stabilized a “half-open and inward facing” conformation (HOIF) that was associated with impaired DA uptake, and diminished AMPH-induced DA efflux and currents in cells. *Drosophila* expressing hDAT ΔN336 displayed phenotypes commonly

associated with ASD, including impaired social interactions and increased fear. Together, the findings from hDAT variants R51W and ΔN336 suggest that impaired DA efflux (albeit induced by AMPH) may also contribute to disease pathology, emphasizing the idea that DA efflux may play a physiological role.

Parkinson's Disease and parkinsonian-like symptoms

PD is a neurodegenerative disorder characterized by deficits in motor symptoms, including bradykinesia (slowed movement) and either resting tremor or rigidity. Common to hDAT variants associated with PD or parkinsonian-like symptoms are deficits in hDAT capacity or regulation (162, 163, 173, 174). A recent study on a cohort of patients with parkinsonian-like movement disorders identified a compound heterozygous mutation in a patient with early-onset PD and ADHD. This patient possessed a heritable variant, hDAT I312F and a *de novo* variant, hDAT D421N (164). hDAT I312F and hDAT D421N cells displayed impaired DA uptake despite normal cell surface expression. hDAT D421N cells also displayed impairments in DA efflux and cocaine sensitive ADE. Further, hDAT D421N altered Na^+ affinity by interfering with the second Na^+ binding site in cells.

Numerous loss-of-function hDAT variants, often resulting from impaired hDAT surface expression have been associated with parkinsonian-like symptoms in DAT deficiency syndrome (DTDS, first termed infantile dystonia-parkinsonism). The details of how these variants, specifically R445C contributes to DAT dysfunction and parkinsonian-like phenotypes will be discussed in detail in Chapter 2.

Drosophila Melanogaster as a Model System

Drosophila melanogaster have proven to be a robust model system for neuroscience research due to powerful and versatile genetic techniques, ease of use, short lifespan and low cost (175-177). *Drosophila* and humans share many of the same neurotransmitters including GABA, glutamate, acetylcholine and some of the same monoamines including histamine, serotonin and DA (175). *Drosophila* also express many of the same proteins that regulate DA

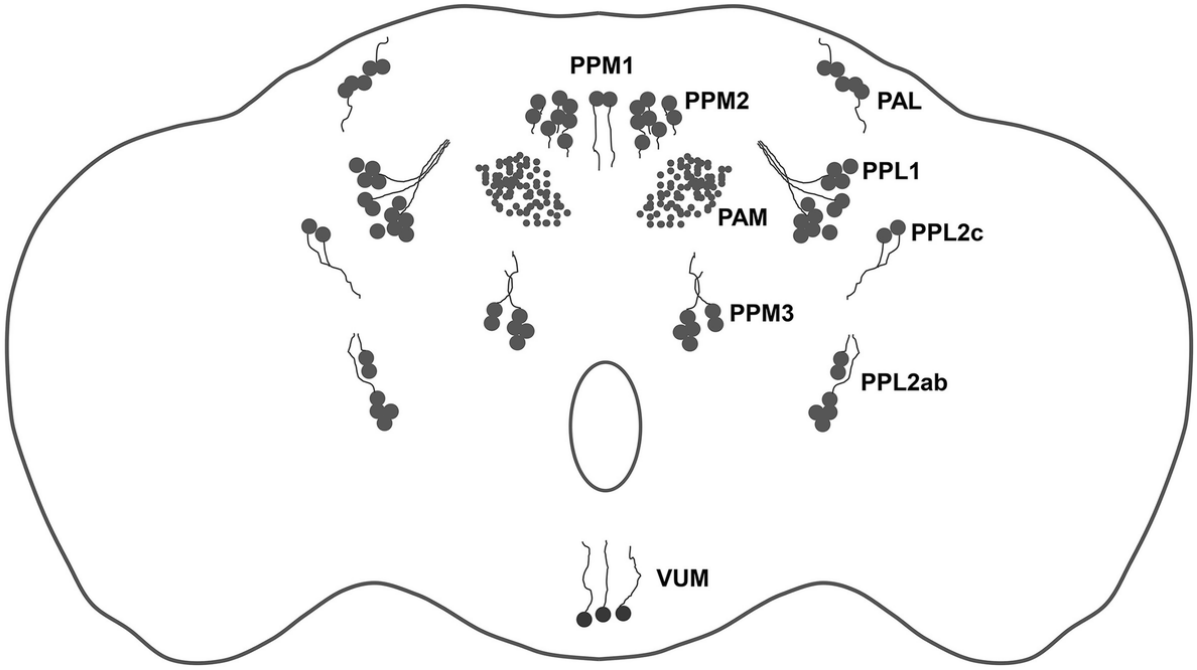

Figure 10: Dopamine projections in the *Drosophila* brain

Schematic of DA clusters in an adult fly brain. Highlighted are PAM, PAL, PPM1, PPM2, PPM3, PPL1, PPL2ab, PPL2c, and VUM neurons.

Dung V.M., Thao D.T.P. (2018) Parkinson's Disease Model. In: Yamaguchi M. (eds) *Drosophila* Models for Human Diseases. Advances in Experimental Medicine and Biology, vol 1076. Springer, Singapore

neurotransmission (synthesis, packaging, transport and metabolism) and signal transduction (receptors and signaling pathways) (178). These include proteins that are proposed molecular targets of vertebrate psychostimulant action, such as DAT, SERT and VMAT (178). Thus, *Drosophila* have been used to the study the molecular mechanisms that underlie DA neurotransmission in healthy and disease states.

In *Drosophila* brains there are approximately ~200 DA neurons that segregate into eight clusters (179), as shown in **Fig. 10**. These DA neurons play key roles in regulating elemental behaviors such as arousal, sleep, locomotion and courtship in flies (180-188). In addition, recent studies, suggest that DA also regulates more complex behaviors such as attention, motivation, fear, learning and memory (165, 189-191). Of note, psychostimulants produce stereotyped, behavioral effects as seen in other vertebrate models. For example, flies exposed to volatilized cocaine show dose-dependent increases in grooming and locomotion paralleling behaviors in mammals (192, 193). AMPH administration promotes hyperlocomotion in both larvae and adult flies consistent with phenotypes in mammals (19, 22, 122). Consequently, flies have become an increasingly valuable model system to study drugs of abuse, and the mechanism that underlie drug reward and preference (64).

Finally, *Drosophila* have been instrumental in the study of human disease. Animals models for various disorders, including PD (177, 194-197) and ASD (51, 165, 176, 198) have shed light on the mechanism that underlie specific disease-related phenotypes. The following chapters will define whether and how DAT and DA dysregulation drive specific behavioral phenotypes in *Drosophila.* Moreover, they will detail how these findings translate to our understanding of these disease states in humans.

CHAPTER II

PARKINSONIAN-LIKE PHENOTYPES IN *DROSPHILA MELANOGASTER* PROMOTED BY INTRACELLULAR GATE DYSFUNCTIONS IN THE HUMAN DOPAMINE TRANSPORTER

The work described in this chapter is part of, and adapted from the manuscript in preparation titled "Aguilar JI *et al*. Parkinsonian-like phenotypes in *Drosophila Melanogaster associated with* channel-like conformation in the human dopamine transporter"

Abstract

Parkinson disease (PD) is a progressive, neurodegenerative disorder affecting over 6.1 million people worldwide. Although the cause of PD remains unclear, studies on highly-penetrant mutations identified in early-onset familial parkinsonism have contributed to our understanding of the molecular mechanisms underlying disease pathology. Dopamine Transporter (DAT) Deficiency Syndrome (DTDS) is a distinct type of infantile parkinsonism-dystonia that shares key clinical features with PD, including motor deficits (progressive bradykinesia, tremor, hypomimia) and altered dopamine (DA) neurotransmission. Here, we define structural, functional, and physiological consequences of a Cys substitution at R445 in human DAT (hDAT), identified in a patient with DTDS. We found that a Cys substitution at R445 disrupts a conserved intracellular (IC) network of interactions, compromising the hDAT IC gate and thus, impairing transport function. Notably, the disruption of this IC network supported a channel-like intermediate in the hDAT. To understand the pathophysiological relevance of this mutation, we used *Drosophila melanogaster* as a model system. We showed that hDAT R445C *Drosophila* exhibit motor deficits, lack of motor coordination (i.e. flight coordination) and phenotypic heterogeneity in these behaviors that is typically associated with DTDS and PD phenotypes. These behaviors were linked with altered dopaminergic signaling stemming from loss of DA neurons and decreased DA

availability. We rescued flight coordination via the lysosomal inhibitor chloroquine that we identified to enhance DAT expression. Together, these studies shed light on how a DTDS-linked DAT underlies DA dysfunction and the clinical phenotypes shared by DTDS and PD, more broadly

Introduction

Parkinson's disease (PD) is the second-most prevalent neurodegenerative disorder, affecting 2–3% of the population over the age of 65 (199). Classically, patients with PD present with motor symptoms, including bradykinesia and either resting tremor or rigidity. A hallmark of PD neuropathology is the loss of dopaminergic neurons in the substantia nigra that results in severe striatal dopamine (DA) depletion, accompanied by α-synuclein inclusions in the remaining neurons (46). Early in PD, α-synuclein, a protein largely expressed in the brain, forms soluble oligomeric aggregates believed to confer neurotoxicity that mature to insoluble fibrils (200, 201). Although a vast majority of PD cases occur idiopathically, affecting people over the age of 50 (late-onset), a subset of genetic mutations are associated with early-onset PD (202). Investigations on these highly-penetrant, inherited forms of PD have provided tremendous insights into specific molecular pathways that underlie neurodegeneration and motor deficits (46).

Recently, mutations in the human DA transporter (hDAT) gene (*SLC6A3*) have been linked with a distinct type of infantile parkinsonism-dystonia, referred to as DA transporter deficiency syndrome (DTDS) (162, 163, 174). Few patients diagnosed with DTDS survive to adulthood, with a majority of patients dying in childhood or adolescence (162, 163, 174). Common to DTDS-linked DAT variants is a multifaceted loss of DAT function, which includes impaired transporter activity and expression (162, 163, 174, 196, 203). DTDS is a complex movement disorder, typically characterized by initial infantile hyperkinesia (dyskinesia/dystonia) that progresses to a parkinsonian movement disorder (bradykinesia/tremor) (162, 163). Other characteristic clinical features include elevated levels of the DA metabolite, homovanillic acid (HVA) in the cerebrospinal fluid and loss of DAT activity in the basal ganglia, as measured by

single-photon emission tomography imaging of the DAT (i.e. DaTSCAN) (162, 163, 174). In DTDS, increased levels of HVA typically reflect increased DA turnover promoted by higher extracellular DA levels. This increase in DA levels likely reflects decreased DA clearance mediated by a loss of DAT activity. Other forms of early-onset parkinsonism have also been associated with impaired DAT function (164). Specifically, a patient with early-onset parkinsonism and attention deficit hyperactivity disorder (ADHD) was identified with *SLC6A3* compound heterozygous missense mutations that gave rise to Phe substitution at I321 and Asn at D421 in the DAT(164, 204). To date, the mechanism through which altered DAT function underlies parkinsonian symptoms remains unclear.

The DAT is a presynaptic membrane protein that spatially and temporally regulates DA neurotransmission by mediating the reuptake of DA from the synapse following vesicular release. Among other roles, DA regulates cognition, emotion, motor activity, and motivation (43, 205, 206). Altered DA neurotransmission has been implicated in several neuropsychiatric and neurological disorders, including ADHD, Autism Spectrum Disorder (ASD) and PD (47-52, 199). Structural and molecular dynamic (MD) studies suggest that DA transport occurs via an alternating access model, wherein the transporter alternates between various “outward-facing” and “inward-facing” conformations (79-81). In addition, it has been shown that hDAT can form an aqueous pore in a channel-like mode (50, 85, 86). Key to the alternating mechanism is a network of interactions occurring at the extracellular and intracellular space, termed EC and IC gates, respectively. Recent work identified a compound heterozygous missense mutation in the *SLC6A3* gene, with the mutation in one allele resulting in a Cys substitution at R445 (R445C) and the mutation in the second allele resulting in a Leu substitution at R85 (R85L) in a patient who presented with classical DTDS (162). Either mutation, when studied individually, has devastating effects on hDAT activity and expression (162), given that these residues regulate either the EC or IC gates of hDAT (62, 207, 208). In this study, we focused on the R445C mutation. R445 is located close to the cytoplasmic end of TM9, facing the IC vestibule and is part of a conserved IC interaction network

that comprises the IC gate (62, 66, 82, 209, 210). This network is thought to coordinate conformational rearrangements in the DAT throughout the transport cycle (62, 82). Specifically, R445-E428 salt bridge is predicted to stabilize the transition of the hDAT to an inward-occluded conformation (58, 66, 209). Previous studies showed that substitutions at R445 impair DAT function (162, 196, 203, 209). However, how and whether R445C impacts the dynamics of the IC gate, and subsequently DA neurotransmission as well as DA-associated behaviors remains unclear. Importantly, how R445C contributes to DA dysfunction in disease and more specifically, DTDS etiology is largely unknown.

We undertook a close examination of the structural and functional consequences of R445C substitution in the hDAT. We integrated molecular insights from X-ray crystallography, electron paramagnetic resonance (EPR) and molecular dynamic (MD) simulations to determine how R445C underlies DAT dysfunction. We adopted *Drosophila melanogaster* as an animal model to examine whether and how this hDAT variant supports brain DA dysfunction, loss of DA neurons and behavioral phenotypes characterized by DTDS. Finally, we assessed a pharmacological agent in its ability to rescue behavioral deficits in *Drosophila* expressing hDAT R445C. Together, this work provides insight into the structural mechanisms underlying DAT dysfunction and the impact of DAT dysfunction on specific behaviors as well as on the molecular mechanisms that underlie DTDS and more broadly, PD pathology.

Results

hDAT R445C compromises movement vigor in *Drosophila*

Drosophila melanogaster have provided unique and critical insights on the pathogenic mechanisms underlying PD (194, 197). *Drosophila* PD models consistently recapitulate essential PD phenotypes, including neurodegeneration as well as motor and non-motor behavioral deficits (177). In addition, mechanisms that mediate DA neurotransmission and signaling observed in other phyla are largely conserved in *Drosophila* (178). As observed in mammals, *Drosophila*

exhibit increased arousal and hyperactivity, among other stereotypies when DAT function is altered (187, 192, 211).

In order to understand whether certain DAT dysfunctions are associated with specific phenotypes in *Drosophila,* we assessed whether the R445C missense mutation in the DAT promoted behaviors associated with common DTDS phenotypes. We adopted the Gal4/UAS system to express hDAT WT or hDAT R445C specifically in DA neurons of flies homozygous for the *Drosophila* DAT null allele (DAT^{fmn}) (51). We tested flies for spontaneous locomotor activity and "anxiety"-related behaviors (i.e. center time). Illustrated are representative trajectories of adult hDAT WT (**Fig. 11A**, *black trace*) and hDAT R445C (**Fig. 11A**, *blue trace*) flies assayed in an open-field test for 5-min. We observed no differences in center time in hDAT R445C flies with respect to hDAT WT flies (**Fig. 11B**; hDAT WT: 0.016 ± 0.003 (t/t_{total}); hDAT R445C: 0.024 ± 0.006 (t/t_{total}); $p > 0.05$). We did observe a significant reduction in spontaneous locomotor activity in hDAT R445C (59.7 ± 6.1 cm) compared with hDAT WT flies (80.1 ± 4.2 cm; $p = 0.008$) (**Fig. 11C**). Given that parkinsonian locomotor deficits can be characterized by hypokinesia (inability to initiate movement) and bradykinesia (slowed movement), we dissected the specific locomotor deficits observed in hDAT R445C flies. We determined the frequency (number of times) with which specific velocities were explored throughout the test period (**Fig. 11D**). We defined "initiating movement" as velocity = 0.74 - 0.94 mm/s and "fast movement" as velocity = 5.3 – 10.0 mm/s and determined their frequency per genotype. hDAT R445C flies spent 5.0 ± 0.3 % of the testing period initiating movement compared with 5.2 ± 0.4 % for hDAT WT flies, suggesting hDAT R445C flies did not have difficulty performing this task ($p > 0.05$; **Fig. 11E**). In contrast, hDAT R445C flies displayed significantly decreased movement vigor, in fast movement for only 9.8 ± 1.4 % of the testing period compared with 14.5 ± 1.1 % for hDAT WT flies ($p = 0.0098$; **Fig. 11F**). Together, these data suggest that motor deficits in hDAT R445C flies are primarily characterized by deficits in movement vigor.

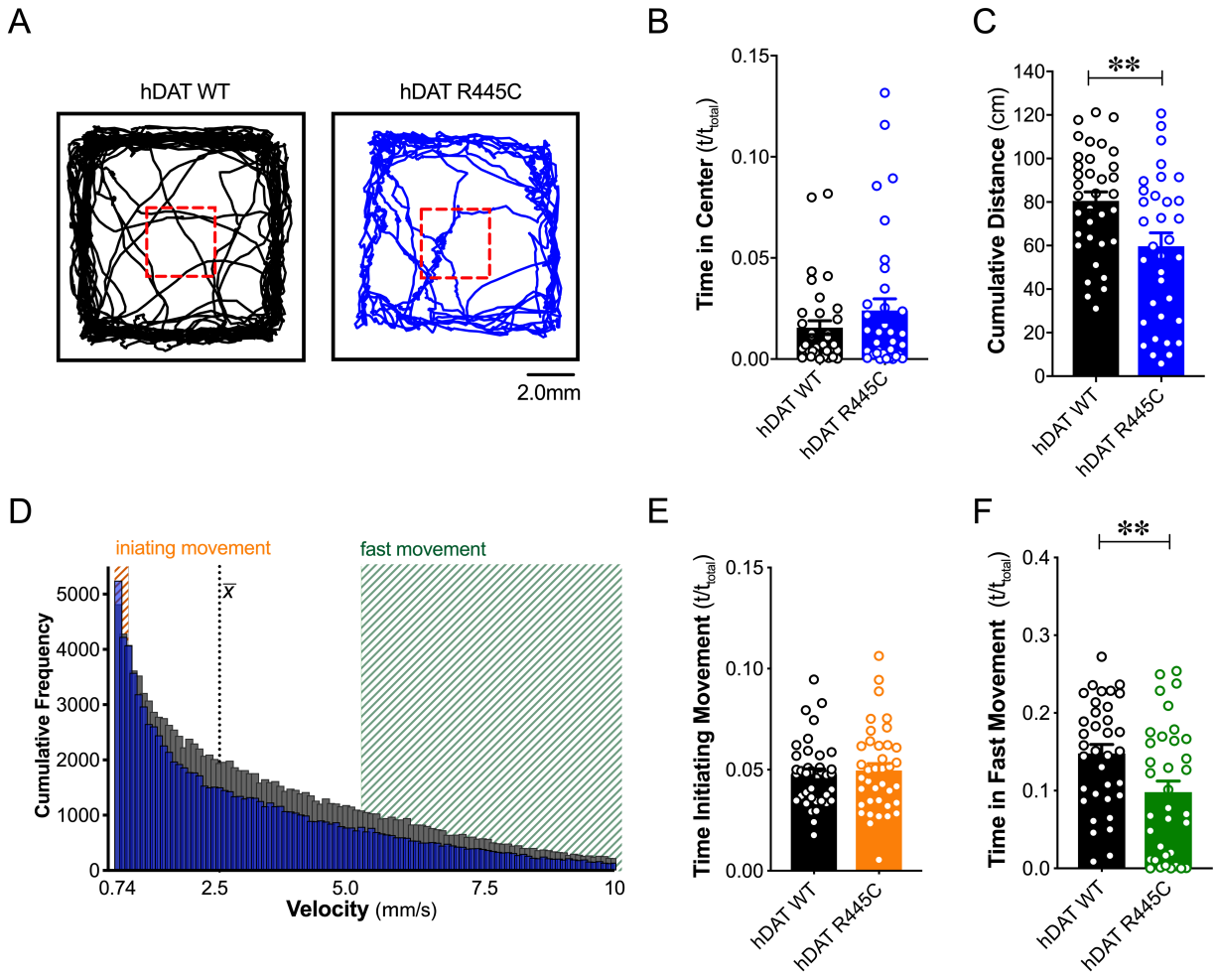

Figure 11: R445C variant disrupts locomotive behaviors

(**A**) hDAT WT or hDAT R445C was selectively expressed in DA neurons in a dDAT KO (*fmn*) background. Representative trajectories of hDAT WT (*black*) and hDAT R445C (*blue*) flies in an open-field test during a 5-min test period. 3 x 3 mm square (*red dashed lines*) delineates the center space. (**B**) hDAT WT and hDAT R445C flies spent comparable time in the center space ($p > 0.05$; n = 35). (**C**) hDAT R445C flies traveled significantly less relative to hDAT WT flies ($p = 0.006$; n = 35). (**D**) Histogram represents instantaneous velocities ranging from 0.74 to 10.0 mm/s (bin width = 0.094 mm/s; see methods) and corresponding frequencies (number of times). Initiating movement velocities (0.74 - 0.94 mm/s, *orange shaded*), fast movement velocities (5.3 - 10.0 mm/s, *green shaded*) and average velocity ($\bar{x}$) are highlighted. (**E**) hDAT R445C flies spent a comparable amount of time initiating movement relative to hDAT WT flies ($p > 0.05$; n = 35). (**F**) hDAT WT flies spent significantly more time in fast movement compared with hDAT R445C flies ($p = 0.001$; n = 35).

Data are presented as mean ± SEM. Student's t-test: (B); Mann-Whitney test (C) and (E - F).

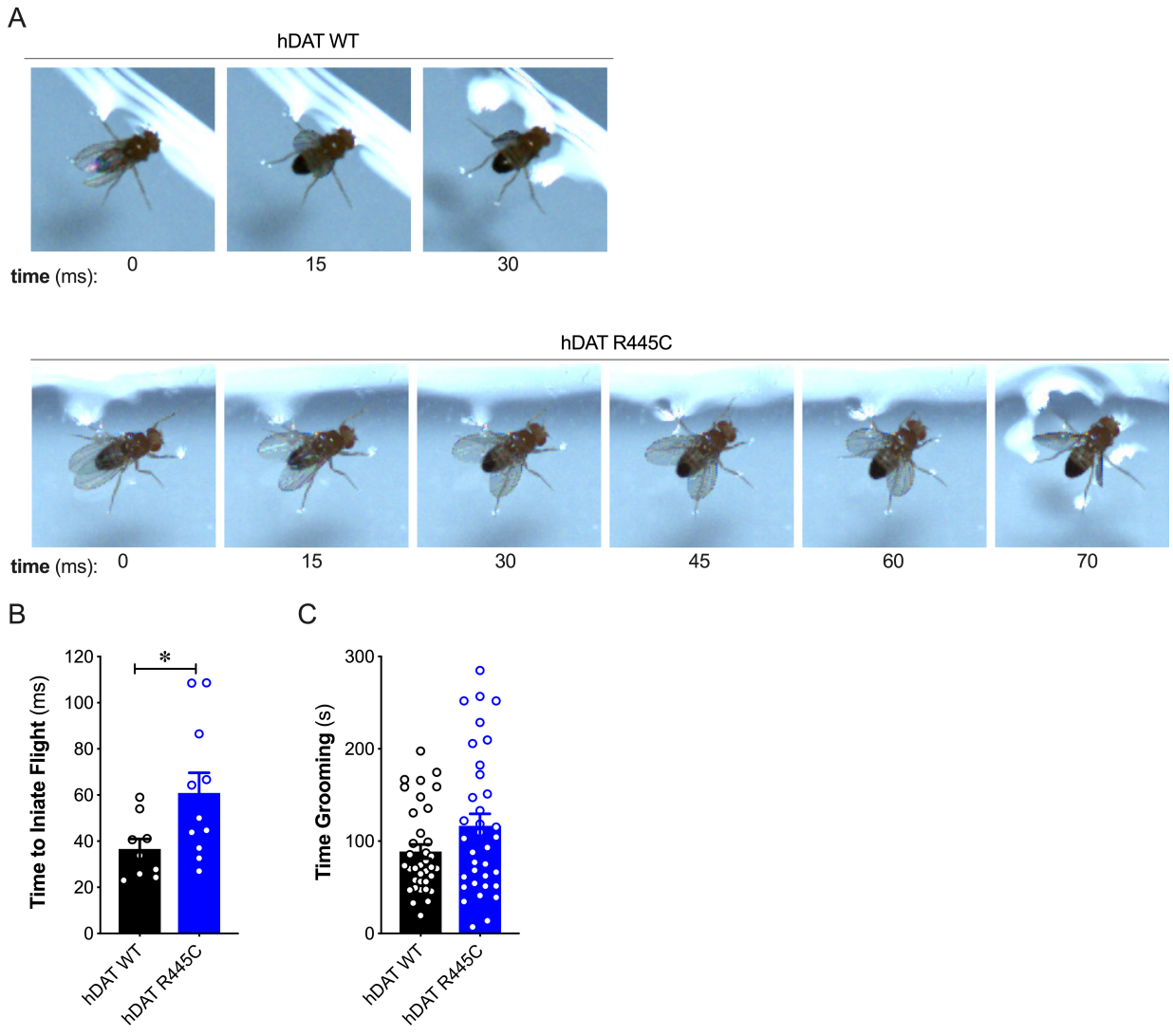

Figure 12: R445C variant selectively impairs flight take-off

(**A**) Single frames of *Drosophila* hDAT WT (*top*) and hDAT R445C (*bottom*) during various phases of coordinated take-off (video recorded at 2000 fps). (**B**) Flight initiation (take-off) was quantified from the initial phase of wing elevation (t = 0) to the second phase of simultaneous wing depression and leg extension. Flight initiation was significantly delayed in hDAT R445C flies relative to hDAT WT ($p = 0.02$; n = 10 - 11). (**C**) hDAT R445C flies spent comparable time grooming compared with hDAT WT flies ($p > 0.05$; n = 35).

Data are presented as mean ± SEM. Student's t-test: (B).

hDAT R445C impairs selective coordinated movements

Patients with early-onset as well as sporadic PD often present with impairments in coordination (212). To understand further the contribution of the DAT to coordinated motor behaviors, we analyzed a quintessential fly behavior: flight. Various monoamines, including DA modulate insect flight (184). Inhibition of specific TH-positive DA neurons has been found to compromise flight, including impaired wing coordination and kinematics (184). Initiating voluntary flight (take-off) consists of an initial phase of wing elevation followed by a second phase of simultaneous left- and right-wing depression and leg extension (213). Using a high-speed camera (2,000 fps), we quantified the time that elapsed between the initiation of wing elevation (t = 0) and final take-off from a water surface (**Fig. 12A**). We found that flight initiation was significantly compromised in hDAT R445C flies as the corresponding duration of take-off was 60.9 ± 8.7 ms compared with 36.6 ± 4.4 ms for hDAT WT flies ($p = 0.03$) (**Fig. 12B**). To determine whether impairments in coordination were consistent across multiple modalities, we assessed grooming. In *Drosophila,* this stereotyped, coordinated movement of the forelegs and hindlegs is prompted by a mechanical or microbial stimulus and is modulated by DAergic neurotransmission (214). Interestingly, grooming was not significantly impaired in hDAT R445C flies (116.7 ± 12.9 s) relative to hDAT WT flies (88.8 ± 7.7 s; $p > 0.05$) (**Fig. 12C**). These data suggest that coordinated movements are selectively impaired in hDAT R445C flies.

Expressing hDAT R445C in *Drosophila* results in DA deficiency

DA dysregulation, specifically the loss of DA signaling, drastically alters the timing, velocity and fluidity with which movement is executed (215, 216). We thus sought to determine whether impairments in movement and coordination were driven by altered DA dynamics. We first measured DA content in whole brains of hDAT WT and hDAT R445C flies. DA content was significantly reduced by 16.9 ± 3.2 % in hDAT R445C (21.4 ± 0.8 ng/mg) relative to hDAT WT brains (25.8 ± 1.0 ng/mg) ($p = 0.02$) (**Fig. 13A, left**). We also measured serotonin (5-HT) content,

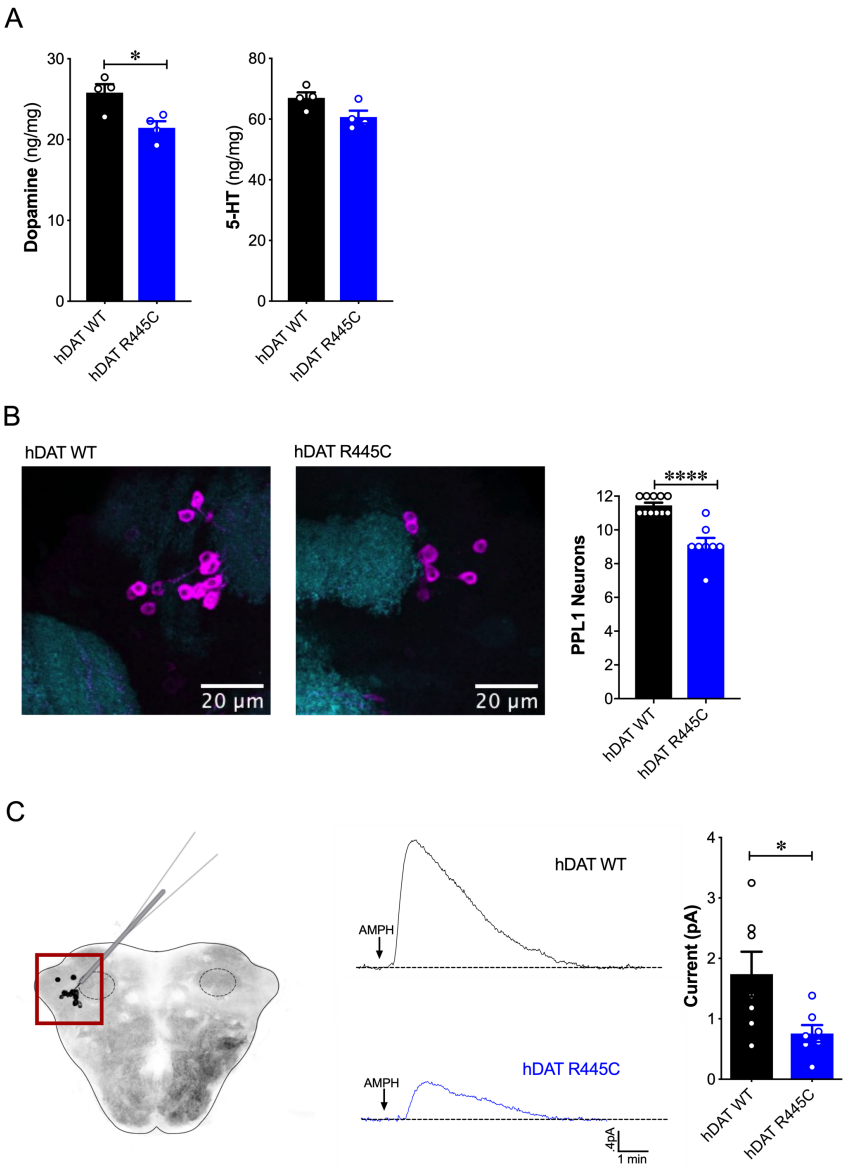

Figure 13: Reduced brain DA content and AMPH-induced DA efflux in hDAT R445C flies

(**A**) Tissue concentration of DA (*left*) and 5-HT (*right*) measured by HPLC (n = 4). DA content was significantly decreased in hDAT R445C relative to hDAT WT brains ($p = 0.01$). 5-HT content in hDAT R445C was comparable to hDAT WT ($p > 0.05$). (**B**) Confocal *z*-stack (5 µm) of hDAT WT (*left*) and hDAT R445C (*center*) brains co-labeled with anti-TH (*magenta*) and anti-n82 (*cyan*) zoomed-in on PPL1 neurons. Quantitation of TH-labeled PPL1 neurons showed a significant reduction of these neurons in hDAT R445C brains relative to hDAT WT ($p < 0.0001$; n = 8 – 11) (**C**) Diagram illustrates an amperometric recording from TH-positive, PPL1 DA region (*red box)* in fly brain. Currents recorded in response to AMPH application (20 µM) in hDAT WT (*black trace*) and hDAT R445C (*blue trace*) brains. Quantitation of peak currents showed a significant decrease in DA efflux in hDAT R445C relative to hDAT WT brains ($p = 0.03$; n = 7).

Data are presented as mean ± SEM. Student's t-test (A)-(B).

as serotonergic dysfunction has also been associated with the development of motor and non-motor symptoms in PD (217) . We found that 5-HT content was comparable in hDAT WT (67.0 ± 1.8 ng/mg) and hDAT R445C (60.7 ± 2.1 ng/mg; $p > 0.05$) brains (**Fig. 13A, right**).

Various *Drosophila* PD models have shown selective neurodegeneration of protocerebral posterior lateral 1 (PPL1) DA neurons (113, 195, 218, 219). These clusters of neurons innervating the mushroom and fan-shaped bodies are implicated in regulating motivated behaviors as well as reward learning and reinforcement, and are thus parallel in their functions to DA projections from the substantia nigra to the striatum in mammals (186, 189, 190, 220, 221). We assessed the number of TH-positive PPL1 neurons in hDAT WT and hDAT R445C brains (**Fig. 13B, left**). We found TH-positive PPL1 neurons to be significantly reduced in hDAT R445C flies (9.1 ± 0.4) relative to hDAT WT controls (11.5 ± 0.2); $p < 0.0001$) (**Fig. 13B, right**). These data demonstrated that specific motor deficits are associated with DA deficiency in hDAT R445C flies.

To determine the effects of DA deficiency on DAT function, we specifically examined if hDAT R445C could support the reverse transport (efflux) of DA evoked by amphetamine (AMPH) from isolated *Drosophila* brains. The psychostimulant AMPH causes DA efflux mediated by the DAT. To measure DA efflux by amperometry, we guided a carbon fiber electrode into mCherry-tagged PPL1 neurons (222) (**Fig. 13C, left, red box**). The representative traces displayed are an integrated current measurement of DA efflux from this population of neurons (**Fig. 13C, middle**). Given the DA deficiency in hDAT R445C brains, it was not surprising that AMPH-induced DA efflux was significantly reduced in hDAT R445C (0.76 ± 0.14 pA) compared with hDAT WT (1.74 ± 0.37 pA; $p = 0.03$) brains. Nonetheless, these brains were capable of DA efflux, suggesting that hDAT R445C can support the reverse transport of DA.

Substitutions at R375 in LeuT (which corresponds to R445 in hDAT) disrupt IC network interactions

LeuT, the bacterial homolog of hDAT, has provided key insights that improved our understanding of Na^+- and substrate-coupled transport in the neurotransmitter sodium symporter (NSS) family (61, 223). Integrating data from LeuT crystal structures, electron paramagnetic resonance (EPR) and single-molecule fluorescence energy transfer (sm-FRET) and MD simulations has defined the alternating access mechanism used by the NSS family to transport substrate. Common to these models is the transition from outward-facing open (OF) to inward-facing open (IF) states through the opening and closing of the IC and EC gates, respectively (81, 224). Here, we use a combination of Rosetta modeling, X-ray crystallography and EPR spectroscopy to determine the consequence of hDAT mutations at R445 on conformational changes in LeuT.

Cysteine residues exist at an equal ratio of protonated (neutral) to deprotonated (acidic) states at physiological pH. Therefore, we determined the effects of a Cys to Ala and Cys to Asp substitution at R445 by introducing the corresponding mutations in LeuT: LeuT R375A and LeuT R375D, respectively, as well as LeuT R375C. Previous studies of LeuT conformational dynamics have shown that the network of interactions between the N-terminus (residues R5, E6, W8), TM6/IL3 (Y265, Y268), TM8 (D369) and TM9 (R375) are key to occluding the IC vestibule in the outward-facing occluded (OO) state (225). In particular, salt bridges R5-D369 and E6-R375 stabilize the N-terminus in the OO state as illustrated in **Fig. 14A** (l**eft**). The residues participating in this network are highly conserved across the NSS family, and are thus, likely critical to transport. First, we constructed molecular models of LeuT R375A and R375D (**Fig. 14A**) using Rosetta to determine potential changes in these interactions and in the thermodynamic stability (ΔΔG) of these variants relative to WT. We found that both, neutralizing and acidic substitutions at R375, likely promote the dissociation of the salt bridge between R375 and E6 (closest atom-atom distances: WT= 2.1 Å; R375A = 5.4 Å; R375D = 4.2 Å), weaken the interaction of R375 and I184 (WT = 2.5 Å; R375A = 6.0 Å; R375D = 4.7 Å), and decrease the thermodynamic stability of LeuT (Rosetta scores: R375A = + 4.4 REU; R375D = + 5.6 REU relative to WT) (**Fig. 14A**, **Fig. 15A-**

B)**.** Other interactions were largely preserved, including R5-D369 and E6-I187 interactions (**Fig. 14A**). One key difference between these models was that K189 moved towards E6 in LeuT R375A, but away from E6 in LeuT R375D (**Fig. 15A**). Together, these models predicted that both, acidic and neutral mutations at the LeuT counterpart (R375) of hDAT R445 disrupt the interactions near the IC vestibule, partially affecting the IC gate, but maintaining other IC network interactions. Moreover, based on the model for LeuT R375C, where K189 also moves away from E6, we conclude that a Cys mutation at R375 more closely resembles an acidic substitution (compare **Fig. 14A** and **Fig. 15A, C**).

To define further the structural consequences of R375 substitutions, we determined the X-ray crystal structures of LeuT WT, LeuT R375A and LeuT R375D solved in an L-Ala and Na^+ bound OO conformation to a resolution of 2.1 Å for WT and R375A and 2.6 Å for R375D (**Fig. 14B,** detailed in **Fig. 16**). Expression of R375C was low and sufficient protein for crystallography. Structures were aligned with a previous structure of LeuT WT in an OO conformation (PDB ID: 3F3E) with an RMSD of 0.134, 0.146 and 0.236 for LeuT WT, R375A and R375D, respectively. In all structures (*superimposed*), L-Ala, Na1 and Na2 (*purple spheres*) could be modeled into their respective binding sites (**Fig. 14B, left**). These crystal structures showed that substitution of Arg to Ala in LeuT R375A (**Fig. 14B, middle bottom**) and of Arg to Asp in LeuT R375D (**Fig. 14B, right top**) precluded salt bridge formation between R375 and E6 and between R375 and the backbone of I184 as was also observed with Rosetta modeling in **Fig. 14A**. In addition, K189 moved towards E6 by 3.4 Å, reducing the distance between residues K189 and E6 from 8.0 Å in LeuT WT to 4.6 Å in LeuT R375A (**Fig. 14B, middle bottom**), as observed in the Rosetta modeling. The distance between residues R5 and D369 and between residues E6 and I187 were conserved in all three structures (**Fig. 14B, right bottom**), as observed also in **Fig. 14A**. As evident from these data as well as the REU versus RMSD plots (**Fig. 15D**), our Rosetta models parallel our crystal structures. In addition, these data indicate that the IC gate is disrupted by substitutions at position R375.

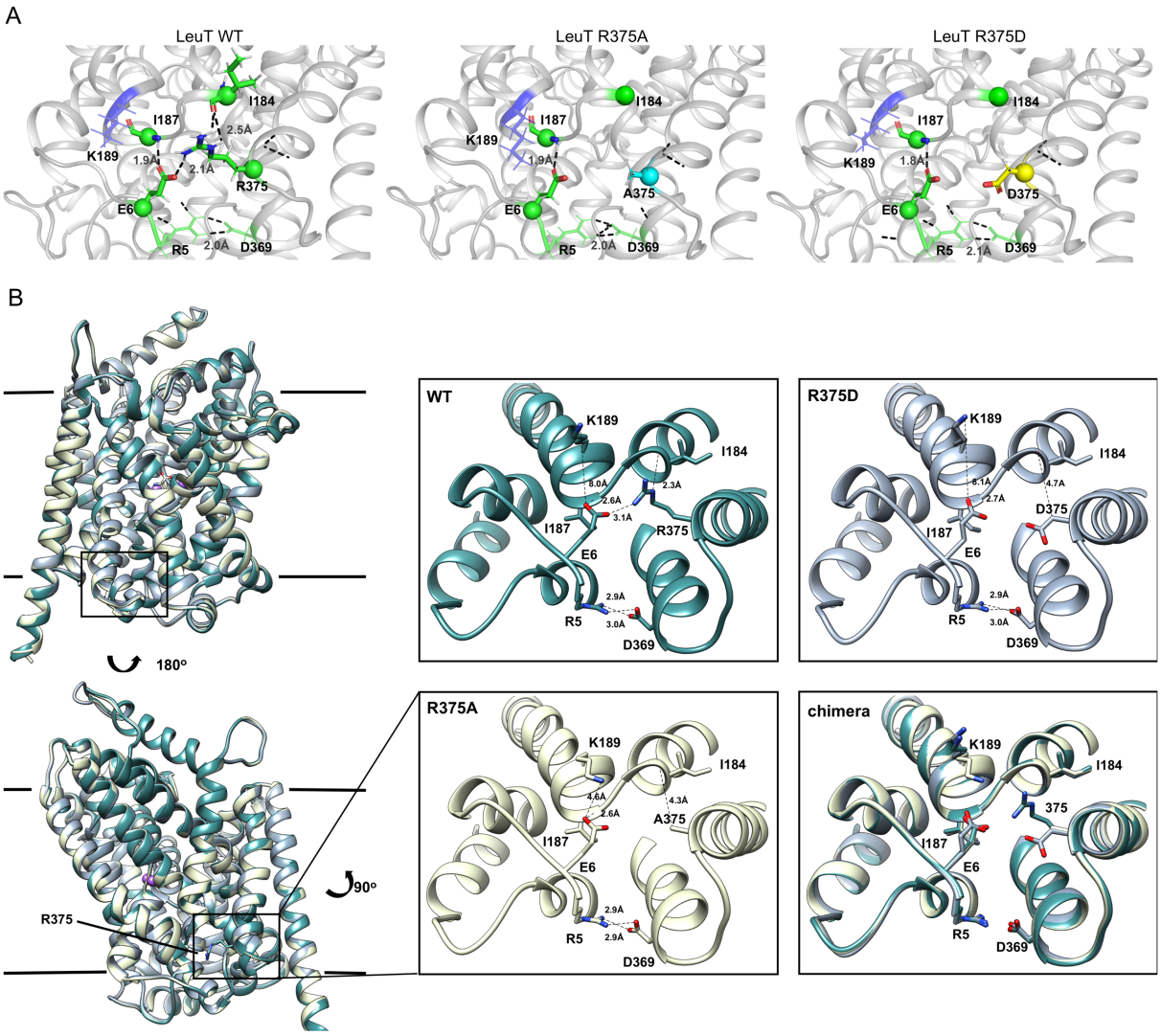

Figure 14: Representative Rosetta models and crystallographic structures of LeuT revealed weakening of E6-R375 salt bridge promoted by substitutions at R375

(**A**) Models derived using Rosetta of LeuT WT (*left*), LeuT R375A (*middle*) and LeuT R375D (*right*) where protein backbones are represented as cartoons and residues E6, I184, I187, R5, and D369 are represented as green spheres and sticks. K189 is colored in blue. R375 is colored in green (*left*). A375 is colored in cyan (*middle*). D375 is colored in yellow (*right)*. All corresponding polar contacts between side chain or backbone atoms in each model are represented as dashed lines in black. R375 substitution to either Ala or Asp disrupted E6-R375 salt bridge. (**B**) Crystal structures of LeuT WT (*green*), LeuT R375A (*cream*) and LeuT R375D (grey) are superimposed. Box indicates area of zoomed-in view of TM1-TM8 IC region for LeuT WT (*top left*), LeuT R375D (*top right*), LeuT R375A (*bottom left*) and overlay of three structures (*bottom right*). Distances between residues are shown in dashed lines.

A

Rosetta Distance Calculations of LeuT R375A/C/D

	WT	R375A	R375C	R375D
	distance (Å)			
R375-I184	2.5	6	3.3	4.7
R375-E6	2.1	5.4	5.7	4.2
E6-I187	1.9	1.9	1.9	1.8
R5-D369	2	2	2.1	2.1
K189-E6	8.2	7.0	9.9	8.5

B

Rosetta ΔΔG Calculations of LeuT R375A/C/D

WT	R375A		R375C		R375D	
score	score	ΔΔG	score	ΔΔG	score	ΔΔG
-2300.2 ± 4.4	-2295.8 ± 4.3	4.4	-2295.4 ± 4.5	4.8	-2294.6 ± 5.2	5.6

C

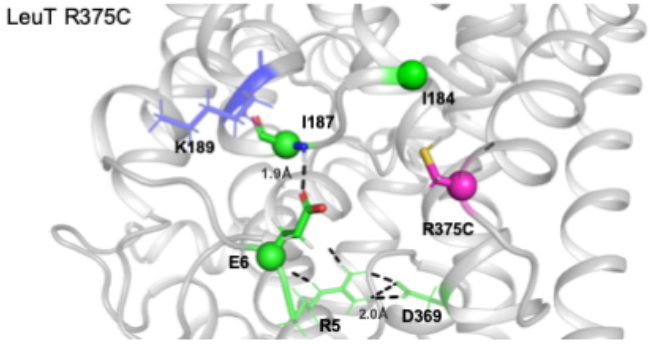

D

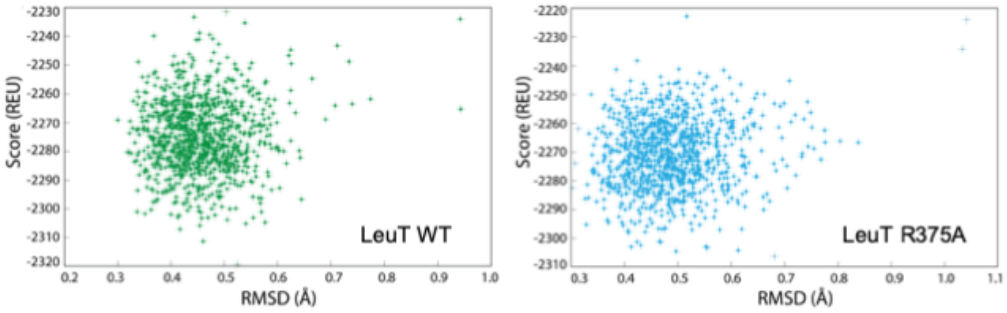

Figure 15: Detailed data for LeuT models

(**A**) Distances between IC residues in angstroms (Å) in LeuT WT, R375A, R375C, and R375D. (**B**) Rosetta scores represent the average scores of the top 5% of models. ΔΔG values are in Rosetta Energy Units (REUs). (**C**) Rosetta modeling of LeuT R375C, where protein backbones are represented in *grey*, amino acid side chains in *green*, K189 in *blue* and R375C in *magenta*. All corresponding polar contacts between side chain or backbone atoms in each model are represented as dashed lines in *black*. (**D**) REU versus RMSD diagrams were obtained from 1000 Rosetta Flex ΔΔG trajectories for LeuT WT (*left*) and LeuT R375A (*right*)**.** The RMSD between the protein backbone and heavy side chain atoms within a 10 Å distance of R375 and R375A was calculated to show the correlation between the energy-optimized models and the experimental model.

	LeuT WT	LeuT R375A	LeuT R375D
PDB ID:	6W99	6W95	6W9F
Data collection			
Space group	C121	C121	C121
Cell dimensions			
a, *b*, *c* (Å)	88.48, 86.87, 81.14	87.58, 86.62, 80.99	86.63, 87.06, 80.59
α, β, γ (°)	90.00, 96.09, 90.00	90.00, 95.64, 90.00	90.00, 95.32, 90.00
Resolution (Å)	43.99 – 2.1	47.31 – 2.1	47.22 – 2.6
R_{sym} or R_{merge}	0.06 (0.54)	0.06 (0.86)	0.26 (2.18)
I / σI	14.9 (3.0)	11.8 (1.6)	7.6(2)
CC1/2	0.99 (0.89)	0.99 (0.71)	0.99 (0.69)
Completeness (%)	99.4 (93.5)	100 (100)	99 (98.9)
Redundancy	7.1 (6.9)	5.1 (5.2)	7.1 (7.4)
Refinement			
Resolution (Å)	43.43 – 2.1	43.58– 2.1	43.53– 2.6
No. reflections	33363	35182	18237
R_{work} / R_{free}	16.87/19.54	18.01/20.44	19.28/23.93
No. atoms	4272	4199	4093
Protein	4043	4040	3984
Ligand/ion			
Ligand	94	102	77
Na	2	2	2
water	135	57	32
B-factors	48.10	53.23	55.19
Protein	46.92	52.18	54.83
Ligand/ion	84.83	94.62	74.36
R.m.s. deviations			
Bond lengths (Å)	0.006	0.003	0.005
Bond angles (°)	0.82	0.54	0.60
Ramachandran (%)			
Favored	97.62	98.22	95.77
Allowed	2.38	1.78	4.02
Disallowed	0.00	0.00	0.20

Figure 16: LeuT crystallographic data in detail

Table delineates crystallographic data for LeuT WT, R375A and R375D regarding data collection, model building, and refinement statistics.

R375 substitutions stabilizes an inward-facing conformation in LeuT

To monitor the ligand-dependent conformational dynamics of the EC and IC gates, we used EPR, and more specifically, double electron-electron resonance (DEER) to obtain distance distributions between spin label pairs 309/480 and 7/86, respectively (**Fig. 17A**). These spin label pairs are used to monitor the isomerization of LeuT between the OF, OO, IF and inward-facing occluded (IO) states, as previously described (165, 226). It is important to note that the spin labels were attached at introduced cysteines hence precluding the investigation of LeuT R375C. Instead, we monitored the effects of Ala and Asp substitutions at R375 on LeuT conformational dynamics. We found that these substitutions had relatively minor effects on the EC gate (left). In the absence of ion and substrate (Apo), LeuT WT dwells between OO and OF conformation, with OO being predominant (**Fig. 17B, left**; *black trace*). Na^+ enhances the OF conformation poised to bind substrate (**Fig. 17B, left**; *red trace*) (224). Leu binding to Na^+-bound LeuT restores the conformational preference to the OO form (**Fig. 17B, left;** *blue trace*). We found that the introduction of an Ala (**Fig. 17C, left**) or Asp (**Fig. 17D, left**) at position R375 did not drastically affect the conformational dynamics of the EC gate. We do note that in R375A, longer-distance components are sampled in the Apo (*black trace)*, Na^+ *(red trace)* and Na^+/Leu state (*blue trace)*. In R375D, the probability distribution of the dominant short-distance component (OO) decreased, such that more open intermediary distances were sampled in the Apo state (*black trace*) (**Fig. 17D, left**).

More substantial changes were observed on the IC gate. Consistent with previous findings, the spin label pair monitoring of the IC gate in LeuT WT showed a bimodal distribution between IF and IO conformations in the Apo state (*black trace*), where Na^+ alone (*red trace)* or Na^+/Leu (*blue trace*) biased LeuT towards the IO conformer (**Fig. 17B, right**). The substitution of R375 to Ala in LeuT increased the probability of an IF conformation in the Apo (*black trace)* and Na^+/Leu states (*blue trace*) (**Fig. 17C, right**). Similarly, the substitution of R375 to Asp suppressed the short-distance component (IO conformation) in favor of an IF conformation in the Apo (*black trace*)

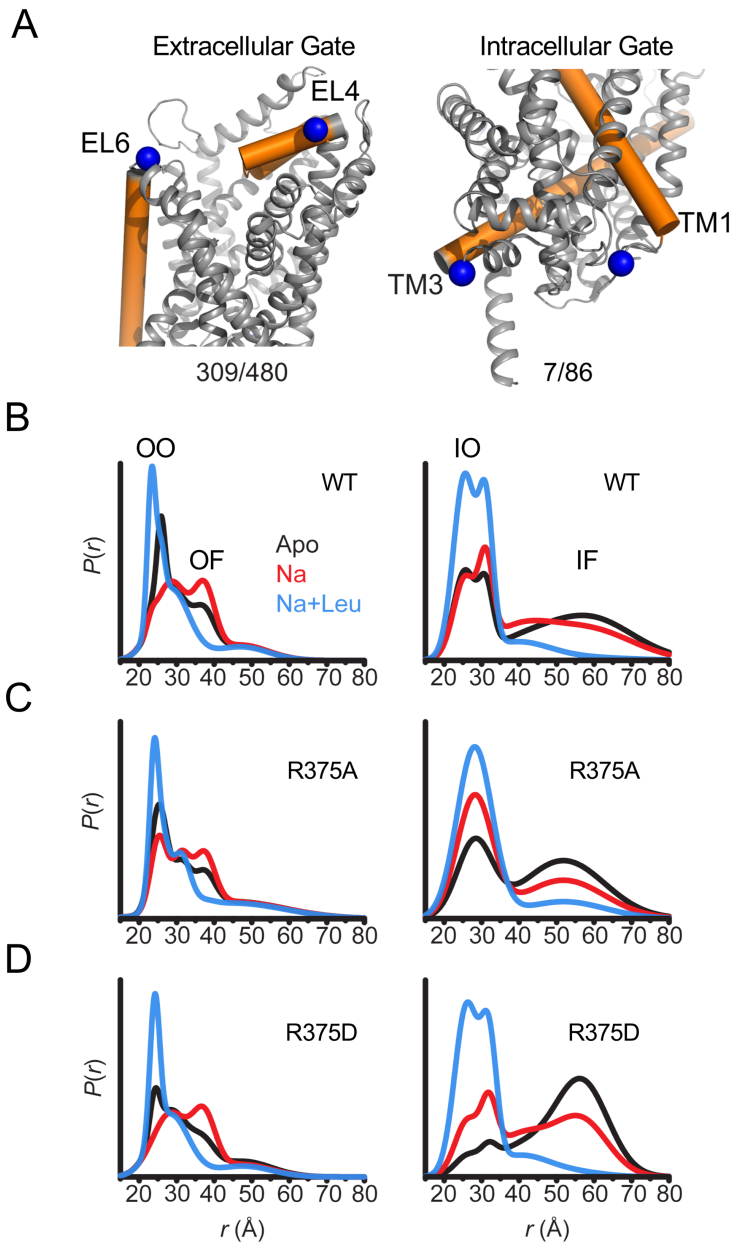

Figure 17: Asp substitution at R375 in LeuT favors an inward facing conformation

(**A**) Probability distance distributions (P(r)) of the spin labels pairs 308/409 and 7/86 reporting the conformational dynamics of the EC (*left*) and IC (*right*) gate of LeuT, respectively. Distance distributions for each pair were obtained in the Apo (*black*), Na^+-bound (Na^+; *red*), and Na^+- and Leu-bound (Na^+/ Leu; *blue*) conformations for (**B**) LeuT WT, (**C**) LeuT R375A and (**D**) LeuT R375D.

(**Fig. 17D, right**). The addition of Na^+ was able to partially rescue the probability distribution of the IO conformer, where Na^+/Leu resets the IC gate to the IO conformation.

Together, DEER distance distributions demonstrate that the substitution of R375 for Asp leads to increased probability of open conformations on both sides of the transporter.

R445 substitutions lead to the intermittent formation of a channel-like intermediate in hDAT

To determine the structural and dynamic changes effected by a Cys substitution at R445, we generated homology models of hDAT based on dDAT structures (PDB ID: 4M48). As illustrated in **Fig. 18A**, salt-bridges at the IC surface (e.g. R445-E428 and R60-D436), a cation-π interaction between R60 and Y335, and a hydrogen bond between E428 and Y335, form an IC network of interactions that stabilizes the occlusion of the IC vestibule in hDAT WT (**Fig. 18A**) (62, 82, 227). *In silico* studies have suggested that disruption or reconfiguration of these IC salt bridges facilitate the opening of the IC vestibule for release of substrate or ions (66, 227). This feature has also been noted in the human serotonin transporter (hSERT) in recent cryo-EM structures (228, 229).

The structural model generated for hDAT R445C showed that a Cys substitution at R445 disrupts this IC interaction network to support an intermittent channel-like intermediate (**Fig. 18B**), characterized by continuous water occupancy in the transporter lumen. Superposition of hDAT WT and R445C structures (**Fig. 18C**) showed an overall opening of the transmembrane (TM) helices on the IC face (TM9, *blue arrow*) in hDAT R445C. MD simulations also showed that Na^+ migrates from either the IC or EC side (**Fig. 18D**), where Na^+ binding occurs prior to the complete dissociation of R60-D436 salt bridge at 150 ns (**Fig. 18E**). We also note that the IC-exposed TM1a-TM6b pair retained their 'closed' state (**Fig. 18F**), in contrast to the usual opening of TM1a in the IF state observed in WT. Finally, Na^+ entry was facilitated by the opening of TM9 and consequent increase in the interhelical distance between TM9 and TM6b (**Fig. 18F**).

Similar channel-like intermediates were observed in hDAT R445A (data not shown) and R445D (**Fig. 19**). In R445D, three Na^+ ions (*cyan, violent and orange spheres*) stabilize along the

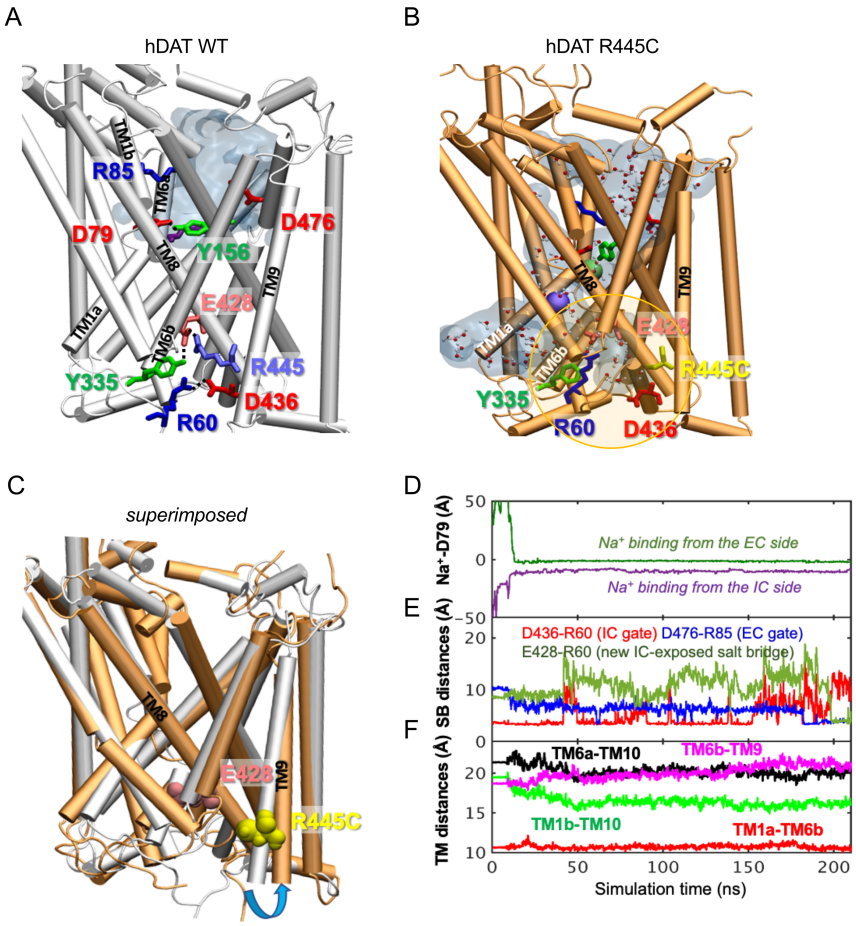

Figure 18: R445C mutation favors the opening of the IC vestibule, leading to intermittent formation of a channel-like intermediate

(**A**) MD stimulations of hDAT WT in the OF state (*white*) illustrates a network of interactions at the IC surface stabilizing the closure of IC vestibule and solvated EC vestibule (*gray shaded region).* (**B**) Substitution of R445 with Cys (*orange*) breaks salt-bridge R445-E428, which weakens IC network interactions and promotes the intermittent formation of a channel-like intermediate. This conformation favors the entry of both water and ions from the IC space. Hydrated regions inside the transporter are indicated in *gray* shaded areas with explicit water molecules displayed in spheres and lines (CPK format). Green and purple spheres are Na^+ migrating from the EC and IC side, respectively. (**C**) Structural alignment of hDAT R445C (*orange*) with hDAT WT (*white*). In hDAT R445C the association between TM8 and TM9 (near the IC exposed region) is weakened. TM9 undergoes an outward titling (*blue curved arrow*) to allow for the 'opening' of IC vestibule along TM8, facilitated by the absence of C445-E428 salt bridge (R445-E428 in hDAT WT holds TM8-TM9 in place). (**D-F**) Results from MD simulations of hDAT R445C. Time evolution of distances between (**D**) Na^+ and D79; (**E**) salt-bridge forming residues at EC and IC regions. On the EC side, D476-R85 distance decreases (EC gate closure). On the IC side, D436-R60 distance increases (IC gate opening). D345-K66 remains closed. After dissociating from D436 (t = 150 ns), R60 interacts with E428 (t = 200 ns). (**F**) Interhelical distances for EC-exposed TM1b-TM10 and TM6a-TM10 shows that the EC region remains exposed to solvent with reduced opening, and IC-exposed TM1a-TM6b is closed, but there is a new opening indicated by the increase in TM6b-TM9 distance. Conformation shown in B is the last snapshot taken from the simulation trajectory in **D-F**.

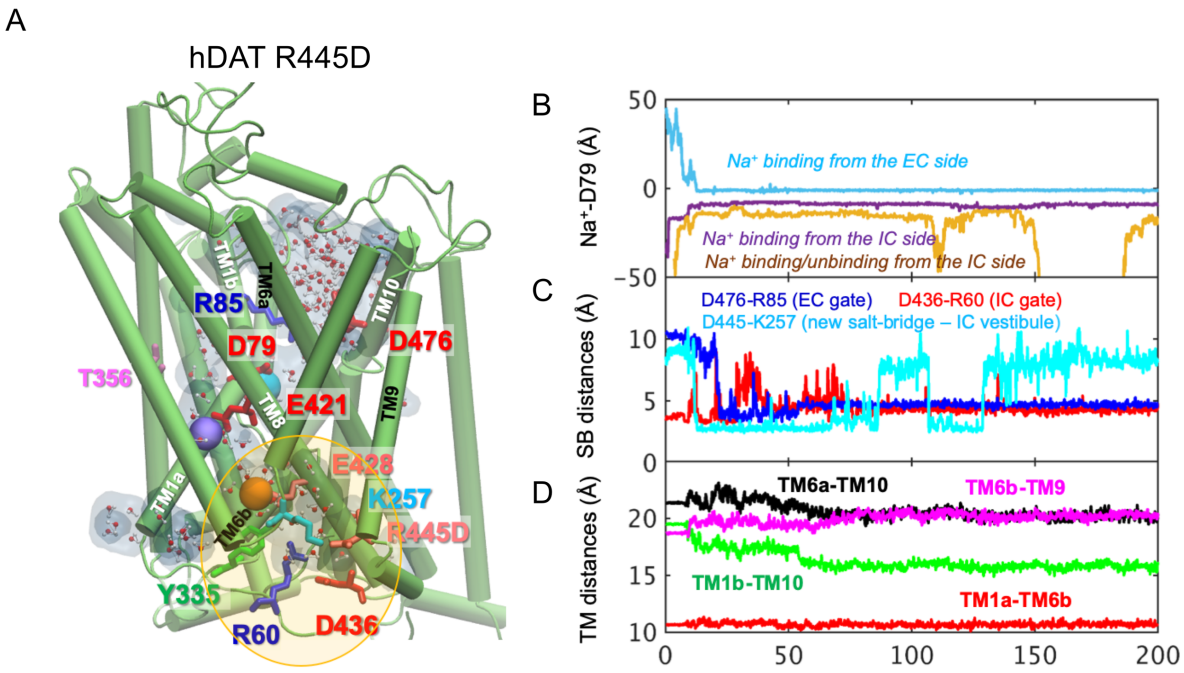

Figure 19: hDAT R445D confers a channel-like conformation with three Na^+ ions

(**A**) Model of hDAT R445D showed the formation of a channel-like intermediate promoted by the opening of the IC vestibule. In hDAT R445D, three Na^+ ions bound along the transport lumen (two diffusing from the IC region, and one from the EC region). The region enclosed in the yellow ellipse is more exposed to the cytosol relative to WT, allowing Na^+ and water entry. Hydrated regions inside the transporter are indicated in *gray* shaded areas with explicit water molecules displayed in spheres and lines (CPK format). The conformation shown is a snapshot (100 ns) taken from the simulation trajectory illustrated in B-D**.** (**B**) Time evolution of distances between Na^+ and D79. (**C**) Time evolution of distances between D476-R85 salt-bridge on the EC side show that this interaction shortens over time (EC gate closure). The distances between D436-R60 on the IC side increase intermittently (IC gate opening). Interestingly, a new salt bridge between D445 and K257 is formed intermittently. (**D**) Time evolution of interhelical distances between EC-exposed TM1b-TM10 and TM6a-TM10 shows that the EC region remains exposed to solvent with reduced opening, whereas IC-exposed TM1a-TM6b shows that the IC region is predominantly closed with a slight opening indicated by the increase in TM6b-TM9 distance.

solvated transporter lumen (one entering from the IC region, one entering from the EC region, and one intermittently diffusing from the IC region) (**Fig. 19B**), as compared with two Na^+ binding sites in R445C (**Fig. 18B**). It is likely that the dissociation of R445-E428 salt bridge promoted by R445D substitution allows E428 to bind an additional Na^+. In contrast, in hDAT R445C, E428 finds an alternative partner, R60. These findings point to a unique feature of the R445 residue, as substitutions associated with DTDS stabilize a channel-like conformation only observed occasionally in previous simulations (230).

We also observe that the dissolution of R445-E428 salt-bridge weakened the IC interaction network as a whole. In particular, R445C weakened the association of TM8-TM9 near the IC entrance, whereby TM9 underwent an outward tilting exposing an egress pathway along TM8 for Na^+ (or a different cation) (**Fig. 18C**). The outward titling of TM9 has been observed previously in the DA-loaded transition from OF to IO states (227). Furthermore, R455C substitution increases the likelihood that the R60-D436 salt bridge breaks, while promoting the formation of a new salt bridge R60-E428 (**Fig. 18E**) at the expense of breaking R60-D436 salt-bridge in both runs.

In addition to structural disruptions, hDAT R445C displays reduced expression that is partially rescued by chloroquine

We determined the expression of hDAT R445C to be significantly compromised in a heterologous expression system, as was also observed in LeuT R375C. Substitution of R445 to Cys reduced the surface expression to 0.06 ± 0.01 of hDAT WT (1.0 ± 0.04; $p < 0.0001$) and the total mature DAT expression to 0.20 ± 0.04 of hDAT WT (marked by #; 1.0 ± 0.05; $p < 0.0001$) (**Fig. 20A**). Given this reduction in transporter expression and structural impairments, we surmised that DA uptake would also be impaired. Indeed, [^{3}H]DA uptake kinetics showed that R445C cells have significantly reduced transport capacity with respect to WT cells as reflected in the Vmax ($F_{(1, 15)} = 160.3$; $p < 0.0001$) (**Fig. 20B**). Instead, the apparent affinity for DA (K_m)

significantly increased in hDAT R445C relative to WT ($p < 0.0001$) cells, suggesting that conformational changes promoting leading to translocation of DA across the membrane are also affected (**Fig. 20B**). To determine if R445C affected the reverse transport function of the DAT (DA efflux), we delivered DA (2mM DA, 10 min) to the inside of the cell through a patch-pipette in whole-cell configuration and used amperometry to measure DA efflux in response to AMPH (10 μM) (64). Thus, we were able to load the cells with equal concentrations of DA despite differences in DA uptake. Consistent with our *ex vivo* brain amperometric recordings, we found that R445C supported DA efflux although significantly reduced compared with WT (hDAT WT = 0.74 ± 0.09 pA; hDAT R445C = 0.28 ± 0.06; $p = 0.001$) (**Fig. 20C**).

We found that both neutralizing and anionic substitutions at R445 (hDAT R445A and hDAT R445D) significantly comprised surface DAT ($p < 0.0001$) and mature DAT expression ($p < 0.0001$) relative to hDAT WT (**Fig. 21A, Fig. 22A**). Given this significant reduction in hDAT surface expression, it was unsurprising that [^{3}H] DA uptake was also significantly reduced in hDAT R445A ($F_{(5,92)} = 22.7$, $p < 0.0001$; **Fig. 21B)** and hDAT R445D cells ($F_{(5,94)} = 42.1$; **Fig. 22B**). Consistent with R445C, we find that the K_m of hDAT R445A and hDAT R445D was also significantly increased. Combining patch-clamp with amperometry (as above), we found that AMPH-induced DA efflux was significantly compromised in hDAT R445D ($p = 0.002$; **Fig. 22C**) compared with hDAT WT cells. Interestingly, we observed that AMPH caused a reduction in the amperometric current in hDAT R445A compared with hDAT WT cells ($p = 0.001$; **Fig. 21C**), consistent with AMPH blocking constitutive DA efflux as previously noted in other DAT mutations (51, 86, 156). Together, these data confirm that substitutions at R445 significantly compromised DAT DAT cell surface expression and function

The severity and onset of clinical phenotypes are associated with residual DAT function in DTDS (162, 163). DAT function is related to its expression in hDAT R445C and other DTDS-associated variants; thus, we assessed the possibility of improving motor coordination deficits in

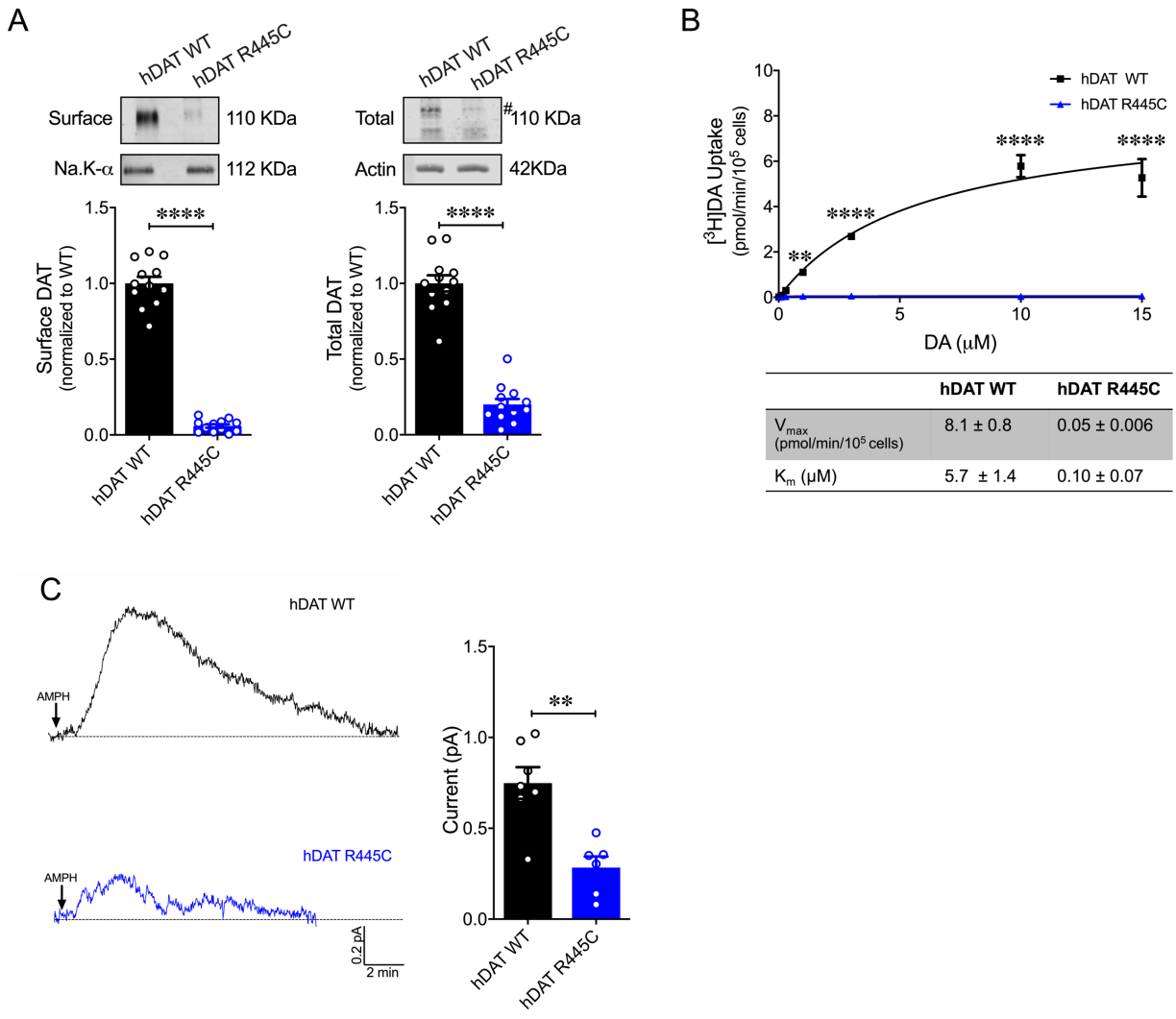

	hDAT WT	hDAT R445C
V_{max} (pmol/min/10^5 cells)	8.1 ± 0.8	0.05 ± 0.006
K_m (μM)	5.7 ± 1.4	0.10 ± 0.07

Figure 20: Cys substitution at R445 compromises hDAT expression and function

(**A**) Representative immunoblots of surface hDAT (top *left*), total hDAT (top *right*) and corresponding Na-K ATPase (*bottom left)* and actin (*bottom right)* loading controls. hDAT expression was normalized to hDAT WT. hDAT R445C displayed significantly reduced surface ($p < 0.0001$; n = 4, in triplicate) and total mature (#) expression relative to hDAT WT ($p < 0.0001$; n = 4, in triplicate). (**B**) ^{3}[H]DA saturation curves of DA uptake measured in hDAT WT (*black*) or hDAT R445C (*blue*) cells (n = 3, in triplicate). Curves were fit to Michaelis-Menten kinetics to derive K_m and V_{max}. DA uptake for hDAT R445C was significantly reduced compared with hDAT WT at every DA concentration measured ($F_{(6,64)} = 52.4$, $p < 0.0001$), as were the kinetic constants, K_m and V_{max} ($p < 0.0001$). (**C**) Representative traces of amperometric currents (DA efflux) recorded in response to AMPH application (*left;* 10 μM, indicated by arrow) from hDAT WT (*black*) and hDAT R445C (*blue*) cells loaded with DA (2 mM, 10 min) with whole-cell pipette. Quantitation of peak current amplitudes illustrated a significant reduction in DA efflux recorded from hDAT R445C compare to hDAT WT (*right*; $p = 0.008$; n = 6-7).

Data are presented as mean ± SEM. Student's t-test (A) and (C); Two-way ANOVA with Bonferroni's multiple comparison test: (B).

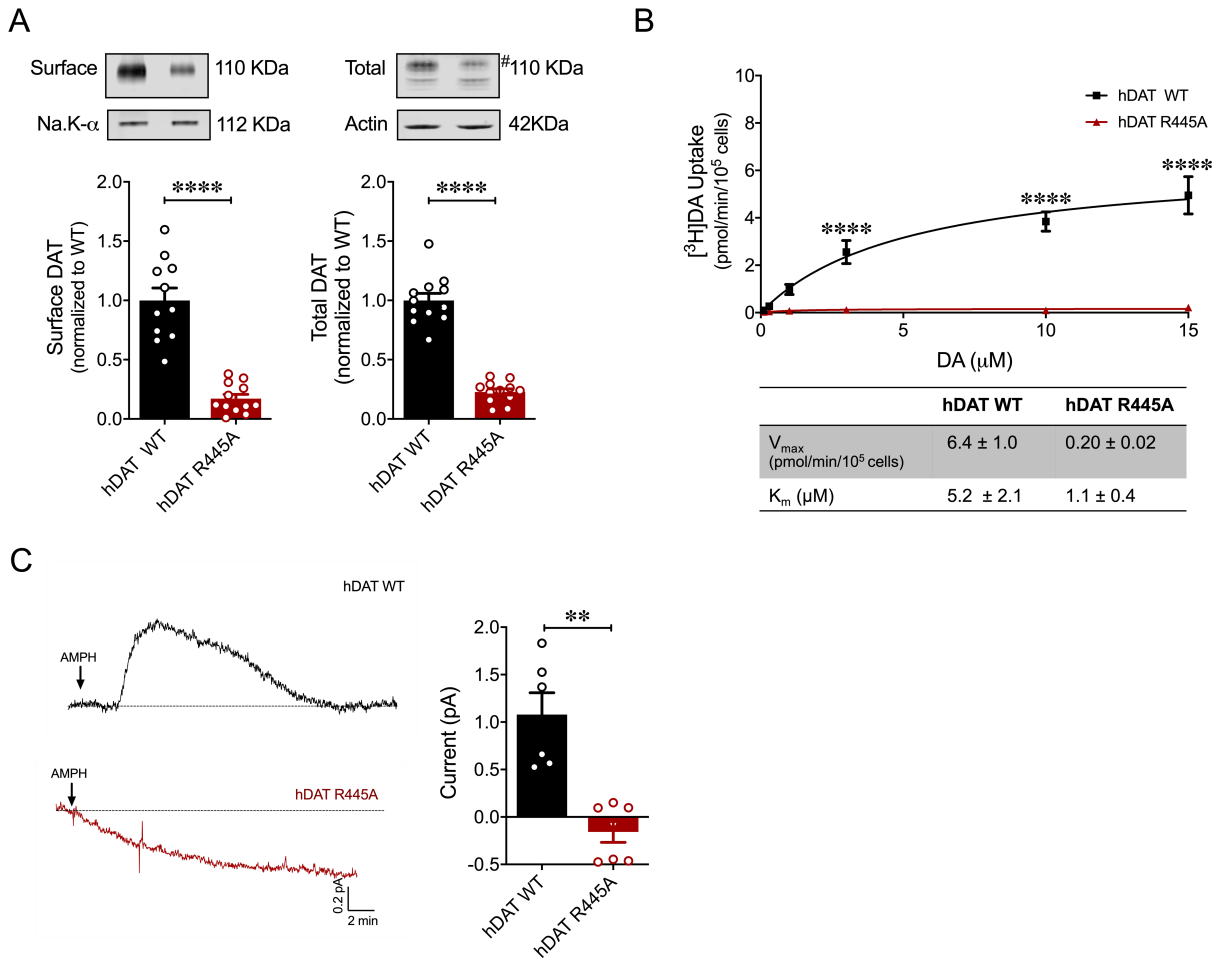

	hDAT WT	hDAT R445A
V_{max} (pmol/min/10^5 cells)	6.4 ± 1.0	0.20 ± 0.02
K_m (μM)	5.2 ± 2.1	1.1 ± 0.4

Figure 21: hDAT R445A cells display AMPH-sensitive DA leak despite reductions in hDAT surface expression and uptake

Representative immunoblots of surface hDAT (top *left*), total hDAT (top *right*) and corresponding Na-K ATPase (*bottom left)* and actin (*bottom right)* loading controls (n = 4, in triplicate). hDAT expression was normalized to hDAT WT. hDAT R445A displayed significantly impaired surface ($p < 0.0001$) and total (#) expression relative to hDAT WT ($p < 0.0001$).
(**B**) [^{3}H]DA saturation curves of DA uptake measured in hDAT WT (*black*) and hDAT R445A (*red*) cells (n = 3, in triplicate). Curves were fit to Michaelis-Menten kinetics to derive K_m and V_{max}. DA uptake for hDAT R445A was significantly reduced compared with hDAT WT ($F_{(5,92)} = 22.7$, $p < 0.0001$) as were kinetic constants, K_m and V_{max} ($p < 0.0001$). (**C**) Representative amperometric traces (DA efflux) recorded in response to AMPH application (*left*; 10 μM, indicated by arrow) from hDAT WT (*black*) and hDAT R445A (*red*) loaded with DA (2 mM, 10 min) via a whole-cell patch electrode in current-clamp. Quantitation of peak amperometric current in hDAT R445A and hDAT WT cells (*right*; $p = 0.002$; n = 6).

Data are presented as mean ± SEM. Student's t-test (A); Two-way ANOVA with Bonferroni's multiple comparison test: (B). Mann-Whitney Test (C).

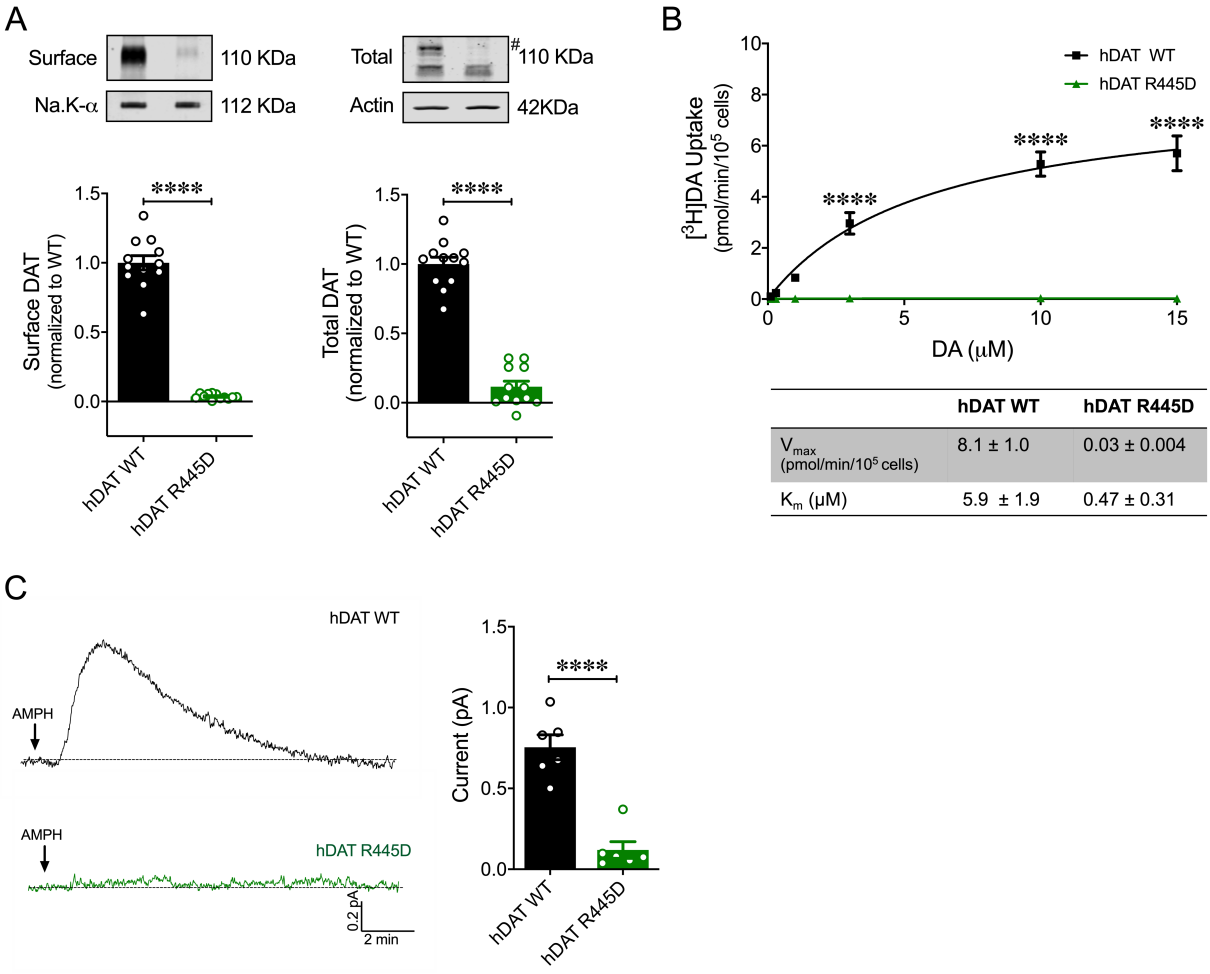

	hDAT WT	hDAT R445D
V_{max} (pmol/min/10^5 cells)	8.1 ± 1.0	0.03 ± 0.004
K_m (μM)	5.9 ± 1.9	0.47 ± 0.31

Figure 22: Asp substitution at R445 impairs hDAT expression and function

(**A**) Representative immunoblots of surface hDAT (top *left*), total hDAT (top *right*) and corresponding Na-K ATPase (*bottom left)* and actin (*bottom right)* loading controls (n = 4, in triplicate). hDAT R445D displayed significantly reduced surface ($p < 0.0001$) and total (#) expression relative hDAT WT ($p < 0.0001$). (**B**) [^{3}H]DA uptake was measured in hDAT WT (*black*), hDAT R445D (*green*) cells (n = 3, in triplicate). Curves were fit to Michaelis-Menten kinetics to derive K_m and V_{max}. DA uptake for hDAT R445D was significantly reduced compared with hDAT WT ($F_{(5,94)} = 42.1$, $p < 0.0001$), as were the kinetic constants, K_m and V_{max} ($p < 0.0001$). (**C**) Left: Representative amperometric traces (DA efflux) recorded in response to AMPH application (10 μM, indicated by arrow) from hDAT WT (*black*) and hDAT R445D (*green*) cells loaded DA (*left*; 2 mM, 10min) with a whole-cell patch electrode. Peak current amplitudes illustrated a significant reduction in DA efflux recorded from hDAT R445D relative hDAT WT (*right*; $p = 0.002$; n = 6).

Data are presented as mean ± SEM. Student's t-test (A); Two-way ANOVA with Bonferroni's multiple comparison test: (B). Mann-Whitney Test (C).

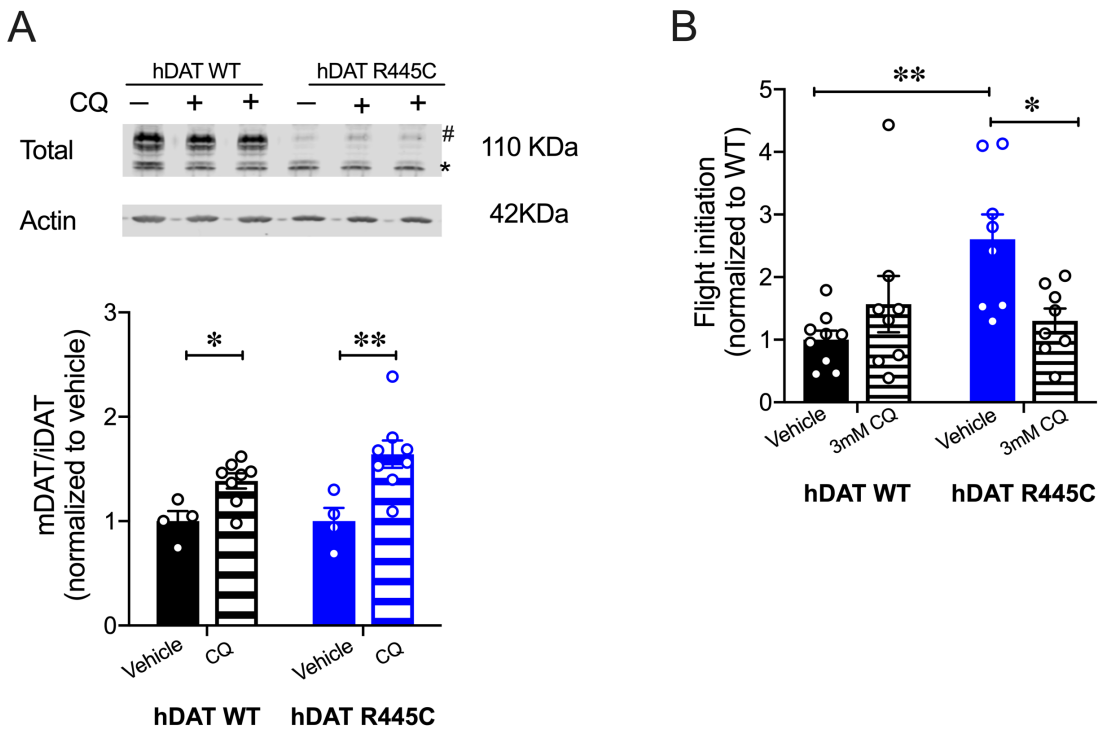

Figure 23: CQ enhances R445C expression ratios and flight coordination

(**A**) Representative immunoblots of total hDAT and actin (*bottom)* loading controls, where glycosylated (#) and non-glycosylated (*) DAT is highlighted. Ratio of mature (glycosylated) to immature (non-glycosylated) DAT (mDAT/iDAT) expression normalized to vehicle conditions was quantified for hDAT WT and hDAT R445C (n = 4, in duplicate). Incubating hDAT R445C cells with CQ (1 mM, 4 h) significantly increased the ratio of mDAT/iDAT ($F_{(1,20)}$ = 18.0), p = 0.003). CQ also significantly increased mDAT/iDAT expression in hDAT WT cells (p = 0.04). (**B**) *Drosophila* expressing hDAT R445C or hDAT WT were fed CQ (3 mM, 72 h) or vehicle supplemented diet. Quantitation showed a significant reduction in the time to initiate flight in hDAT R445C flies ($F_{(1,10)}$ = 7.6 , p = 0.01) in response to CQ (1.54 ± 0.60) compared with vehicle (4.07 ± 0.48). Time for flight initiation was comparable in hDAT WT flies exposed to CQ and vehicle supplemented diet (p > 0.05).

Data are presented as mean ± SEM. Two-way ANOVA with Bonferroni's multiple comparison test: (A-B).

hDAT R445C flies by enhancing or correcting DAT expression. DAT expression and degradation are regulated by endocytic, recycling, and lysosomal pathways (100, 231-233). Previous studies have shown that chloroquine (CQ), a lysosomotropic weak base that inhibits lysosomal activity, limits DAT lysosomal degradation (231, 234).

In DTDS-associated variants the ratio of mature (glycosylated) to immature (unglycosylated) DAT is shifted where the immature form predominates (**Fig. 20A**) (162), suggesting DAT degradation. Here, we determined whether CQ by inhibiting DAT lysosomal degradation could improve this ratio. We found that CQ treatment (1mM, 4h) significantly increased the ratio of mature (marked by #) to immature DAT (marked by *) in hDAT WT ($p = 0.04$) and R445C ($p = 0.003$) cells relative to vehicle ($F_{(1,20)} = 18.0$) (**Fig. 23A**). As specified above in DTDS, the severity of clinical phenotypes is correlated with DAT function/expression. Thus, we sought to determine whether the improvement in DAT expression promote by CQ translated to improvements in motor phenotypes. We supplemented fly food with CQ (3mM, 72 h) for both hDAT WT and hDAT R445C flies and measured the timing of flight initiation. We found that CQ treatment significantly improved the time for flight initiation in hDAT R445C flies relative to vehicle ($F_{(1,10)} = 7.6$, $p = 0.01$) (**Fig. 23B**). CQ did not have significant effects on motor coordination in hDAT WT flies ($p > 0.05$). These data suggest that CQ, by enhancing DAT expression, can improve flight initiation in hDAT R445C flies and that when a threshold DAT expression is reached, further increases in DAT expression do not further enhance flight initiation time.

Discussion

PD is a multi-system, heterogenous neurodegenerative disorder characterized clinically by core motor symptoms, including resting tremors, bradykinesia, rigidity and postural instability. As the disease progresses, additional motor symptoms develop, such as impairments in gait and balance, eye movement control, speech and swallowing, and bladder control. Mood disorders (e.g. anxiety and depression), sleep disorders (e.g. insomnia, disrupted circadian rhythm),

hyposmia (impaired olfaction), gastrointestinal symptoms and other non-motor features usually precede full PD diagnosis (235). Additionally, cognitive impairment, including dementia, typically manifests after diagnosis and progresses steadily over time (236). Some motor and behavioral symptoms can be alleviated by DA replacement therapies, such as levodopa (L-DOPA, a DA precursor), DA metabolism inhibitors and DA receptor agonists (237). However, as the disease progresses, there is often a “loss of drug” effect, with symptoms largely refractory to therapeutic interventions (237). In some patients, DA replacement can promote new behavioral phenotypes, most commonly: impulse control disorder (ICD) and DA dysregulation syndrome (DDS). In ICD, patients impulsively or compulsively engage in reward-seeking behaviors, including gambling, eating, or sexual activities (238). In DDS, patients display addictive behaviors with dependence or withdrawal-type symptoms towards their DA medications (239). Essential to developing new pharmacotherapies is understanding the underlying disease pathology.

Although the cause of PD is not completely understood, the combination of aging, neuronal susceptibility, genetic risks and environmental factors are thought to underlie its etiology. Studies on highly-penetrant mutations identified in familial parkinsonism, as well as candidate gene and genome-wide association findings in idiopathic PD have contributed to our understanding of the molecular mechanisms underlying disease pathology (46). DTDS is a distinct type of infantile parkinsonism-dystonia associated with DAT dysfunction that shares various clinical phenotypes with PD, including motor deficits and altered DA homeostasis (162, 163, 174). Investigations on DTDS-linked DAT variants are essential to understating the impact of DAT dysfunction on DA neurocircuits and signaling pathways. Further, these studies may shed light on the molecular mechanisms that underlie the clinical phenotypes shared by DTDS and PD (240).

In this study, we define how a specific DAT variant identified in DTDS (R445C) confers DAT dysfunction by altering the structure and gating dynamics of an IC interaction network as well as DAT expression. In the NSS superfamily, which includes DAT and LeuT, thermodynamic

coupling of substrate and Na^+ -co-transport occurs via an alternating access mechanism that comprises the opening and closing of the IC and EC gates (61, 223). R445 corresponds to R375 in LeuT, which forms R375-E6 salt-bridge as part of the IC gate (225). Our crystallographic data, supported by modeling and ΔΔG calculations in LeuT, revealed that substitutions at R375 in LeuT disrupt key IC interactions, including R375-E6 salt-bridge, promoting an IF conformation.

These findings are consistent with previous *in silico* studies which suggest that the transition to an IF conformation is defined by the dissolution of IC salt-bridges D369-R5 and R375-E6 in LeuT (225). Furthermore, from our EPR studies, we surmise that R375 substitutions disrupt the IC network and bias LeuT to an IF conformation, subsequently altering transport, which requires LeuT to isomerize toward an OF conformation. We have previously shown that other mutations associated with neuropsychiatric disorders (i.e. ΔV269) that disrupt this IC network also bias LeuT to an IF conformer, impairing transporter function (165). It is important to note that R375A does not alter LeuT IC gate to the extent of R375D, suggesting that some variants at this site are more tolerated, likely due to nearby residues conferring resiliency to this IC interaction network. Indeed, it has been previously noted that the microenvironment surrounding the IC gate is enriched with putative interaction partners that reinforce this IC network (82).

Using homology models and MD simulations, we were able to determine the structural and dynamic changes effected by a Cys substitution at R445 in hDAT. In hDAT, R445 forms a salt bridge with E428, an association that is highly conserved among the eukaryotic NSS members and is proposed to be part of the IC gate (209). Although this association is distinct from the R375-E6 salt-bridge in LeuT, they are thought to serve similar functions as part of the IC network. We found that R445C promotes the dissociation of salt-bridge R445-E428 (209). MD simulations suggested that the dissolution of R445-E428 salt-bridge weakened IC network interactions as a whole, giving rise to a channel-like intermediate filled with water molecules. This channel-like intermediate was also observed in hDAT R445D, with an additional Na^+ binding the transporter from the IC environment. Previous studies have shown that DAT undergoes

uncoupled DAT-mediated ionic fluxes (88) as well as reverse transport of DA (efflux) via channel-like pathways (85). We have previously uncovered that the hDAT coding variant A559V identified in patients with ADHD supports a channel-like mode in the DAT which is associated with persistent DAT-mediated reverse transport of DA (DA leak) uncovered by AMPH blockade (50, 156). This DA leak was also identified in hDAT T356M, a *de novo* missense mutation in ASD (51). We conclude that the channel-like intermediate observed in our simulations of R445 substitutions may be associated with a channel-like mode supporting ion fluxes. Interestingly, we found that a neutral substitution at R445 (hDAT R445A) results in constitutive, anomalous DA leak blocked by AMPH. These data highlight the possibility that anomalous DA efflux may increase risk for various psychiatric disorders (51, 156, 164). It is important to note that constitutive DA efflux is not observed in cells expressing hDAT R445C nor hDAT R445D. This underscores the complexity of the IC network and the possibility that distinct amino acid substitutions at R445 differentially affect the IC dynamics, promoting different hDAT functions.

Our *in vitro* analysis, combined with our *in silico* data, revealed that impaired DAT R445C transport capacity stems both from a reduction in transporter expression as well as impaired hDAT function that reflects compromised DA uptake, but partially supported DA efflux. Our findings are consistent with previous studies highlighting impaired transporter expression and uptake in hDAT R445C cells (162, 196, 203). In addition, these data support the idea that the IC gate differentially regulates inward versus outward transport of DA (165), as R445C supports DA efflux (albeit reduced). In addition, we find that specific substitutions at this IC interaction network are distinctly tolerated in LeuT versus hDAT, as has been previously noted with other substitutions at this site (241). In hDAT, neither neutral (R445A) nor acidic (R445D) substitutions support normal hDAT function. These findings contrast EPR measurements, which suggest that neutral (R375A) but not acidic (R375D) substitutions are tolerated in LeuT. These findings highlight key differences in the IC and perhaps redundancy existing in LeuT within this network that is absent in the hDAT.

Despite neuroanatomical differences between mammalian and fly brains, increasing evidence on the evolutionary relationships between molecules, neural networks and organization within mammalian and invertebrate brains, as well as studies on animal models of disease, suggest many similarities (177, 178, 194, 197, 242-244). We used *Drosophila* as an animal model to explore the physiological and phenotypic consequences of a Cys substitution at Arg445 of the DAT. Our studies found that hDAT R445C promotes altered motor and coordinated behaviors in *Drosophila*. Specifically, hDAT R445C *Drosophila* displayed impaired locomotion that was driven by compromised movement vigor (fast movement). This behavioral phenotype is parallel to bradykinesia observed in patients with DTDS and PD, more broadly (162, 163, 174, 199) as well as in various mammalian and *Drosophila* models of PD (177, 197, 245).

In patients with PD, loss of DA neurons elicits impaired movement and motor symptoms as well as compromised fine and gross motor coordination. In flies, flight initiation requires exquisite sensory-motor integration, where a fly first raises its wings to a ready position and subsequently, simultaneously extends its mesothoracic legs and depresses its wings to coordinate a jump with the initial downstroke (246). Here, using a high-speed camera, we studied flight initiation in a *Drosophila* model of DTDS to understand the effects of hDAT R445C on sensory-motor integration. We found spontaneous flight initiation to be significantly delayed in *Drosophila* expressing hDAT R445C. Similarly, recent studies have observed wing coordination defects in flies with reduced neurotransmitter release from DAergic neurons (184). These data suggest that there may be a reduction in DA tone in hDAT R445C flies that contributes to flight deficits. In addition, we found a disparate repetitive motor behavior requiring fine-motor coordination, grooming to be unaffected in hDAT R445C *Drosophila.* These findings point to the phenotypic heterogeneity commonly observed in DTDS and PD (46, 162, 163, 174, 202, 235) and suggest that specific coordinated movements are selectively impaired or alternatively, present in a progressive nature in this model of DTDS. It is important to note that this study focused on the

motor symptoms exhibited in DTDS and PD; however, whether and if R445C promotes non-motor deficits, including cognitive impairment and hyposmia, has not been explored.

Our studies in fly brains also demonstrate that the hDAT R445C mutation drives reduced transporter function (i.e. DA efflux), impaired DA synthesis and reduction in TH-labeled DA neurons. Our findings of diminished transporter function align with our previous *in vitro* findings showing reduced hDAT R445C expression (162). In PD, core motor deficits are ascribed to the loss of DA neurons in the substantia nigra and their projections to the striatum (46). To date, neurodegeneration in DTDS has not been studied in depth; however, given that affected individuals develop parkinsonism-dystonia, including resting and acting tremor, difficulty initiating movements, bradykinesia and rigidity, it is likely that DA circuits are affected. To this end, we observed a reduction in TH-labeled DA neurons in hDAT R445C flies, consistent with various *Drosophila* models of PD that show selective neurodegeneration of protocerebral posterior lateral 1 (PPL1) DA neurons (113, 195, 218, 219). Although these findings suggest neurodegeneration in PPL1 neurons, given the reduction in measured DA levels, it is also possible that there is an overall reduction in TH, which limits the labeling of this neuronal population. However, our behavioral data points to a decrease in DA function, as observed in PD.

Together, these findings support a mechanism where reduced DAT-mediated DA reuptake results in excessive EC dopamine and depleted presynaptic stores. Synaptic hyperdopaminergia leads to overstimulation of presynaptic D_2 autoreceptors which suppress DA release and down-regulate tyrosine hydroxylase (TH), the rate limiting enzyme in DA synthesis; thereby, decreasing DA synthesis (13). This mechanism aligns with previous findings in DAT knockout animals and those with compromised DAT function (166, 247, 248).

DTDS presents in a phenotypic continuum, where clinical phenotypes appear to be associated with varied, residual DAT function. Thus, higher residual DAT activity is suggested to reduce symptom severity and/or postpone the age of disease onset (162, 163). Previous studies have used pharmacological chaperones that stabilize the DAT in an IF conformation to rescue

transporter expression (162, 196, 203). hDAT R445C function was not consistently rescued with these agents (196, 203), in alignment with our EPR and *in silico* data, which showed that hDAT R445C can isomerize and is even biased toward the IF conformer. In light of previous studies which showed that CQ inhibits DAT lysosomal degradation (231, 234), we tested CQ in its ability to improve motor deficits in hDAT R445C flies. We found that CQ was able to increase motor coordination in hDAT R445C flies, reducing the time to initiate flight significantly. This improvement in flight coordination was associated with improved DAT expression. It is important to note that in some studies, lysosomal dysfunction has been associated with PD (46, 199). In these instances, lysosomotropic agents should not considered, as they may exacerbate disease progression. In addition, although CQ and other quinines have been used for more than 400 years to treat malaria and more recently, re-purposed to treat cancer, these agents are not without substantial adverse side effects (249, 250). Thus, the use of lysosomotropic agents, such as CQ should be considered as therapeutic agents to ameliorate motor deficits only in specific cases of DTDS.

Our study reveals how a specific DAT variant identified in DTDS contributes to DAT dysfunction and subsequently, how DAT dysfunction supports altered DA neurotransmission as well as behaviors in *Drosophila*. Moreover, this experimental paradigm supports *Drosophila* as a model system in the study of DTDS, and PD, more broadly. Our investigation on hDAT R445C provides a blueprint to gain valuable insights on the mechanisms regulating transporter function, gating and expression, and how dysfunction of these processes translates to abnormal DA physiology and behaviors.

Materials and Methods

Cell culture: peGFP expression vector was engineered to contain synhDAT WT (hDAT WT), R445C (hDAT R445C), R445D (hDAT R445D) and R445A (hDAT R445A). All vectors were sequenced via Sanger sequencing to confirm no off-target mutations. Vector DNA was transiently

transfected into human embryonic kidney (HEK) cells using Fugene-6 (Roche Molecular Biochemicals) transfection reagent. eGFP (enhanced green fluorescence protein was used for cell selection and quantitation of transfection efficiency. Cells were maintained in a 5% CO_2 incubator at 37°C in Dulbecco's Modified Eagle Medium (DMEM) supplemented with 10% fetal bovine serum (FBS), 1 mM L-glutamine, 100 U/mL penicillin, and 100 µg/mL streptomycin. All assays were conducted ~48 h post transfection.

[^{3}H] DA uptake assays: Cells were washed in KRH buffer composed of (in mM): 130 NaCl, 25 HEPES, 4.8 KCl, 1.2 KH_2PO_4, 1.1 $MgSO_4$, and 2.2 $CaCl_2$, 10 d-glucose, 1.0 ascorbic acid, 0.1 pargyline, and 1.0 tropolone. KRH was titrated to pH 7.3 - 7.4. Cells were equilibrated in KRH at 37°C for 5 min. Saturation kinetics of DA were measured by incubating cells in a range of 0.1 to 15 µM DA, comprised of a mixture of [^{3}H]DA (PerkinElmer Life Sciences, Waltham, MA) and unlabeled DA. Uptake was terminated after 10 min by washing cells twice in ice-cold KRH buffer. Nonspecific binding was measured in the presence of 10 µM cocaine. K_m and V_{max} values were derived by fitting Michaelis-Menten kinetics to specific binding data.

Amperometry and patch-clamp electrophysiology: Cells were washed twice with 37°C Lub's external solution composed of (in mM): 130 NaCl, 1.5 $CaCl_2$, 0.5 $MgSO_4$, 1.3 KH_2PO_4, 10 HEPES and 34 d-glucose. Lub's external solution adjusted to pH 7.3 - 7.4 and 300-310 mOsms/L. To intracellularly load DA, a programmable puller (Model: P-2000; Sutter Instruments; Novato, CA) was used to fabricate quartz patch-pipettes with a resistance of 3-8 mΩ. Pipettes were filled with an internal solution containing (in mM): 110 KCl, 10 $NaCl_2$, 2 $MgCl_2$, 0.1 $CaCl_2$, 1.1 EGTA, 10 HEPES, 30 d-glucose and 2.0 DA. The pH of the internal solution was adjusted to pH 7.3 - 7.4 and 280-290 mOsms/L. Upon gaining whole-cell access, the internal solution was allowed to diffuse for 10 min. To record DA efflux, a carbon fiber electrode was juxtaposed to the plasma membrane of the cell and held at +600 mV. After establishing a baseline, 10 µM AMPH was added to the bath. Amperometric currents were low pass filtered at 1 Hz (Model: 3382; Krohn-Hite Corporation; Brockton, MA), sampled at 100 Hz (Model: Axopatch 200B; Molecular Devices; San

Jose, CA), and analyzed off-line using pCLAMP 9 software (Molecular Devices). DA efflux was quantified as the peak of the amperometric current.

Biotinylation assays: Cells were washed on ice with 4 °C phosphate-buffered saline (PBS) supplemented with 0.9 mM $CaCl_2$ and 0.49 mM $MgCl_2$. Cells were incubated in 1.0 mg/ml sulfosuccinimidyl-2-(biotinamido)ethyl-1,3-dithiopropionate-biotin (sulfo-NHS-SS-biotin; Pierce, Rockford, IL) in PBS for 20 min at 4 °C. Excess biotin was quenched by incubating cells in 100 mM glycine in PBS for 15 min. Cells were solubilized in radioimmunoprecipitation assay buffer (RIPA) composed of 150mM NaCl, 1.0% NP-40, 0.5% Sodium Deoxycholate, 0.1% SDS , 50 mM Tris, 1 mM EDTA, 1 mM EGTA, 1 mM PMSF and protease inhibitors (1:100), and titrated to pH 7.4. Cellular extracts were centrifuged for 30 min at 16,000 × g at 4 °C. The supernatant was added to immunopure immobilized streptavidin beads (Pierce Chemical Company; Rockford, IL) and incubated overnight at 4 °C. Beads were extensively washed and eluted in sample buffer. Samples were processed according to a standard western blot protocol (see below).

Western blotting protocol: Cells were incubated in vehicle or 1 mM chloroquine (CQ) for 4 h. Cells were solubilized in RIPA, sonicated and centrifuged. Supernatants were denatured in sample buffer, run on SDS-PAGE gel and transferred to polyvinylidene fluoride membrane (PVDF) (Millipore, Bedford, MA). Membranes were immunoblotted for DAT (1:1000) (MAB369; Millipore), β-actin (1:5000) (A5441; Sigma-Aldrich; St. Louis, MO), and Na-K ATPase (1:100; Developmental Studies Hybridoma Bank (DSHB), Iowa City, Iowa). The secondary antibodies used were Li-COR goat-anti-rat IRDye 800 (1:15,000), goat-anti-rabbit IRDye 680 (1:15,000) and goat-anti-mouse IRDye 680 (1:15,000). Band densities were quantified using Image Studio (Odyssey Infrared Imaging System (LI-COR, Lincoln, Nebraska).

***Drosophila* Rearing and Stocks:** All *Drosophila melanogaster* strains were grown and maintained on standard cornmeal-molasses media at 25 °C under a 12:12 h light-dark schedule. Fly stocks include w^{1118} ((Bloomington Indiana Stock Center (BI) 6326), TH-GAL4 (BI 8848), $DAT^{MB07315}$ (BI 25547), UAS-mCherry (Kyoto Stock Center 109594), and M[vas-int.Dm]ZH-2A;

(M[3xP3-RFP.attP']ZH-22A (BI 24481) and *DAT*^{fmn} (dDAT KO). *Drosophila* expressing homozygous dDAT null allele *DAT*^{fmn} (dDAT KO) (187), TH-Gal4 (251), and UAS-mCherry were outcrossed to a control line (*w*^{1118}) for 5 - 10 generations and selected by PCR or eye color. Transgenes (hDAT WT and hDAT RT445C) were cloned into pBID-UASC (252) and constructs were injected into embryos from M[vas-int.Dm]ZH-2A, M[3xP3-RFP.attP']ZH-22A (BI 24481) (Rainbow Transgenic Flies Inc; Camarillo, CA). Initial potential transformants were isolated and selected. Flies containing transgenes were outcrossed to dDAT KO flies (in w^{1118} background) for 5–10 generations. Age-paired adult male flies (10 days post eclosion) containing a single copy of hDAT WT or hDAT R445C in DA neurons in a *DAT*^{fmn} background were used for all subsequent experiments.

Drosophila **amperometry assays:** *Drosophila* brains were dissected with surgical forceps in ice-cold Schneider's *Drosophila* Medium supplemented with 1.5% BSA. Whole brains were placed in a mesh holder in Lub's external solution (see previous). A carbon fiber electrode was held at +600 mV and positioned in the TH-positive PPL1 DA neuronal region. After establishing a baseline, 20 μM AMPH was added to the bath. Amperometric currents were processed as previously (see above).

Drosophila **locomotion analysis:** Spontaneous locomotor activity in an open field was measured using custom 3D printed activity chambers (1.1 x 1.1 cm). Locomotion was detected using NIS Elements AR (Melville, NY). Animals were placed in the activity chambers, where activity was recorded for 5 min following 2-min acclimation period. Data from this test was also used to measure anxiety-like behaviors. Thigmotaxis, the tendency of an animal to remain close to the walls of an open field was measured by as the percent of time flies spent in center square (3.0 x 3.0 mm). Total distance traveled, center time and velocity distribution were quantified using MATLAB 2018b (MathWorks; Natick, MA). Velocity thresholds for movement initiation were set based on the average velocity during non-movement phases ($\chi + 0.5\sigma = 0.50 + 0.24$ mm/s),

whereas, fast movement was determined from the average velocity during the test period ($\chi + \sigma$ = 2.7 + 2.6 mm/s).

***Drosophila* grooming analysis:** Flies were observed for a period of 5 min (~19 fps). Forelimb and hindlimb grooming incidents were quantified per frame, where total grooming time was calculated as the total number of frames spent grooming.

***Drosophila* flight assay:** Coordinated flight was measured using custom 3D-printed chambers (3.9 x 1.0 x 1.0 cm) filled with 2600 μL of water. Flight initiation was recorded at 2,000 frames per second using a Phantom v1212 Camera (Ametek; Wayne, New Jersey), after a short acclimation period. Delay in flight initiation was quantified as the time from the outset of the first wing motion to the coordinated jump response.

HPLC: Biogenic amines were quantified by the Neurochemistry Core Facility at Vanderbilt University. Briefly, *Drosophila* brains were dissected quickly in ice-cold PBS and immediately frozen in liquid nitrogen. Brains were homogenized using a tissue dismembrator in 100 - 750μl of solvent containing (mM) 100 TCA, 10 Na, 0.1 EDTA and 10.5% methanol (pH 3.8). Homogenate was spun (10,000 g, 20 min) and supernatant was removed for biogenic monoamines analysis. Biogenic amine concentrations were determined utilizing an Antec Decade II (oxidation: 0.65) electrochemical detector operated at 33 °C. Supernatant was injected using a Water 2707 autosampler onto a Phenomenex Kintex C18 HPLC column (100 x 4.60 mm, 2.6μm). Biogenic amines were eluted with a mobile phase 89.5% of solvent (see previous) and 10.5 % methanol (pH 3.8). Solvent was delivered at 0.6 ml/min using a Waters 515 HPLC pump. Biogenic amines elute in the following order: Noradrenaline, Adrenaline, DOPAC, Dopamine, 5-HIAA, HVA, 5-HT, and 3-MT. HPLC control and data acquisition are managed by Empower software. Isoproterenol (5ng/mL) was included in the homogenization buffer for use as a standard to quantify the biogenic amines. Protein concentration was determined by BCA Protein Assay Kit (ThermoFisher Scientific).

Immunohistochemistry: Fly brains were dissected in PBS and fixed in 4% paraformaldehyde for 20 mins at RT. Brains were washed 3 times with PBST (0.3% Triton X100). Brains were blocked in 1% BSA and 5% normal goat serum. Brains were labeled for TH (1:200; Millipore, AB152) and nc82 (1:50; DSHB) overnight at 4 °C, washed and labeled with secondary antibodies Alexa 488–conjugated goat anti-rabbit (1:200; A11034, ThermoFisher Scientific) and Alexa 566–conjugated goat anti-mouse (1:200, A11031, ThermoFisher Scientific) overnight at 4 °C. Brains were washed and mounted with ProLong Diamond Anti-Fade mounting solution (ThermoFisher Scientific). Imaging was performed using a Nikon A1R confocal microscope. The resolution of the image stack was 1024 × 1024 with 0.5 µm step size. Neurons were counted manually using FIJI (Bethesda, MD)

Rosetta Homology Modeling and Stability Calculations: The Rosetta Flex ΔΔG protocol (253, 254) and the Rosetta Membrane all-atom energy function (255) were used to estimate free energy changes and sample conformational changes of the LeuT, hDAT and corresponding variants. The Flex ΔΔG protocol models mutation-induced conformational and energetic changes through a series of “backrub” moves of the protein backbone together with side-chain repacking around the mutation site. 15,000 backrub steps were used in this study to sample backbone and side chain degrees of freedom for neighboring residues within an 9 Å boundary of the mutation site. This is subsequently followed by side chain optimization using the Rosetta “packer.” Global minimization of the backbone and side chains torsion angles is performed with harmonic Cα atom-pair distance restraints. The restraints are used to prevent large structural deviations from the input model. Models are scored with the Rosetta Membrane all-atom energy function (255). This is carried out in parallel for the WT input model and the mutant of interest. For the LeuT calculations, the LeuT crystal structure (PDB ID: 2A65) (61) was used and 1000 independent trajectories were carried out for both LeuT WT(control) and each variant. For the hDAT calculations, homology models for hDAT WT were created in the Rosetta molecular modeling suite (revision 57712, Rosetta Commons) as previously described (165) using the *Drosophila melanogaster* DAT (PDB ID:

4XP9) (59) as a structural template. 500 independent trajectories were carried out for each hDAT R445 mutant and hDAT WT (control). This protocol was used for the top three scoring hDAT homology models resulting in 1500 trajectories total per mutant. The Rosetta energy change (ΔΔG) was calculated as score difference between the average of the top 5% of LeuT WT and corresponding variants as well as of hDAT WT and corresponding variants. Rosetta ΔΔG values are in Rosetta Energy Units (REU). Representative structural models for LeuT, hDAT, and all variants were selected for visualization in Pymol by removing outliers and taking the lowest-energy model within the lowest interquartile range of a box plot.

Protein expression and purification: Escherichia coli C41 (DE3) cells were transformed with the pET16b plasmid containing LeuT, LeuT-R375A, LeuT-R375C or LeuT-R375D tagged with a C-Terminal 8xHis-tag and thrombin cleavage site. Transformed cells were grown in Terrific broth media to an OD_{600} of 0.6. Cells were induced with 0.1mM isopropyl-β-D-1-thiogalactopyranoside (20 h, 20 °C), harvested by centrifugation and disrupted with a french press in 20 mM HEPES-Tris pH 7.5, 190 mM NaCl, 10 mM KCl, 1 mM EDTA, 5 mM L-Alanine, 100 μM AEBSF and 0.004 mg/mL DNAse I. Cells membranes were isolated by ultracentrifugation at 200,000 x g (45 min) and solubilised with 40 mM n-dodecyl-β-D-maltopyranoside (DDM, Anatrace). Solubilised membranes were incubated with Ni-NTA resin (Qiagen) (1 h, 4 °C). Protein bound to the Ni-NTA resin was washed with 50 mM imidiazole and then eluted with 300 mM imidiazole. The histidine tag was subsequently removed by digestion with thrombin (10 U/mg protein) and the protein further purified on a size exclusion column in 10 mM Tris-HCl pH 8.0, 45 mM NaCl, 5 mM KCl, 5 mM L-Alanine and 40 mM n-Octyl-β-D-glucopyranoside (OG, Anatrace). Purified protein was concentrated to 8 mg/mL using 30 kDa cut-off AMICON concentrators (Merck).

Crystallography and structure determination: Crystals were grown at 18 °C using the hanging-drop vapor diffusion method, by mixing protein (~8mg/ml) and well solution (1:1 vol:vol), 100 mM HEPES-NaOH pH 7-7.5, 200 mM NaCl, 17-22 % PEG550 MME. Protein crystals were

cryoprotected by soaking in the well solution supplemented with 25 – 35 % PEG550 MME. All diffraction data was collected on the EIGER 16M detector at the Australian Synchrotron (ACRF ANSTO) beamline MX2 at a wavelength of 0.954 Å (256). Datasets were indexed, integrated and scaled using XDS (257). Initial phases were obtained by molecular replacement with Phaser (258) using the structure of LeuT with bound L-Leu (PDB ID: 3F3E) as the search model. The protein model was built manually in Coot (259) and refined using REFMAC (260) with TLS and non-crystallographic symmetry (NCS) restraints (261). Phases were further improved by rounds of manual rebuilding followed by restrained refinement in REFMAC. Validation was carried out using MolProbity (262). Unit cell parameters, data collection and refinement statistics are presented in Table1. All structural figures were prepared using USCF Chimera (263).

Electron Paramagnetic Resonance (EPR) protocol: Cysteine residues were introduced using site directed mutagenesis into LeuT, LeuT R375A, and LeuT R375D constructs. Experiments were conducted as in Claxton *et al.* (224). The apo conformation refers to Na^+ and leucine-free transporter, while the +Na/Leu state was obtained in 200 mM NaCl and 4-fold molar excess of Leu relative to LeuT. Double Electron Electron Resonance (DEER) (264) was performed at 83K on a Bruker 580 pulsed EPR spectrometer operating at Q-band frequency using a standard 4-pulse sequence (265). DEER echo decays were analyzed to obtain distance distributions (266).

Statistical methods: Experiments were designed using statistical power calculations considering means and standard errors from preliminary data. Statistical analyses were performed using GraphPad Prism 8 (San Diego, CA). Shapiro-Wilk normality tests were performed to determine if data was normally distributed and displayed equal variances; parametric or non-parametric tests were chosen accordingly. All data was acquired unblinded, but analyzed blinded to genotype.

Molecular dynamics (MD) simulations: The structural model for *apo h*DAT (residues Q58-D600) in the outward-facing open (OF) unbound state, based on dDAT structure (PDB ID: 4M48), was taken from previous study (230). Four simulation systems using this initial structure were constructed: wild-type (WT), R445C, R445A, and R445D. In each case, the transporter is

embedded into 1-palmitoyl-2-oleoyl-sn-glycero-3-phosphocholine (POPC) membrane lipids using CHARMM-GUI Membrane Builder module (267). TIP3P waters and Na^+ and Cl^- ions corresponding to 0.15M NaCl solution were added to build a simulation box of ~110 ×110 ×118 Å (268). Each simulation system contained ~ 131,000 atoms, the transporter, ~ 300 lipid molecules, and 27,000 water molecules. All simulations were performed using NAMD (268) (version NAMD_2.12) following previous protocol (230). For each mutant, two independent runs of 200 ns are performed to verify the reproducibility of the results. VMD (269) with in-house scripts was used for visualization and trajectory analysis.

.

CHAPTER III

A NETWORK OF PHOSPHATIDYLINOSITIOL (4,5)-BISPHOSPHATE (PIP_2) BINDING SITES ON THE DOPAMINE TRANSPORTER REGULATE AMPHETAMINE BEHAVIOR IN *DROSOPHILA MELANOGASTER*

The work described in this chapter is part of, and adapted from the published manuscript: Belovich AN*, Aguilar JI*≠, et al. A Network of Phosphatidylinositol (4,5)-bisphosphate (PIP_2) Binding Sites on the Dopamine Transporter Regulates Amphetamine Behavior in *Drosophila* Melanogaster. *Molecular Psychiatry*. 2020. * denotes equal contribution ≠ denotes corresponding author

Abstract

Reward modulates the saliency of a specific drug exposure and is essential for the transition to addiction. Numerous human PET-fMRI studies establish a link between midbrain dopamine (DA) release, DA transporter (DAT) availability, and reward responses. However, how and whether DAT function and regulation directly participate in reward processes remains elusive. Here, we developed a novel experimental paradigm in *Drosophila melanogaster* to study the mechanisms underlying the psychomotor and rewarding properties of amphetamine (AMPH). AMPH principally mediates its pharmacological and behavioral effects by increasing DA availability through the reversal of DAT function (DA efflux). We have previously shown that the phospholipid, phosphatidylinositol (4, 5)-bisphosphate (PIP_2), directly interacts with the DAT N-terminus to support DA efflux in response to AMPH. In this study, we demonstrate that the interaction of PIP_2 with the DAT N-terminus is critical for AMPH-induced DAT phosphorylation, a process required for DA efflux. We showed that PIP_2 also interacts with intracellular loop 4 at R443. Further, we identified that R443 electrostatically regulates DA efflux as part of a

coordinated interaction with the phosphorylated N-terminus. In *Drosophila,* we determined that a neutralizing substitution at R443 inhibited the psychomotor actions of AMPH. We associated this inhibition with a decrease in AMPH-induced DA efflux in isolated fly brains. Notably, we showed that the electrostatic interactions of R443 specifically regulate the rewarding properties of AMPH without affecting AMPH avoidance. We present the first evidence linking PIP_2, DAT, DA efflux and phosphorylation processes with AMPH reward.

Introduction

Overshadowed by the current opioid epidemic, the resurgence of amphetamine (AMPH) and its derivatives (e.g. methamphetamine) in the United States has gone largely underreported (270). While AMPHs are used clinically, the potential for AMPH abuse and dependency is high (271). Underscoring this possibility is the observation that there are 37 million illicit AMPH users globally (272).

AMPH's rewarding and reinforcing effects, as well as its psychomotor stimulant properties, are associated with its ability to increase extracellular dopamine (DA) levels (19, 128). AMPH perturbs DA homeostasis maintained by the DA transporter (DAT) as a competitive inhibitor and substrate of the DAT. The DAT is a presynaptic membrane protein that, under normal physiological conditions, drives the high-affinity transport (reuptake) of synaptically released DA, thereby regulating the spatial and temporal dynamics of extracellular DA levels. AMPH alters psychomotor behaviors, at least in part, by promoting the reversal of the DAT function (a non-vesicular event), here defined as DA efflux. Indeed, selective inhibition of DA efflux impairs AMPH psychomotor behaviors (63, 122). Thus, in order to develop pharmacotherapies that mechanistically target and limit AMPH action (i.e. DA efflux), it is critical to understand how AMPH alters DAT function.

DA efflux is regulated by several molecular mechanisms and protein post-translational modifications. We and others have shown that phosphorylation of the DAT N-terminus is required

for AMPH-induced DA efflux (140, 141). This phosphorylation process is mediated by several kinases, protein-protein interactions, as well as protein-lipid interactions (68-70, 72, 96, 97, 153). Various other proteins and lipids regulate DA efflux through DAT association, including Syntaxin 1 (STX1) (52, 69, 153), G protein βγ subunits (Gβγ) (71, 72) and phosphatidylinositol (4,5)-bisphosphate (PIP_2) (63).

Phospholipid molecules are an integral component of cell function and metabolism (273, 274), comprising approximately 50% of the plasma membrane. Among these, PIP_2 is the principal substrate of receptor-stimulated phospholipases C (PLC) and the precursor to second messengers inositol trisphosphate (IP_3), diacylglycerol (DAG), and phosphatidylinositol (3,4,5)-trisphosphate (PIP_3). Moreover, PIP_2 itself acts as a second messenger and cofactor, regulating protein function (273, 275-278) and trafficking (279). Additionally, PIP_2, through its electrostatic interactions, has been shown to modulate the function of ion channels and transporters, including the serotonin transporter (SERT) (124, 273) and the DAT (63). In earlier studies, we have shown that PIP_2 directly interacts with the DAT through electrostatic interactions with basic, positively charged DAT N-terminal residues (Lys3, Lys5). Substitution of these residues with uncharged amino acids decreases DAT/PIP_2 interactions, and AMPH-induced DA efflux and behaviors (63). This was the first demonstration that PIP_2, through its interaction with a plasma membrane protein, regulates DA-associated behaviors, underscoring the importance of elucidating the mechanism through which PIP_2 regulates DAT function and DAT-associated behaviors.

Recently, *in silico* experiments pointed to the possibility that PIP_2 also associates with the DAT intracellular loop 4 (IL4; specifically at R443) to regulate conformational rearrangements of the DAT N-terminus (66). These simulations proposed that the interaction between the N-terminus and IL4, mediated by PIP_2, may coordinate the dynamics of the intracellular gate. However, the biochemical, physiological or behavioral relevance of these findings remained unclear. Using a combination of *in silico* and biochemical assays, we show that R443 physically interacts with PIP_2 as well as the N-terminus. We demonstrate *in silico*, *in vitro* and *ex vivo* that R443 electrostatic

interactions with PIP_2 and the N-terminus are required for specific DAT conformations that support DAT-mediated DA efflux in response to AMPH. In *Drosophila,* these interactions regulate fundamental behaviors, such as AMPH-induced hyperlocomotion and, notably, the rewarding properties of AMPH. Disrupting R443 electrostatic interactions does not affect the physiological function of the DAT, namely, uptake, nor basal locomotion. Thus, we have uncovered how a single residue in DAT IL4, R443 modulates AMPH actions, including reward.

Results

N-terminus/PIP_2 interactions are required for AMPH-induced DAT phosphorylation

We have previously shown that neutralizing substitutions of Lys3 and Lys5 disrupt N-terminus/PIP_2 interactions and DA efflux (63). Here, we sought to understand the molecular mechanism through which N-terminus/PIP_2 interactions regulate DA efflux. Specifically, does the interaction between the N-terminus DAT and PIP_2 support DAT phosphorylation which is pivotal for robust AMPH-induced DA efflux (141)? To address this question, we disrupted N-terminus/PIP_2 interactions using hDAT K/A and hDAT K/N cells, where Lys3 and Lys5 were substituted for Ala or Asn, respectively, and measured DAT phosphorylation in response to AMPH (10 μM, 30 min) relative to hDAT WT cells. We quantified DAT phosphorylation by metabolic labeling ($^{32}PO_4$) as illustrated in representative autoradiographs under vehicle and AMPH conditions (**Fig. 24A, top left**). The corresponding hDAT immunoblots for these autoradiographs are shown below (**Fig. 24A, bottom left**). Post AMPH treatment, hDAT WT cells displayed an increase in hDAT phosphorylation relative to vehicle-treated hDAT WT cells ($p = 0.002$). In contrast, neither hDAT K/A nor hDAT K/N cells displayed a significant increase in hDAT phosphorylation in response to AMPH ($p > 0.05$). Vehicle-treated (baseline) hDAT phosphorylation was comparable for hDAT WT, hDAT K/A and hDAT K/N ($p > 0.05$) (**Fig. 24A, right**). Since Lys3 and Lys5 on the N-terminus are required for PIP_2 binding, these data suggest

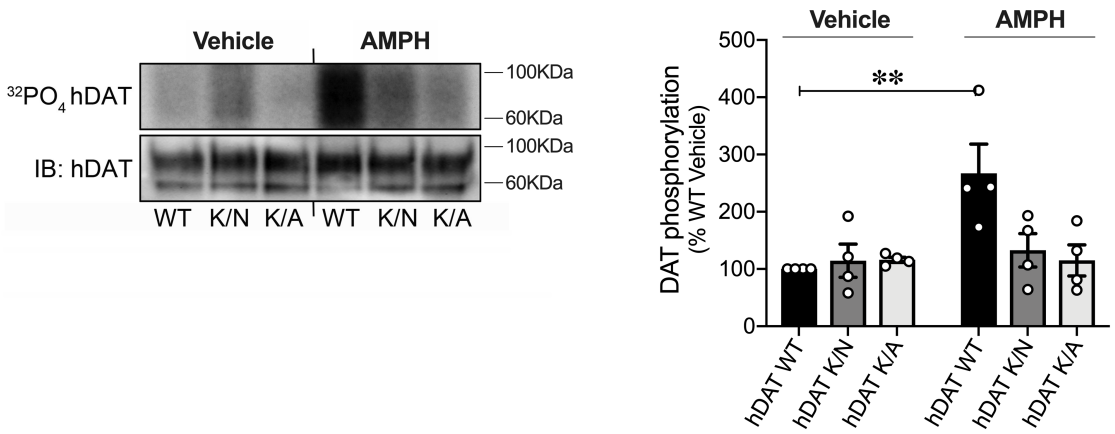

Figure 24: PIP_2/N-terminus interactions regulate DAT phosphorylation

hDAT WT, hDAT K/N or hDAT K/A cells were labeled with ^{32}P prior to vehicle or AMPH (10 μM, 30 min) incubation. Equal amounts of DAT determined by immunoblotting were immunoprecipitated and subjected to SDS-PAGE/autoradiography. Left: Representative autoradiographs showing hDAT phosphorylation after vehicle or AMPH exposure, along with respective immunoblots of total hDAT. Right: DAT phosphorylation is quantified as ^{32}P labeling normalized to basal hDAT ^{32}P labeling. hDAT WT phosphorylation increased post-AMPH treatment relative to vehicle ($n = 4$; $F_{(2, 18)} = 5.05$, $p = 0.002$). In hDAT K/N and hDAT K/A cells, displayed no changes in DAT phosphorylation in response to AMPH compared with vehicle ($p > .05$).

Data are presented as mean ± SEM. Two-way ANOVA with Bonferroni's multiple comparison test: (A).

that the interaction between the N-terminus and PIP_2 is required for AMPH to elicit DAT phosphorylation.

Given PIP_2's integral role in DAT phosphorylation, we next sought to understand whether DAT/PIP_2 interactions were required for the reverse transport of DA by phosphorylated DAT. We used amperometry to measure DA efflux in response to AMPH (10 μM) in hDAT WT cells and in cells where all N-terminal serines (2,4,7,12,13) were mutated to Asp (hDAT S/D) to mimic N-terminus phosphorylation. We depleted PIP_2, thereby disrupting DAT/PIP_2 interactions with phenylarsine oxide (PAO, 20 μM, 10 min), a PI-4 kinase inhibitor, which limits the synthesis of PIP_2 from phosphatidylinositol and effectively decreases PIP_2 levels. Consistent with our previous findings in hDAT WT cells (63), PIP_2 depletion by PAO pre-treatment significantly reduced AMPH-induced DA efflux compared with vehicle conditions (**Fig. 25A, top**) ($p = 0.04$). In contrast, in hDAT S/D cells PAO did not significantly reduce AMPH-induced DA efflux compared with vehicle (**Fig. 25A, bottom**) ($p > 0.05$). Thus, our data strongly suggest that once DAT N-terminus phosphorylation occurs, DAT/PIP_2 interactions do not regulate DA efflux (**Fig. 25A, right**).

To validate these findings further, we sequestered PIP_2 at the plasma membrane with a basic peptide (pal-HRQKHFEKRR), which consists of a palmitic acid, a fatty acid moiety that tethers the peptide to the plasma membrane and the putative PIP_2 binding domain of the Kv7.2 channel (280). This pal-HRQKHFEKRR acts as a competitive inhibitor, sequestering plasma membrane PIP_2, and subsequently reducing AMPH-induced DA efflux in hDAT WT cells (63). Here, we perfused hDAT S/D cells with DA and either the basic peptide pal-HRQKHFEKRR (3 μM, 10 min) or the control peptide pal-HAQKHFEAAA (3 μM, 10 min) using a whole cell electrode while recording DA efflux with an amperometric electrode (**Fig. 25B, left**). We found that pal-HRQKHFEKRR did not significantly change DA efflux relative to control peptide (**Fig. 25B, right**). Together, these data underscore that PIP_2 interactions are unlikely to regulate DA efflux once DAT is phosphorylated.

R443 electrostatic interactions coordinate AMPH-induced DA efflux *in vitro*

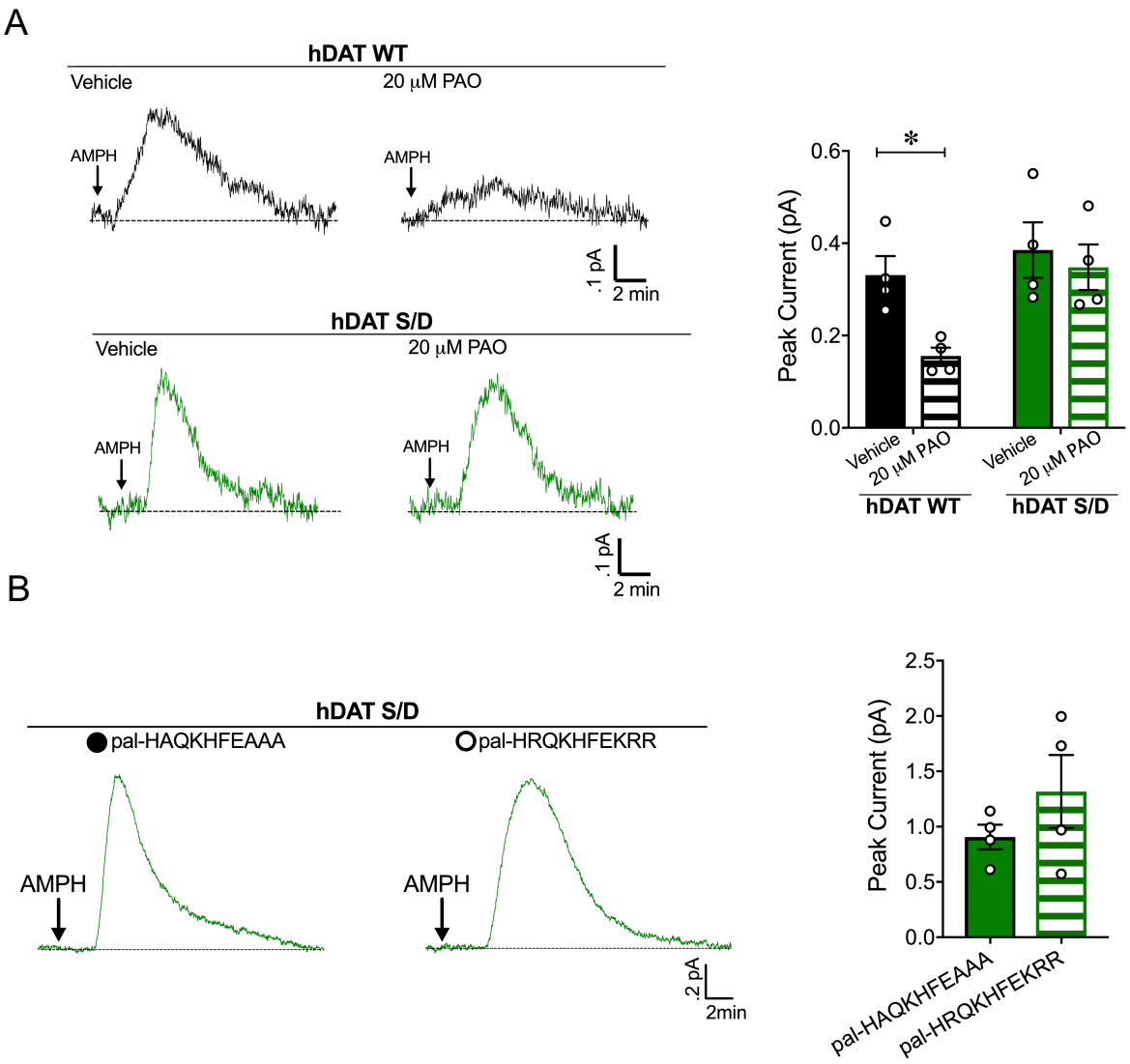

Figure 25: DAT phosphorylation supports PIP_2 independent DA efflux

(**A**) Left: Representative traces of amperometric currents recorded from hDAT WT (black traces) and hDAT S/D (green traces) pre-incubated in either vehicle or PAO (20 μM, 10 min) and subsequently treated with AMPH (10 μM; indicated by arrow). Right: Quantitation of mean peak current amplitudes in hDAT WT and hDAT S/D cells. Pre-incubation with PAO significantly decreased DA efflux in hDAT WT cells (0.33 ± 0.04 pA) with respect to vehicle (0.16 ± 0.02 pA; p = 0.03; n = 4), but not in hDAT S/D cells (vehicle: 0.38 ± 0.06 pA, PAO: 0.35 ± 0.05 pA; p>0.05; n = 4). (**B**) Representative traces from hDAT S/D cells after whole-cell patch delivery of control peptide (3 μM, pal-HAQKHFEAAA) or PIP_2 sequestering peptide (3 μM, pal-HRQKHFEKRR) to the cytoplasm of the cell prior (10 min) to the application of AMPH (10 μM, indicated by arrow). Delivery of control or PIP_2 sequestering peptides resulted in comparable peak currents in response to AMPH (n = 4; p >.05).

Data are presented as mean ± SEM. Two-way ANOVA with Bonferroni's multiple comparison test: (B); Student's t-test: (C).

Increasing evidence from TRPV1, $Kir_{2.1}$ and other channels suggest that the effect of PIP_2 is mediated by multiple binding sites that may have different and/or interacting functions (281). Thus, we sought to understand the contribution of other putative PIP_2 binding sites to reverse transport of DA. PIP_2 binds basic amino acids, frequently in the proximity of hydrophobic amino acids (273, 274). The fourth intracellular loop (IL4) of the DAT contains a basic motif (H442-R443-H444-R445) surrounded by hydrophobic residues, thus, a likely site for PIP_2 binding. Indeed, our molecular dynamic simulations (see below), as well as others, predicted that the IL4 and more specifically, R443, is enriched and interacts with PIP_2 lipids (66). To test whether this possibility had biological and functional relevance, we measured the effect of a charge-neutralizing substitution of R443 to Ala (R443A) on DAT/PIP_2 interactions. Purified His-eGFP tagged hDAT WT or hDAT R443A was incubated with a water-soluble analog of PIP_2 conjugated to an orange fluorophore (BODIPY® TMR-PIP_2). Protein-lipid complexes were pelleted and PIP_2 binding was assayed as a ratio of PIP_2 to eGFP fluorescence. hDAT R443A displayed a significant 34.8 $\pm$ 9.9% reduction in PIP_2 binding compared with hDAT WT ($p = 0.007$) (**Fig. 26A**). The His-eGFP tag (negative control) had significantly diminished PIP_2 binding compared with hDAT WT, as well as to hDAT R443A. These data demonstrate that R443 contributes to the DAT/PIP_2 binding network.

In order to determine whether DAT functions are altered by disrupting this IL4/PIP_2 association, we first measured [^{3}H]DA uptake in both hDAT WT and hDAT R443A cells. DA uptake kinetic curves for hDAT WT and hDAT R443A cells show that DA uptake is comparable through a range of concentrations ($p > 0.05$) (**Fig. 26B, top**). Additionally, neither the maximal velocity of DA uptake (V_{max}) nor apparent affinity for DA (K_m) in hDAT R443A cells were significantly different from that of hDAT WT ($p > 0.05$) (**Fig. 26B, bottom**). Thus, DA uptake is not regulated by the electrostatic interactions of R443.

Considering our previous findings that N-terminus/PIP_2 interactions support AMPH actions (63), we reasoned that disrupting IL4/PIP_2 interactions might alter the ability of AMPH to cause

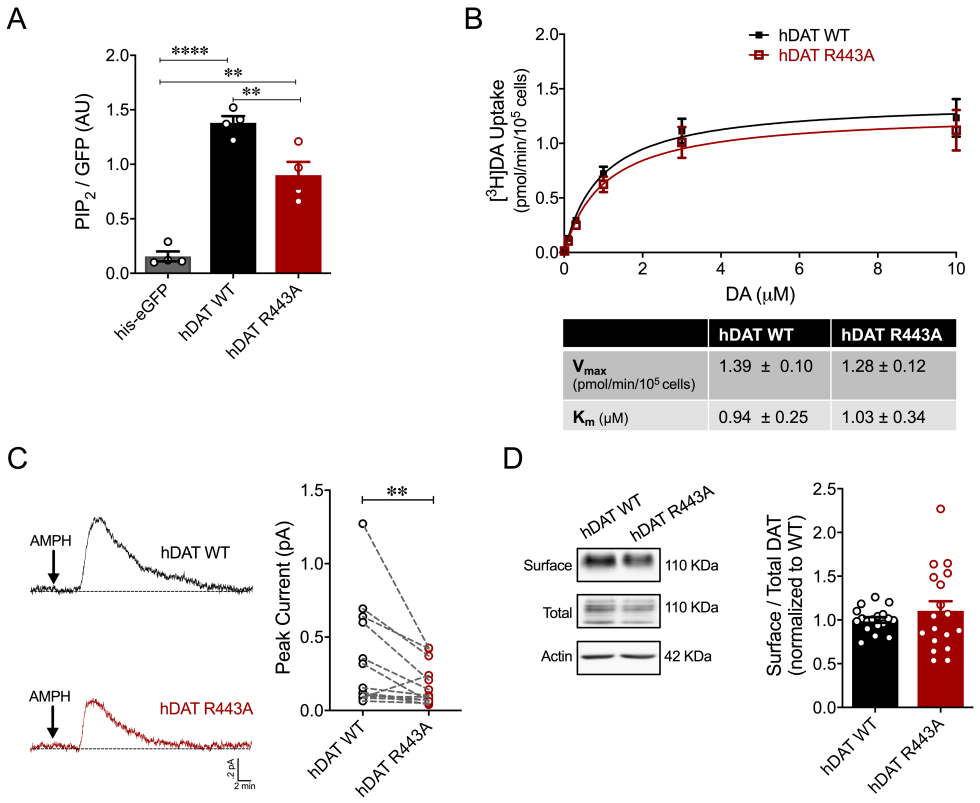

	hDAT WT	hDAT R443A
V_{max} (pmol/min/10^5 cells)	1.39 ± 0.10	1.28 ± 0.12
K_m (μM)	0.94 ± 0.25	1.03 ± 0.34

Figure 26: R443A substitution reduced PIP2 binding and inhibited AMPH-induced DA efflux in vitro

(**A**) hDAT WT or hDAT R443A (containing a His-eGFP tag on the N-terminus) were purified from cellular extracts. Solubilized hDAT WT or hDAT R443A proteins were incubated with a water-soluble analog of PIP_2 conjugated to an orange fluorophore (BODIPY® TMR-PIP_2). Specific binding was quantified as a ratio of PIP_2 fluorescence to eGFP. Minimal PIP_2 binding was measured in the presence of His-eGFP only (0.16 ± 0.05 AU) relative to hDAT WT (1.38 ± 0.12 AU) or hDAT R443A (0.90 ± 0.24 AU) ($F_{(2,9)}$ = 55.11, $p < 0.0001$; n = 4). hDAT R443A displayed a 34.8 ± 9.9% reduction in PIP_2 binding compared with hDAT WT ($p = 0.007$). (**B**) Top: ^{3}[H]DA saturation curves of DA uptake measured in hDAT WT (*closed squares*) or hDAT R443A (*open squares*) cells (n = 4, in triplicate). Curves were fit to Michaelis-Menten kinetics to derive K_m and V_{max}. DA uptake for hDAT R443A was comparable to hDAT WT at every DA concentration measured ($F_{(1,120)}$ = 1.40, $p > 0.05$), as were the kinetic constants, K_m and V_{max} ($p > 0.05$). (**C**) Left: Representative traces of amperometric currents (DA efflux) recorded from hDAT WT (*top*) and hDAT R443A (*bottom*) cells, in response to AMPH application (10 μM, indicated by arrow). Right: Quantitation of peak current amplitudes. hDAT R443A display a 50.6 ± 15.1% decrease in AMPH-induced DA efflux relative to hDAT WT ($p = 0.003$; n = 14). (**D**) Left: Representative immunoblots of surface hDAT (*top*), total (glycosylated and non-glycosylated) hDAT (*middle*), and actin as loading control (*bottom*). Right: hDAT expression is quantified as a ratio of surface to total glycosylated hDAT normalized to hDAT WT. hDAT R443A and hDAT WT had comparable expression ($p > 0.05$; n = 6, in triplicate).

Data are presented as mean ± SEM. One-way ANOVA with Bonferroni's multiple comparisons test: (A); Two-way RM ANOVA with Bonferroni's multiple comparison test: (B); Students t-test: (B) and (D); Wilcoxon matched-pairs signed rank test: (C).

DA efflux. **Figure 26C** (**left**) displays representative amperometric traces recorded from hDAT WT and hDAT R443A upon AMPH application. hDAT R443A cells displayed a significant 50.6 ± 15.1% decrease in AMPH-induced DA efflux relative to hDAT WT ($p = 0.003$) (**Fig. 26C, right**). The disruption of the R443A mutation on DA efflux was so robust that PAO-mediated PIP_2 depletion in hDAT R443A cells (as described above) did not further reduce DA efflux compared with vehicle ($p > 0.05$; **Fig. 27, bottom**)**.** In contrast, PAO significantly reduced AMPH-induced DA efflux in hDAT WT cells compared with vehicle ($p = 0.04$; **Fig. 27, top**). Thus, the electrostatic interactions of R443 with PIP_2 and/or other negatively charged motifs of the DAT regulate the reverse transport of DA (**Fig. 27, right**).

Although we demonstrate no differences in DA uptake between hDAT WT and hDAT R443A, we used cell-surface biotinylation to confirm that this reduction in DA efflux was not due to changes in DAT plasma membrane expression. Surface fractions for hDAT WT and hDAT R443A were quantitated, normalized to total DAT (glycosylated), and expressed as a ratio of hDAT WT (**Fig. 26D**). This analysis yielded no significant differences in hDAT R443A and hDAT WT expression ($p > 0.05$).

N-terminus phosphorylation and R443 electrostatic interactions are necessary for DA efflux

Given the fundamental role of DAT phosphorylation in supporting DA efflux, we reasoned that disrupting R443 electrostatic interactions would be ineffective in regulating this process once the N-terminus DAT was phosphorylated. To test this, we mutated R443 to Ala in the hDAT S/D background (hDAT S/D R443A). We first assessed whether this mutation affected DAT surface expression. This charge neutralizing substitution at R443 did not affect DAT expression compared with controls (hDAT S/D) (**Fig. 28A**, $p > 0.05$).

We also quantified the forward transport of DA supported by cells expressing hDAT S/D R443A relative to hDAT S/D cells (**Fig. 28B, top**). [^{3}H]DA uptake kinetic curves showed comparable uptake in hDAT S/D R443A compared with hDAT S/D cells through a range of DA

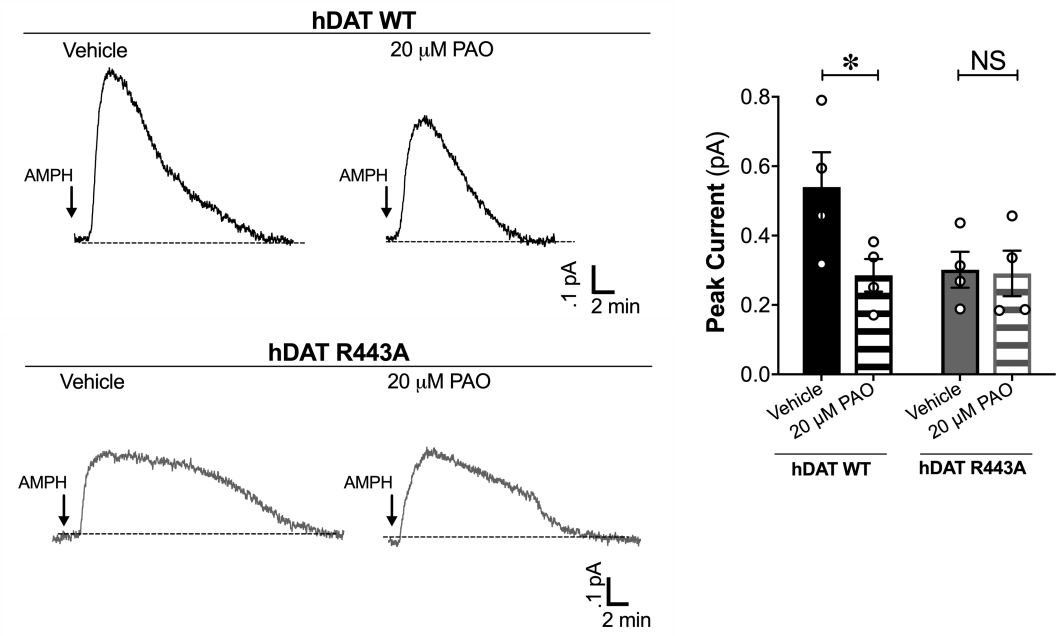

Figure 27: PIP_2 depletion does not decrease DA efflux in hDAT R443A cells

Left: Representative traces of amperometric currents recorded from hDAT WT (black traces) and hDAT R443A (gray traces) pre-incubated in either vehicle or PAO (20 μM, 10 min) and subsequently treated with AMPH (10 μM; indicated by arrow). *Right:* Quantitation of mean peak current amplitudes in hDAT WT and hDAT R443A cells (n = 4). PIP_2 depletion by PAO reduced DA efflux in hDAT WT cells (0.28 ± 0.05 pA) with respect to vehicle (0.54 ± 0.10 pA; $F_{(1,12)}$ = 3.64, p = 0.04), but did not affect hDAT R443A cells (vehicle: 0.30 ± 0.05 pA. PAO: 0.29 ± 0.07 pA; p > 0.05).

Data are presented as mean ± SEM. Two-way ANOVA with Bonferroni's multiple comparison test.

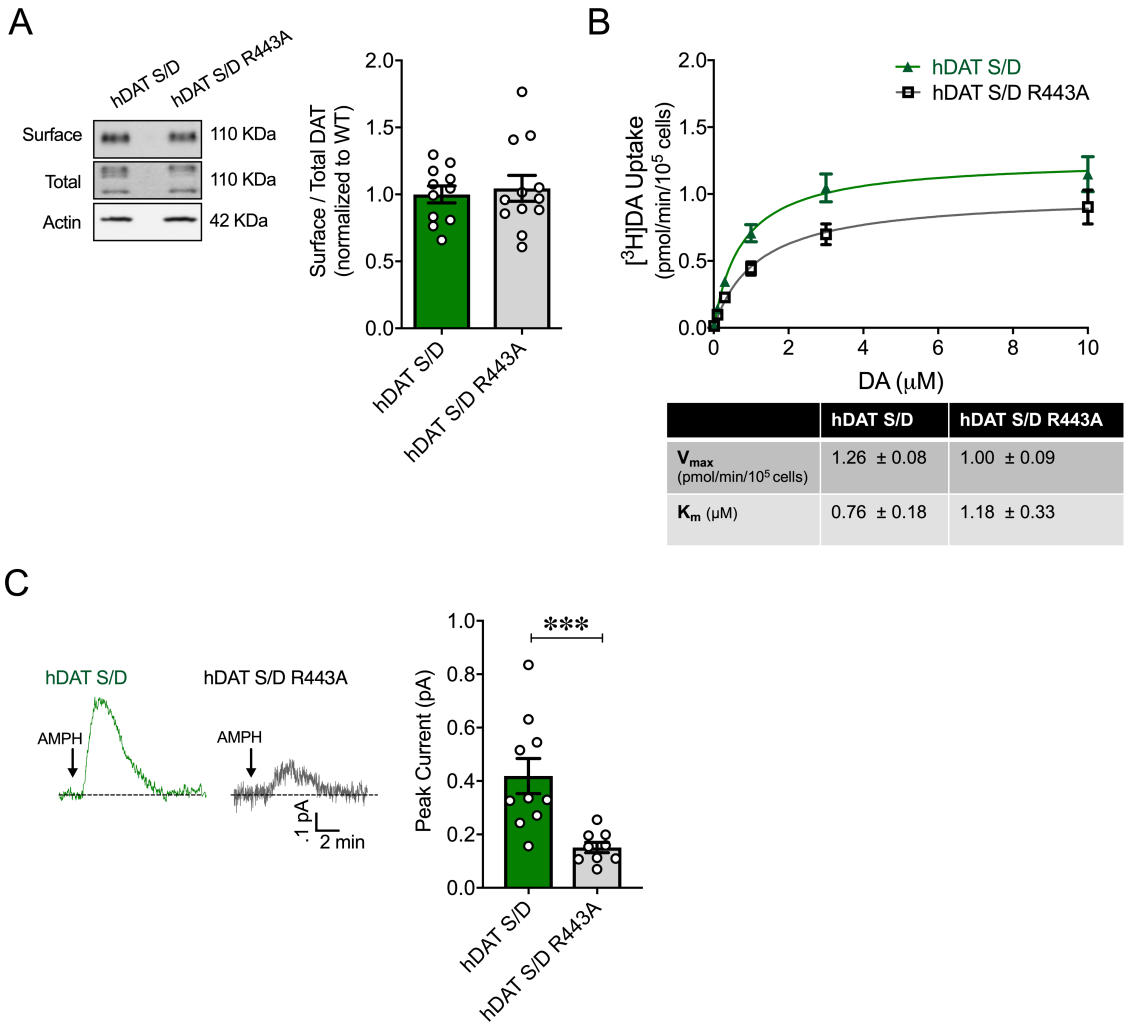

Figure 28: Disrupting R443 electrostatic interactions inhibits DA efflux independent of DAT N-terminus phosphorylation

(**A**) Left: Representative immunoblots of surface hDAT (*top*), total hDAT (*middle*), and actin (*bottom*). Right: hDAT expression is quantified as a ratio of surface to total glycosylated hDAT normalized to hDAT S/D. hDAT S/D R443A had comparable expression to hDAT S/D ($p > 0.05$; $n = 4$ in triplicate). Dashed lines indicate separate sets of experiments. (**B**) Top: Average ^{3}[H]DA uptake kinetics measured in hDAT S/D R443A (grey line open squares) and hDAT S/D (green line closed triangle) cells ($n = 4$, in triplicate). Curves were fit to Michaelis-Menten equation to derive K_m and V_{max}. Bottom: The V_{max} and K_m for hDAT S/D R443A were comparable to hDAT S/D cells ($p > 0.05$). (**C**) Left: Representative traces of DA efflux recorded from hDAT S/D (green trace) and hDAT S/D R443A cells (grey trace) in response to AMPH application (10 μM, indicated by arrow). Right: Quantitation of peak current amplitudes ($n = 9$ - 10). DA efflux from hDAT S/D R443A (0.15 ± 0.02 pA; $p = 0.01$) was significantly lower compared with hDAT S/D cells (0.42 ± 0.07 pA; $p = 0.0004$).

Data are presented as mean ± SEM. Students t-test: (A) - (C); Two-way RM ANOVA with Bonferroni's multiple comparison test: (B).

concentrations ($p > 0.05$) (**Fig. 28B, top**). The V_{max} and K_m in hDAT S/D R443A were not significantly different from that of hDAT S/D cells ($p > 0.05$) (**Fig. 28B, bottom**). Finally, we measured the reverse transport capacity of hDAT S/D R443A cells compared with hDAT S/D in response to AMPH. Representative amperometric traces illustrated a significant 63.9 $\pm$ 0.3% reduction in DA efflux in hDAT S/D R443A cells compared with hDAT S/D cells ($p = 0.0004$) (**Fig. 28C**). hDAT S/D R443A cells displayed amperometric currents in response to AMPH, which were comparable in magnitude to previous recordings from hDAT R443A cells (compare **Fig. 28C** to **Fig. 26C**). These data emphasize the role of R443 in DA efflux, even when N-terminus phosphorylation has occurred.

To determine whether other putative PIP_2 binding sites on the DAT could further modulate the decrease in DA efflux promoted by R443 substitution, we reduced PIP_2 levels in hDAT S/D R443A cells by either pre-treating cells with PAO or through patch delivery of a PIP_2 sequestering peptide (pal-HRQKHFEKRR) and measured DA efflux. As shown previously, PAO significantly reduced AMPH-induced DA efflux in hDAT WT cells compared with vehicle **(**$p = 0.001$; **Fig. 29A**). Notably, PAO did not further inhibit DA efflux in hDAT S/D R443A cells compared with vehicle ($p > 0.05$; **Fig. 29A).** Similarly, we found that pal-HRQKHFEKRR significantly reduced DA efflux relative to control peptide in hDAT WT cells ($p = 0.02$, **Fig. 29B**), but did not significantly affect DA efflux in hDAT S/D R443A cells ($p > 0.05$, **Fig. 29B)**. Together, these data illustrate that once PIP_2 binding to R443 is impaired, N-terminus phosphorylation does not rescue impairments in DA efflux, and other DAT/PIP_2 interactions do not further regulate reverse transport of DA. These data also raise the possibility that an electrostatic interaction between the positively charged R443 and negatively charged, phosphorylated N-terminus may be important to DA efflux.

Our MD simulations showed that PIP_2 coordinates the interactions between the N-terminus and IL4 (**Fig. 30A**). However, once the N-terminus is phosphorylated, it interacts directly with IL4 (R443) displacing PIP_2 (**Fig. 30B**). Notably, we showed *in vitro* that pseudophosphorylation of the N-terminus significantly increases its affinity for IL4 ($p < 0.0001$;

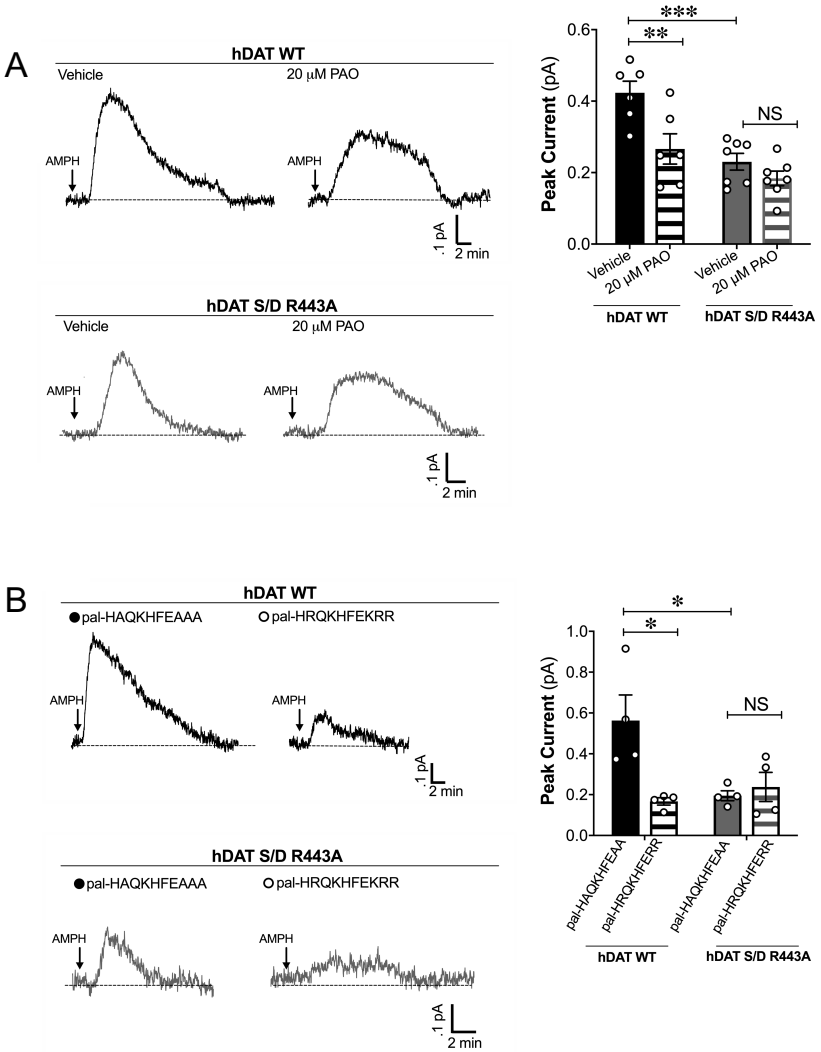

Figure 29: PIP_2 does not regulate DA efflux in hDAT S/D R443A cells

(**A**) *Left:* Representative traces of amperometric currents recorded from hDAT WT (black traces) and hDAT S/D R443A (gray traces) pre-incubated in either vehicle or PAO (20 μM, 10 min) and subsequently treated with AMPH (10 μM; arrow). *Right:* Quantitation of peak current amplitudes in hDAT WT and hDAT S/D R443A cells (n = 4; $F_{(1,22)} = 11.70$). Pre-incubation with PAO decreased DA efflux in hDAT WT cells (0.27 ± 0.04 pA) with respect to vehicle (0.42 ± 0.03 pA; p = 0.001), but not in hDAT S/D R443 cells (vehicle: 0.23 ± 0.02 pA. PAO: 0.18 ± 0.02 pA; p > 0.05). (**B**) Representative traces from hDAT WT cells after patch delivery of control peptide (3 μM, pal-HAQKHFEAAA) or PIP_2 "sequestering" peptide (3 μM, pal-HRQKHFEKRR) to the inside of cells prior AMPH application (10 μM, indicated by arrow). Delivery of PIP_2 sequestering peptides significantly reduced peak currents in response to AMPH in hDAT WT cells (control peptide: 0.56 ± 0.12 pA, PIP_2 peptide: 0.18 ± 0.02 pA; $F_{(1,12)} = 5.38$, p = 0.02). Delivery of PIP_2 sequestering peptides did not affect response to AMPH in hDAT S/D R443A cells (control peptide: 0.19 ± 0.02 pA, PIP_2 peptide: 0.24 ± 0.07 pA; p > 0.05).

Data are presented as mean ± SEM. Two-way ANOVA with Bonferroni's multiple comparison test: (A) – (B).

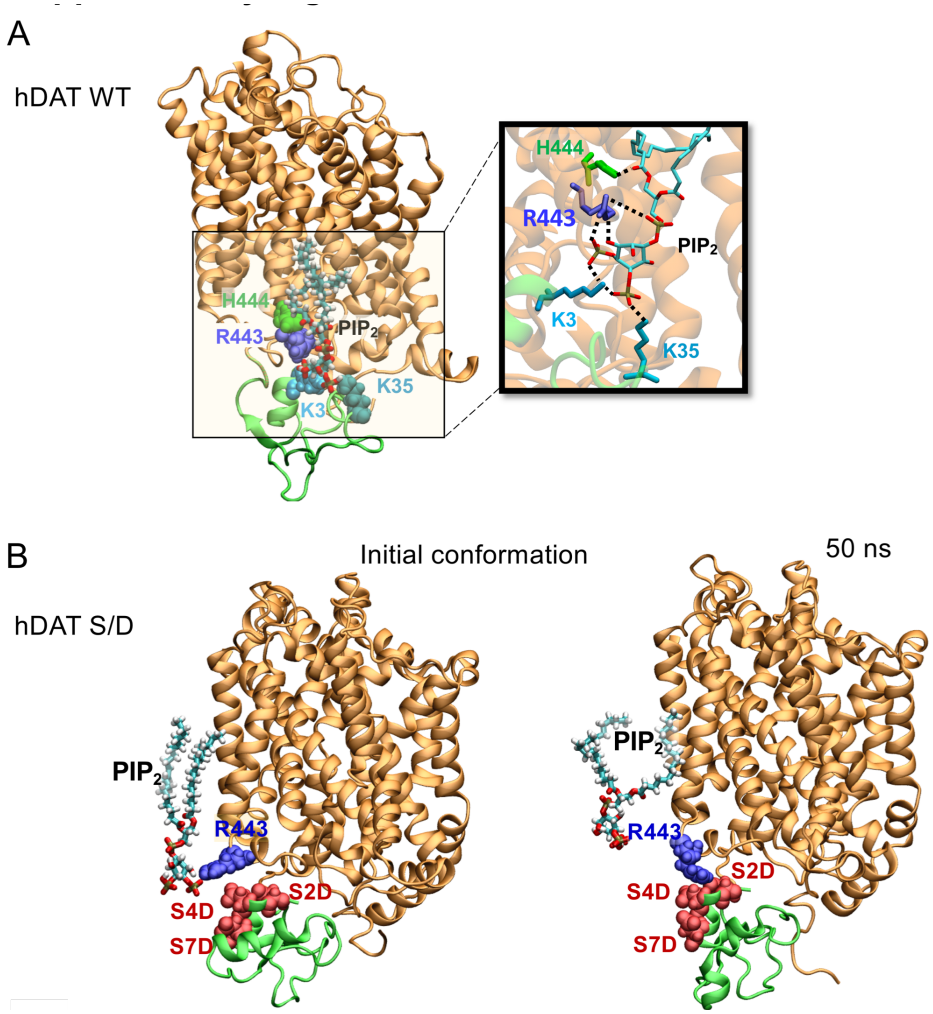

Figure 30: R443 coordinates the interaction between phosphorylated N-terminus and IL4

(**A**) MD stimulations of hDAT WT showed the propensity of PIP_2 (*licorice*) head group to form a hydrogen bond with H444 (*green*, van der Waals (*vdW*) representation), and three salt-bridges with R443(*light blue*, *vdW*), K3 (*bright cyan, vdW*), and K35 (*dark cyan*, *vdW*). The inset illustrates the interactions in more detail. *Red*, *tan*, white and *cyan* in PIP_2 represent oxygen, phosphorus, hydrogen and carbon atoms, respectively. (**B**) MD simulation of hDAT S/D in its initial conformation (left) and at 50 ns (right). In hDAT S/D, the probability of PIP_2 binding N-terminal Lys3 decreased to 20 ± 15% relative to 80 ± 20% for hDAT WT. Simulations illustrate the intermittent formation of a salt bridge between R443 (*blue, vdW*) and S2D/S4D (*red, vdW*), which resulted in unbinding PIP_2 from R443. N-terminus (S2D/S4D)/IL4 (R443) interactions maintained the acidic N-terminal cluster (S2D/S4D/S7D) near the entrance of the intracellular vestibule.

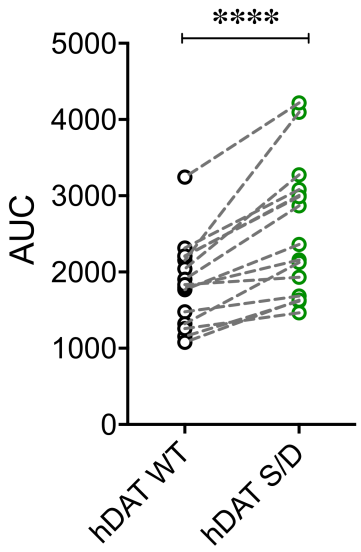

Figure 31: N-terminus pseudophosphorylation increases N-terminus/IL4 association *in vitro*

(**C**) N-terminus/IL4 binding was assayed by incubating purified N-terminus of hDAT WT or hDAT S/D (1 - 68) with rhodamine tagged IL4 (RHodamine-(PEGx3)-IDEFQLLHRHRE). The N-terminus of hDAT S/D had increased binding to IL4 (2567 ± 228 AUC) compared that of hDAT WT (1851 ± 145 AUC; n = 3, in quintuplet; $p < 0.0001$).

Data are presented as mean ± SEM. Wilcoxon matched-pairs signed rank test: (C).

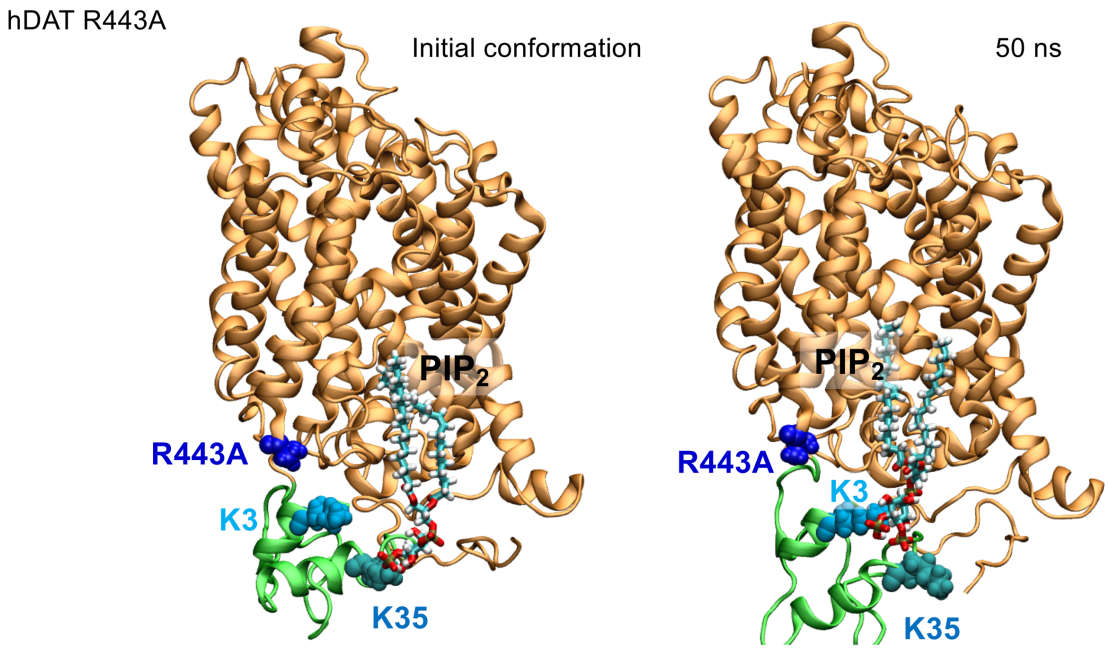

Figure 32: A neutralizing substitution at R443 disrupts N-terminus/ IL4 associations

Illustrated are two conformations of hDAT R443A at t = 0 ns (initial conformation, left) and at 50 ns (right) from MD simulations. Here, the PIP_2 phospholipid head group made close contacts with K3/K35 and remained bound to K3/K35, but did not interact with A443. R443A substitution reduced the probability that PIP_2 bound IL4 to 2 ± 2% compared with 92 ± 5% in hDAT WT. Likewise, it decreased the probability that PIP_2 bound Lys3 to 35 ± 15% compared with 80 ± 20% in hDAT WT.

hDAT S/D R443A

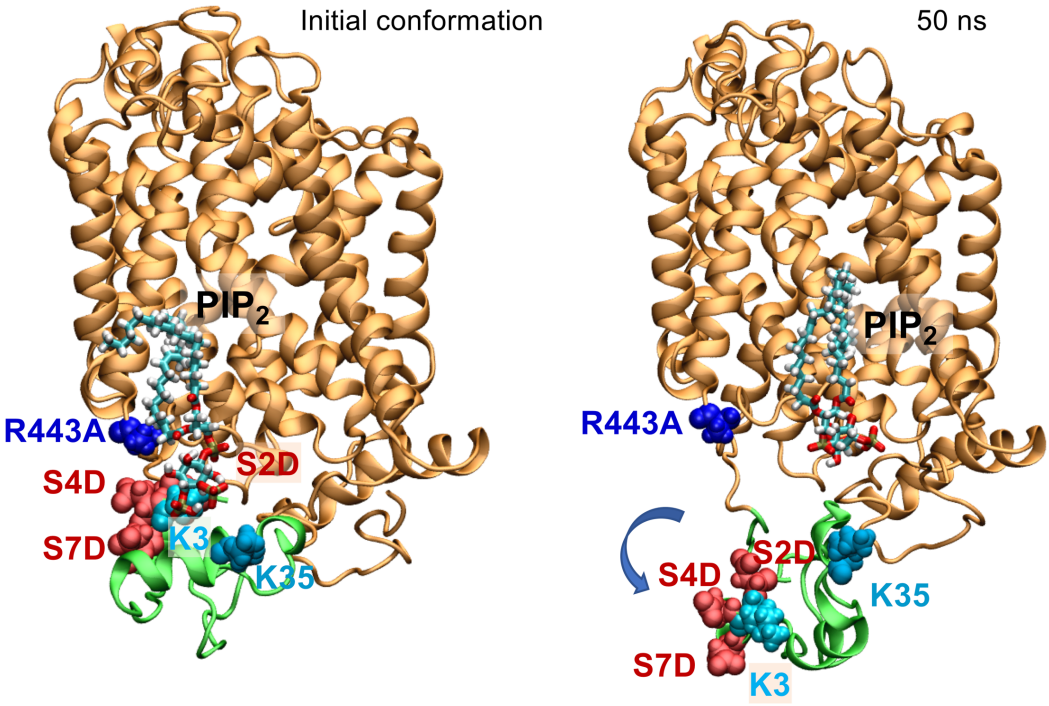

Figure 33: R443A disrupts N-terminus/ IL4 associations even if N-terminus is pseudophosphorylated

Illustrated are two conformations of hDAT S/D R443A at t = 0 ns (initial conformation, left) and at 50 ns (right) from MD simulations. hDAT S/D R443A exhibited significant disordering at the N-terminal segment during the simulations, as the comparison of the initial (left) to 50 ns (right) conformation shows. Here, PIP_2 phospholipid head initially interacted with K3 (*left*), then with K35, and ultimately, lost contact with the disordered N-terminus. This disordering was driven by repulsion between the N-terminal acidic cluster (S2D/S4D/S7D) and the PIP_2 phospholipid head group and the inability of A443 to bind the acidic N-terminus cluster and maintain it in close proximity to the IC vestibule.

Fig. 31). As indicated by our *in vitro* experiments, our MD simulations confirmed that a neutralizing substitution at R443 impairs the interaction between PIP_2 and IL4 (**Fig. 32**). Furthermore, R443A substitution in the presence of N-terminal phosphorylation weakens and eventually impairs the interaction between the anionically charged N-terminus and IL4 (**Fig. 33**), an interaction we show is required for DA efflux.

Disrupting the electrostatic interactions of R443 limits central and behavioral responses to AMPH

We utilized the genetic tractability of *Drosophila melanogaster* to study the *ex vivo* and *in vivo* consequences of a charge-neutralizing substitution at R443. *Drosophila* is a powerful model system to study DA signaling *in vivo* due to conserved mechanisms of DA neurotransmission, including synthesis, packaging and transport (178). We used phiC31-based integration to insert our UAS-driven transgene of interest (hDAT WT or hDAT R443A) in the fly genome of a *Drosophila* DAT (dDAT) null background (DAT^{fmn}), as previously described (51).

We first determined whether hDAT R443A expressing flies supported normal DAT functions. We found that isolated hDAT R443A brains have comparable DA uptake to hDAT WT brains ($p > 0.05$) (**Fig. 34A**). Next, we measured the reverse transport capacity of DAT in hDAT WT or hDAT R443A isolated fly brains using amperometry. Upon the addition of AMPH, DA efflux was measured from posterior inferior-lateral protocerebrum 1 (PPL1) neurons (**Fig. 34B, white box inset**), a dense cluster DA neurons that innervate the mushroom-body modulating reward and punishment learning (190, 220, 282). Consistent with our *in vitro* data, hDAT R443A displayed a significant reduction in DA efflux compared with hDAT WT brains ($p = 0.004$).

Consequently, we focused on understanding the role of DA efflux in complex behaviors using hDAT R443A flies. We first studied an elemental behavior regulated by DA, locomotion. Based on our new findings that hDAT R443A supports normal DA uptake in *Drosophila* brains, we hypothesized that hDAT R443A flies would have normal circadian locomotor activity.

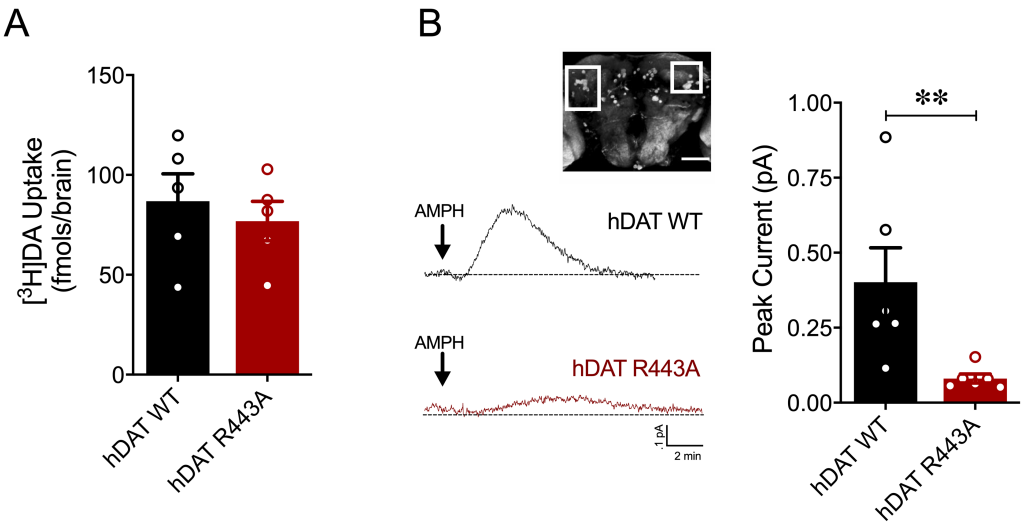

Figure 34: hDAT R443A limits AMPH-induced DA efflux in *Drosophila* brain

(**A**) hDAT WT or hDAT R443A was expressed in DA neurons in a dDAT KO (fmn) background. ^{3}[H]DA uptake (200 nM, 10 min) was measured in adult isolated *Drosophila* brain (n = 5). DA uptake measured in hDAT WT flies (86.9 ± 13.7 fmol/brain) was comparable to that measured in hDAT R443A flies (76.9 ± 9.9 fmol/brain; p > 0.05). (**B**) Left: Representative traces of amperometric currents recorded from a dense cluster of DA neurons (PPL1, boxed in *inset, scale bar: 50* µm*)* in response to AMPH application (20 µM; indicated by arrow) in hDAT WT (black trace) and hDAT R443A (red trace) brains. Right: Quantitation of peak current amplitudes. hDAT WT flies displayed higher peak currents (0.40 ± 0.11 pA) than hDAT R443A flies (0.08 ± 0.02 pA; n = 6; p = 0.004).

Data are presented as mean ± SEM. Students t-test: (A) Mann-Whitney test: (B).

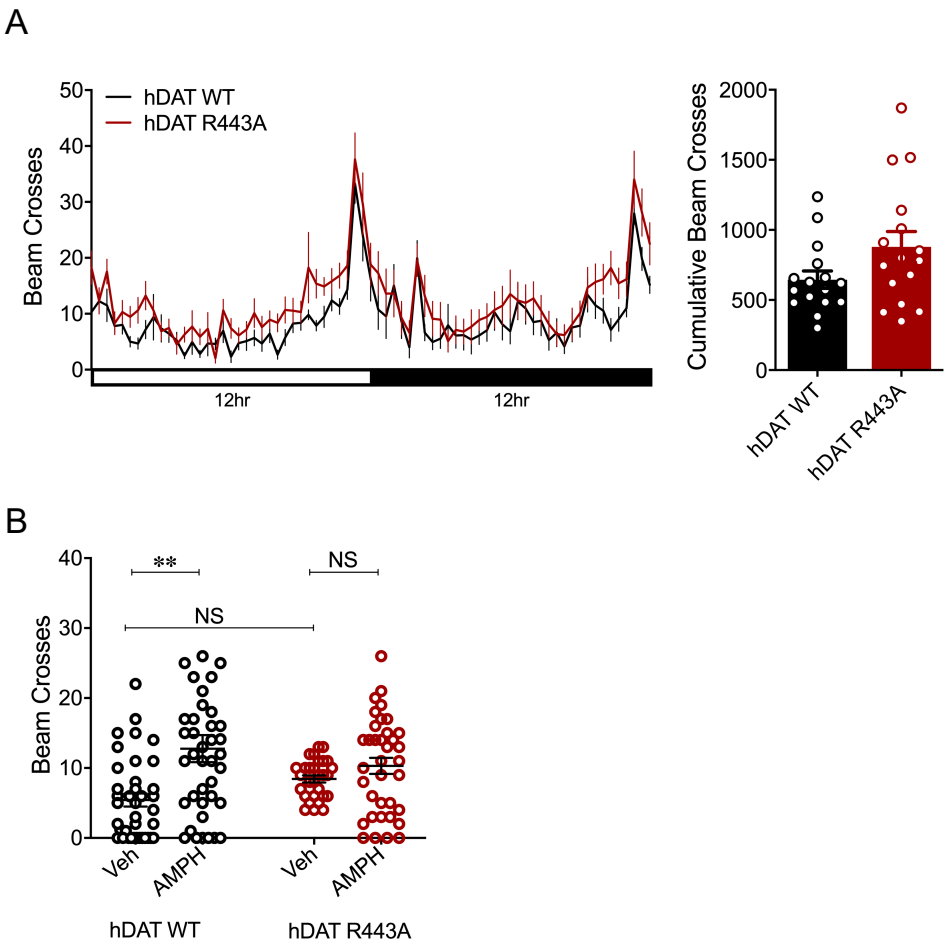

Figure 35: hDAT R443A *Drosophila* display limited psychomotor responses to AMPH

(**A**) Left: Locomotor activity was assayed over a 24-hour period including both the light (horizonal white bar) and dark (horizontal black bar) cycle. Circadian activity curves show average beam crosses (20-min interval) during the 24-h period for hDAT WT (black line) and hDAT R443A (red line) *Drosophila.* Right: Cumulative beam crosses were not significantly different for hDAT WT (654 ± 61) versus hDAT R443A *Drosophila* (879 ± 110; $p > 0.05$; n = 16). (**B**) Locomotor activity was measured after a 30-min exposure to vehicle or 1 mM AMPH. The total beam crosses increase in the AMPH (12.8 ± 1.9; n = 39) compared with vehicle group (5.4 ± 0.9; n = 38) of hDAT WT *Drosophila* ($F_{(1,138)} = 11.83$, $p = 0.0005$). In hDAT R443A *Drosophila,* AMPH (10.3 ± 1.2; n = 36; $p > 0.05$) did not increase the total beam crosses compared with vehicle group (8.5 ± 0.5; n = 29) and with respect to hDAT WT vehicle group ($p > 0.05$).

Data are presented as mean ± SEM. Students t-test: (A); Two-way ANOVA with Bonferroni's multiple comparison test: (D).

Consistent with our hypothesis, circadian locomotor activity in hDAT R443A flies did not significantly differ from that of hDAT WT flies (**Fig. 35A,** $p > 0.05$).

Previous studies have shown that commonly abused drugs effect behavioral phenotypes in flies, similar to those observed in rodents and humans (187, 192, 211). To this end, we and others have shown that acute AMPH exposure increases locomotor activity in *Drosophila* (19, 22, 63, 122). AMPH elicits these behaviors by increasing levels of extracellular DA, a process mediated (at least in part) by DA efflux (128, 132). We reasoned that given deficits in DA efflux in hDAT R443A flies, AMPH-induced hyperactivity would also be diminished in these animals. Exposure to AMPH (1 mM, 30 min) significantly increased activity in hDAT WT flies compared with vehicle (**Fig. 35B,** $p = 0.0005$), but not in hDAT R443A flies relative to vehicle ($p > 0.05$). Thus, charge neutralizing R443 blunts the acute psychomotor response to AMPH.

R443 electrostatic interactions selectively regulate AMPH preference

Reward is a fundamental behavior regulated across phyla by DA neurotransmission (283, 284).; however, the role of DA efflux in this process is not well understood. Increasing evidence supports DAT's role in regulating reward (285, 286). Thus, we took advantage of our fly model to determine the role of DAT-mediated DA efflux in reward processes. To quantify possible differences in AMPH preference in hDAT WT and hDAT R443A flies, we adapted the CApillary FEeding assay (287-289) to measure AMPH consumption. In this redesigned paradigm, adult male flies were acclimated to custom-built testing chambers containing two capillaries filled with either (a) sucrose or (b) sucrose-blue food (**Fig. 36A**). Following this acclimation period, on day 1, baseline consumption, defined as a ratio of sucrose-blue (nL_{blue}) to total food consumed (nL_T), was measured. Consumption levels of 0.5 indicate no preference across the two capillaries. Levels greater than 0.5 indicate preference, and levels lower than 0.5 indicate avoidance. On day 2, experimental groups were given the choice of (a) sucrose or (b) sucrose-blue food supplemented with AMPH (1 mM or 10 mM; solid lines). Notably, hDAT WT flies displayed preference for AMPH (day 2: 0.62 ± 0.04) compared with baseline (day 1: 0.46 ± 0.03; $p = 0.005$)

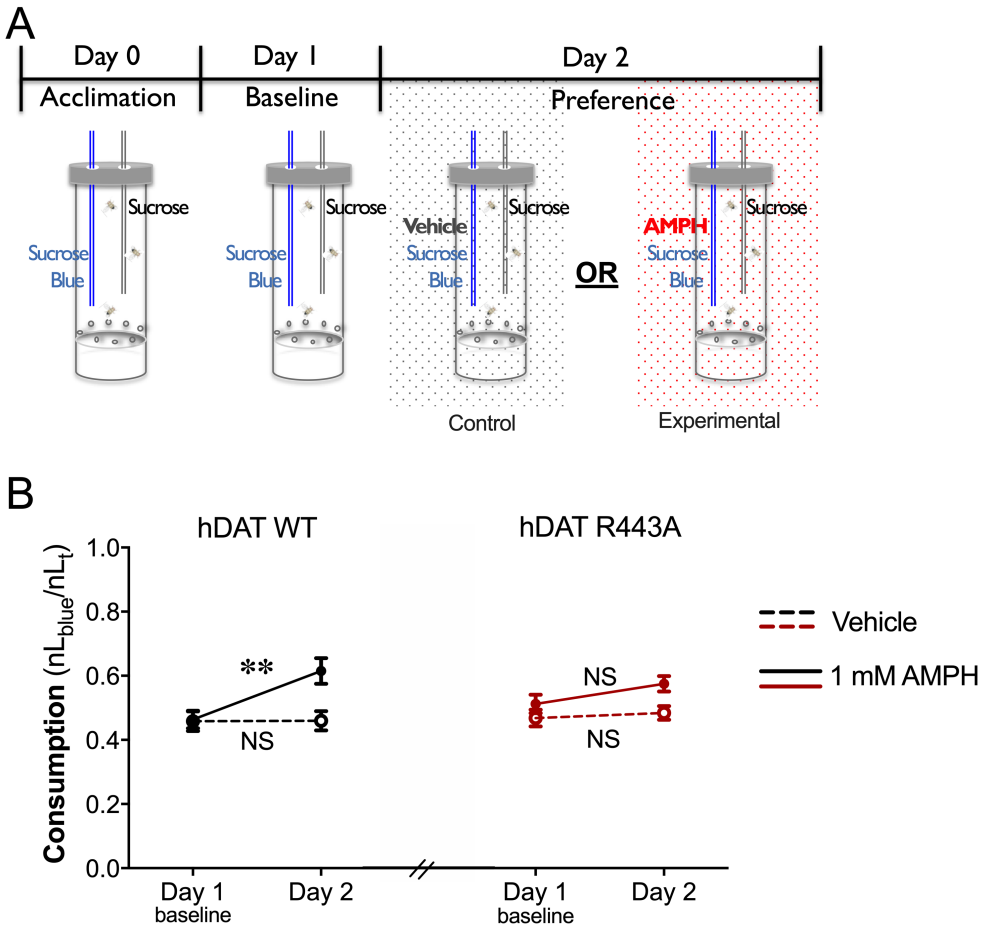

Figure 36: In a two-choice consumption paradigm, hDAT R443A flies display diminished AMPH preference

(**A**) Schematic illustrating a two-choice consumption paradigm developed to measure AMPH preference in flies. The paradigm is comprised of three 24-h testing periods: acclimation, baseline, and preference, where capillaries were replaced every 24-h period to measure AMPH consumption. Adult *Drosophila* were placed in custom chambers containing two volumetric capillaries filled with either clear (100 mM sucrose) or blue food (100 mM sucrose, 500 µM blue). During AMPH preference testing, blue food was supplemented with either AMPH (1 mM or 10 mM) for experimental groups (solid line) or vehicle for control groups (dashed line). Preference is presented as a ratio of blue food to total food consumption. (**B**) Left: hDAT WT *Drosophila* exposed to 1 mM AMPH (solid black line) consumed more AMPH (61.5 ± 4.0 %) relative to baseline vehicle (46.3 ± 2.8 %; n = 12-13, $F_{(1, 49)} = 5.23$, p = 0.005). hDAT WT control groups consumed equal amounts of blue food during day 1 (45.8 ± 3.1%) and day 2 (46.0 ± 3.0 %; n = 14; p > 0.05). Right: hDAT R443A *Drosophila* (solid red line) did not consume more AMPH (57.4 ± 2.4%) compared with baseline vehicle (51.1 ± 2.8%; n = 13, $F_{(1, 50)} = 0.86$, p > 0.05). hDAT R443A control groups consumed comparable amounts of blue food during day 1 (46.7 ± 2.6%) and day 2 (48.3 ± 2.2%; n = 14, p > 0.05).

Each data point represents the mean of 10-14 measurements ± SEM. Two-way ANOVA with Bonferroni's multiple comparison test: (B).

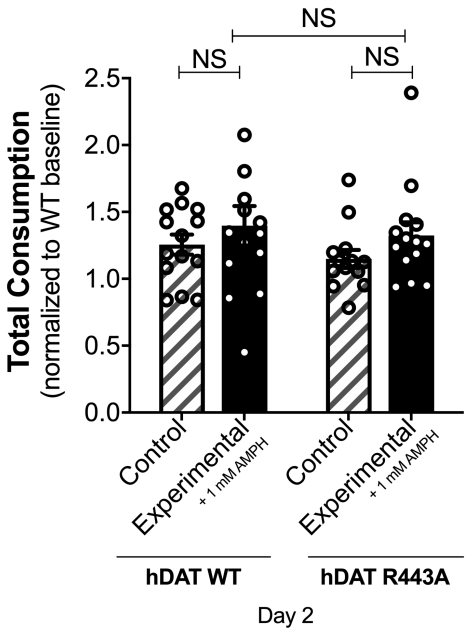

Figure 37: 1mM AMPH does not alter total food consumption

Total food consumed by hDAT WT flies in the control (vehicle) groups was not statistically different from that of experimental (1 mM AMPH) groups (n = 13-14; $p > 0.05$) on day 2. Similarly, food consumption by hDAT WT R443A flies in the control (vehicle) groups was comparable to that of flies in the experimental (1 mM AMPH) groups (n = 13-14; $p > 0.05$) day 2. In addition, there was no significant difference in food consumption between hDAT WT and hDAT R443A experimental groups ($F_{(1,51)} = 0.03$, $p > 0.05$).

Data are presented as mean ± SEM. Two-way ANOVA with Bonferroni's multiple comparison test: (A).

(**Fig. 36B**). To ensure that the increase in AMPH consumption was not due to a developed preference for sucrose-blue food, control groups (dashed lines) were given the choice of (a) sucrose or (b) sucrose-blue food supplemented with vehicle on day 2. hDAT WT control groups (dashed black lines) did not develop a preference for sucrose-blue food (day 1: 0.46 ± 0.03 versus day 2: 0.46 ± 0.03; $p > 0.05$). These data confirm that hDAT WT animals displayed a preference specifically for 1 mM AMPH. Interestingly, hDAT R443A flies did not show preference for AMPH relative to baseline (red solid line, $p > 0.05$). hDAT R443A control groups also did not develop a preference for sucrose-blue food (red dashed line, $p > 0.05$). To account for potential changes in feeding behavior, we compared total food consumption across genotypes (hDAT WT versus hDAT R443A) and groups (control: vehicle versus experimental: 1mM AMPH). Total food consumption on day 2 was not statistically different in control groups (lined bars) compared with AMPH groups (solid bars) in either hDAT WT or hDAT R443A flies (**Fig. 37**; $p > 0.05$). Moreover, total food consumption in hDAT WT (1.40 ± 0.15) compared with hDAT R443A flies (1.32 ± 0.10) exposed to 1 mM AMPH was also not statistically different ($p > 0.05$). Thus, there were no measurable changes in feeding across groups or genotypes. These data show that a single amino acid substitution at position R443 decreases the rewarding properties of AMPH in flies without altering food reward or consumption.

In hDAT WT flies, higher concentrations of AMPH (10 mM) resulted in a significant $39.2 \pm 1.9\%$ decline in AMPH consumption compared with baseline (day 2 vs. day 1, $p = 0.0004$) (**Fig. 38**). hDAT R443A flies also displayed an avoidance for AMPH, where consumption decreased by $33.8 \pm 3.9\%$ on day 2 compared with day 1 ($p = 0.03$). Neither control groups for both hDAT WT or hDAT R443A saw a change in sucrose-blue food consumption on day 2 relative to baseline ($p > 0.05$). Given AMPHs well known anorexigenic effects (290), we confirmed that avoidance for AMPH was not skewed by significant changes in total food consumption on day 2 relative to day 1, neither in hDAT WT nor hDAT R443A flies (**Fig. 39**, $p > 0.05$). Therefore, an Arg at position

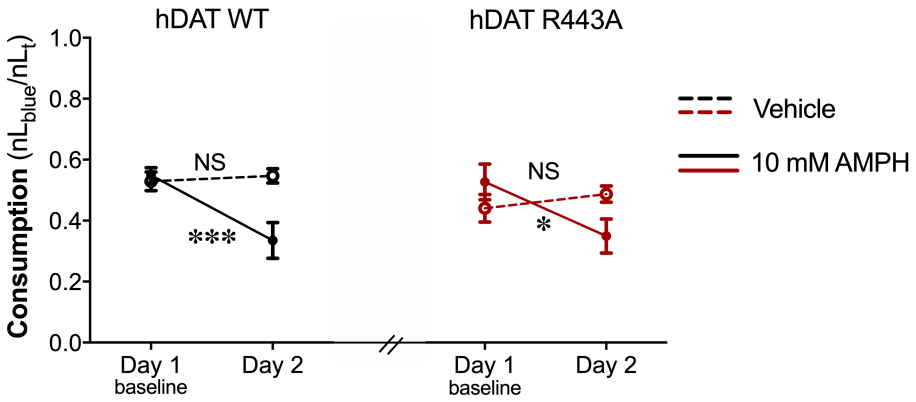

Figure 38: hDAT R443A *Drosophila* display avoidance to high AMPH concentrations

(**C**) Left: hDAT WT *Drosophila* exposed to 10 mM AMPH (solid black line) consumed drastically less AMPH (33.5 ± 5.9%) compared with baseline vehicle (54.9 ± 2.5%; n = 12; $F_{(1,44)}$ = 9.55, p = 0.0004). Control groups for hDAT WT (black dashed line) consumed comparable food on day 1 and day 2 (n = 12; p > 0.05). Right: hDAT R443A *Drosophila* consumed significantly less 10 mM AMPH (35.0 ± 5.6%) compared with baseline vehicle (52.9 ± 5.9%; n = 11; $F_{(1,39)}$ = 5.18, p = 0.03). Control groups for hDAT R443A (red dashed line) consumed comparable food on day 1 and day 2 (n = 10-11; p > 0.05).

Each data point represents the mean of 10-14 measurements ± SEM. Two-way ANOVA with Bonferroni's multiple comparison test.

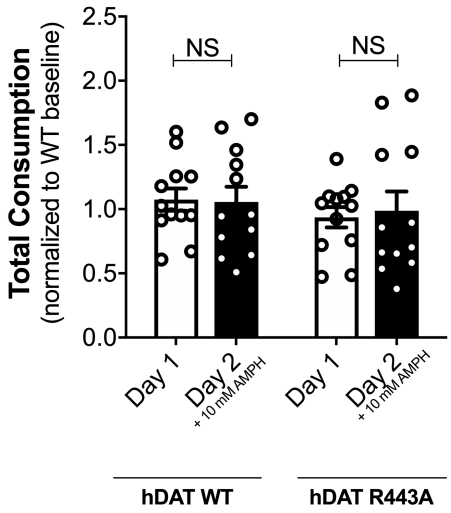

Figure 39: 10mM AMPH does not alter total food consumption

Total food consumption in hDAT WT exposed to 10 mM AMPH on day 2 did not significantly differ compared with baseline (day 1) consumption (n = 12; $F_{(1,44)} = 0.03$, $p > 0.05$). Food consumption in hDAT R443A flies exposed to 10 mM AMPH on day 2 was comparable to that of day 1 (n = 12; $p > 0.05$). Food consumption is normalized to hDAT WT baseline (day 1).

Data are presented as mean ± SEM. Two-way ANOVA with Bonferroni's multiple comparison test: (A) - (B).

443 is a hDAT residue that regulates AMPH reward, although it does not modulate AMPH avoidance.

Discussion

Within the central nervous system, psychostimulant exposure modifies phospholipid profiles in a brain region-dependent manner (291-293). Phospholipid levels increase in response to psychostimulants in the striatum and hippocampus, regions critical for drug reward and reinstatement, respectively (291, 294). In contrast, phospholipid levels decrease in the cerebellum (294). Altered phospholipid levels and metabolism have also been reported in psychostimulant users (293, 295). These findings support the notion that psychostimulant action is regulated by phospholipids and, possibly, by the interaction of phospholipids with plasma membrane proteins. In this study, we sought to understand how phospholipids, as well as their association with the DAT, regulate the psychomotor and rewarding actions of AMPH.

We have previously shown that pharmacologically limiting PIP_2 availability impairs AMPH's actions at DAT (63), as well as its ability to induce hyperlocomotion. However, how the interaction between PIP_2 and the DAT N-terminus supported AMPH behaviors remained unclear. Here, we found that limiting PIP_2 binding through neutralizing substitutions of Lys3 and Lys5 at the N-terminus limits AMPH-induced DAT phosphorylation, which is required for AMPH actions (68, 140, 141). Significantly, neither "sequestering" PIP_2 with a positively charged palmitoylated peptide nor pharmacologically depleting PIP_2 by inhibiting PIP_2 synthesis affected DA efflux once the DAT N-terminus had been pseudophosphorylated. Therefore, the electrostatic interactions between N-terminus Lys and PIP_2 regulate DAT phosphorylation. Moreover, following DAT phosphorylation, PIP_2 levels, as well as its interactions, are not critical to DA efflux.

Molecular dynamic simulations and biochemical experiments show that residue R443 also contributes to PIP_2 interactions. A neutralizing substitution at R443 (hDAT R443A) significantly decreased DAT/PIP_2 interactions. Specifically, this substitution was sufficient to disrupt the

electrostatic interactions between R443 (IL4) and PIP_2, as well as downregulate those between PIP_2 and N-terminus. Unsurprisingly, hDAT R443A displayed limited AMPH-induced DA efflux, suggesting that R443 electrostatic interactions are important for the reverse transport of DA.

Probing further the contribution of R443 to AMPH action, we found that a neutralizing substitution at R443 to Ala in a pseudophosphorylated hDAT (hDAT S/D) background (hDAT S/D R443A) reduced DA efflux relative hDAT S/D controls. Our MD simulations show that once phosphorylated, the N-terminus disrupts the interaction between IL4 and PIP_2. Also, we show *in vitro* that pseudophosphorylation of the N-terminus increases its affinity for IL4. Thus, a neutralizing substitution at R443 limits the physical interaction of an anionically charged N-terminus (phosphorylated) with the positively charged motif at IL4, an interaction we believe is required for DA efflux and behaviors.

It is important to note that reducing PIP_2 levels in hDAT S/D R443A cells did not further impair DA efflux. Once R443 electrostatics are neutralized with Ala substitution, PIP_2 levels lose their ability to regulate DA efflux. However, in this model, we cannot exclude the possibility that the amino acids surrounding R443, in the positively charged motif (His442-Arg443-His444-Arg445), also contribute to DA efflux. It is also important to consider the role of other DAT interacting proteins, including STX1 and Gβγ. STX1 interacts with the DAT N-terminus to support AMPH-induced DA efflux (69, 153, 296). In addition, Gβγ interacts with the carboxy terminus of DAT, whereby activation of Gβγ promotes AMPH-induced DA efflux and behaviors (71, 72). The actions of both Gβγ and STX1 are thought to be modulated by PIP_2 (71, 72, 155). Future studies are necessary to determine how and if these protein-protein and protein-lipid interactions work in concert to promote DA efflux.

Notably, in this study, we show that a neutralizing substitution of R443 in the DAT reduces the ability of AMPH to elicit psychomotor behaviors without altering basal locomotion. Locomotion is a fundamental behavior that enables seeking for rewarding stimuli including sex, food, and drugs. AMPH induces increased locomotor activity in *Drosophila* as in mammals (19, 43, 63, 122,

297). We found that hDAT R443A *Drosophila* were insensitive to locomotor actions of AMPH. These data are consistent with our *ex vivo* findings showing that DA efflux was significantly diminished in hDAT R443A compared with hDAT WT *Drosophila* brain. Intrigued by these results, we further explored whether R443, as well as DA efflux, played a role in the rewarding properties of AMPH.

Reward modulates the saliency of a specific drug exposure and is essential for the transition from drug exposure to addiction (298). We developed a new behavioral paradigm to measure AMPH preference in *Drosophila*. We show that a single amino acid substitution that disrupts IL4 electrostatic interactions, reduces DA efflux and preference for AMPH without affecting avoidance. Numerous human PET-fMRI studies have established a link between midbrain DA release/DAT availability and reward responses (285, 286). Recent findings showed that clinical subgroups with the lowest DAT levels displayed the lowest functional anticipatory reward activation (285). Based on these findings, it is not surprising that we found that animals with limited physiological responses to AMPH (i.e. DA efflux) displayed a lack of preference for AMPH. Finally, previous findings demonstrated inverted responses to higher concentrations of AMPH (290, 299). Here, in flies, we show that high AMPH concentrations cause avoidance. In contrast to AMPH preference, in our animal model, neutralizing the electrostatic interaction of R443 did not affect avoidance. Thus, AMPH avoidance in *Drosophila* is likely mediated by mechanisms that are independent of reverse transport of DA and/or are DAT independent (300). One possibility is that at higher concentrations, the bitter taste of AMPH itself drives an avoidance response. Alternatively, AMPH avoidance may also be regulated by glutamatergic and serotonergic inputs (301, 302) that are modified by AMPH and fine-tuned DA neurons. Recent studies in *Drosophila* illustrate that preference for other stimulants such as cocaine is sex-specific, thus, further studies to determine this potential contribution for AMPH preference are necessary.

We sought to understand the molecular mechanism through which structural domains of the DAT regulate the psychomotor and rewarding properties of AMPH. We developed a novel

behavioral paradigm in *Drosophila* to quantify AMPH's rewarding properties by measuring relative preference for AMPH and associate it with the ability of AMPH to cause DA efflux in brain. We uncovered how a specific residue in the DAT tightly regulates DA efflux and the rewarding properties of the psychostimulant AMPH.

Materials and Methods

Cell culture: pCIHygro expression vector was engineered to contain synhDAT WT (hDAT WT), synhDAT S/D (Ser 2, 4, 7, 12, 13 mutated to Asp; hDAT S/D), synhDAT R443A (Arg 443 mutated to Ala; hDAT R443A) and synhDAT S/D R443A (hDAT S/D R443A). Vector DNA was transfected into Chinese hamster ovary (CHO) cells as previously described (165).

^{3}H[DA] uptake assays: Cells were washed and equilibrated in KRH (37°C, 5 min) buffer composed of (in mM): 130 NaCl, 25 HEPES, 4.8 KCl, 1.2 KH_2PO_4, 1.1 $MgSO_4$, 2.2 $CaCl_2$, 10 d-glucose, 0.1 ascorbic acid, 0.1 pargyline, and 1.0 tropolone (pH 7.4). DA uptake kinetics were performed from 10 nM to 10 μM [^{3}H]DA (PerkinElmer Life Sciences, Waltham, MA) as previously described (63).

Amperometry and patch-clamp electrophysiology: Cells were washed with 37°C Lub's external solution composed of (in mM): 130 NaCl, 1.5 $CaCl_2$, 0.5 $MgSO_4$, 1.3 KH_2PO_4, 10 HEPES and 34 d-glucose (pH 7.4; 300-310 mOsms/L). Quartz patch-pipettes were used to intracellularly load DA (2 mM, Sigma Aldrich, St. Louis, MO) and/or PIP_2 inhibitory/control peptides (3 μM pal-HRQKHFEKRR or pal-HAQKHFEAAA) in internal solution containing (in mM): 110 KCl, 10 $NaCl_2$, 2 $MgCl_2$, 0.1 $CaCl_2$, 1.1 EGTA, 10 HEPES, 30 d-glucose and 2.0 DA (pH 7.4; 280-290 mOsms/L). To record AMPH-induced DA efflux (10 μM), a carbon fiber electrode held at +600 mV was juxtaposed to cells as previously described (63).

Biotinylation assays: Cells were washed with 4°C phosphate-buffered saline (PBS) supplemented with 0.9 mM $CaCl_2$ and 0.49 mM $MgCl_2$, incubated in 1.0 mg/ml sulfosuccinimidyl-2-(biotinamido)ethyl-1,3-dithiopropionate-biotin (sulfo-NHS-SS-biotin; Pierce, Rockford, IL) and

processed as previously described (165). Membranes were immunoblotted for DAT (1:1000) (MAB369; Millipore, Billerica, MA) and β-actin (1:5000) (A5441; Sigma-Aldrich; St. Louis, MO), and then quantified as previously described (165).

Immunoprecipitation assay: Cells expressing 6X-His, eGFP-tagged hDAT variants were lysed in buffer containing (mM): 20 Tris, 100 NaCl, and 20 n-Dodecyl-β-D-Maltopyranoside (DDM) supplemented with 10% glycerol and Protease Inhibitor Cocktail (1:100; Sigma Aldrich, St. Louis, MO). Equivalent hDAT concentrations were isolated using batch cobalt-based immobilized metal affinity chromatography. Cobalt beads were washed, incubated for 4 h with 1 uM BODIPY® TMR Phosphatidylinositol 4,5-bisphosphate, washed, and eluted in buffer supplemented with 300 mM Imidazole. Eluates were assayed in a TECAN Infinite 200 Pro microplate reader for eGFP (ex 454 / em 505 $\pm$ 9 nm) and PIP_2 (ex 542 / em 574 $\pm$ 9 nm).

DAT phosphorylation: hDAT WT, hDAT K/A and hDAT K/N cDNAs were generated within pcDNA 3.0 plasmid using site-directed mutagenesis. Griptite 293 MSR cells (ThermoFisher Scientific, Grand Island, NY) were transfected and metabolically labeled with $^{32}PO_4$ (>8500 Ci/mmol, Perkin Elmer) as described previously (140). DATs were immunoprecipitated with DAT C-terminal antibody C-20 (1433, Santa Cruz Biotech; Santa Cruz, CA) crosslinked to protein A sepharose followed by SDS-PAGE and autoradiography.

***Drosophila melanogaster* rearing and stocks:** All *Drosophila melanogaster* strains were grown and maintained on standard cornmeal-molasses media at 25°C under a 12:12 h light-dark schedule. Fly stocks include w^{1118} ((Bloomington Indiana Stock Center (BI) 6326), TH-GAL4 (BI 8848), $DAT^{MB07315}$ (BI 25547), UAS-mCherry (Kyoto Stock Center 109594), M[vas-int.Dm]ZH-2A; M[3xP3-RFP.attP']ZH-22A (BI 24481) and DAT^{fmn} (dDAT KO). *Drosophila* expressing homozygous dDAT null allele DAT^{fmn} (dDAT KO) (187), TH-Gal4 (251), and UAS-mcherry were outcrossed to control lines for 10 generations. Transgenes were cloned into pBI-UASC (252) and constructs were injected into embryos from BI 24481 (Rainbow Transgenic Flies Inc; Camarillo,

CA). Flies containing transgenes were outcrossed to dDAT KO flies (in w^{1118} background) for 10 generations. Final transgene generations were crossed to dDAT KO/TH-GAL4 flies.

^{3}H[DA] *Drosophila* uptake assays: *Drosophila* male brains were dissected quickly in ice-cold Schneider's Drosophila Medium (ThermoFisher Scientific) supplemented with 1.5% BSA. Single point DA uptake was measured by preincubating brains in either vehicle or 100 μM cocaine for 10 min followed by 200 nM [^{3}H]DA, as previously described (165). Cocaine values were subtracted from vehicle values to determine specific counts.

***Drosophila* amperometry assays:** *Drosophila* male brains were dissected in ice-cold Schneider's Drosophila Medium supplemented with 1.5% BSA. Whole brains were placed in a mesh holder in Lub's external solution (see previous). A carbon fiber electrode held at +600 mV was positioned in the TH-positive PPL1 DA neuronal region and DA efflux was recorded as previously described (165).

***Drosophila* locomotion analysis:** *Drosophila* male flies were transferred individually to activity tubes containing standard food. TriKinetics *Drosophila* Activity Monitoring (DAM) system (Waltham, MA) was used measure basal and AMPH-induced locomotion, as previously described (51, 52).

***Drosophila* two-choice AMPH administration paradigm:** To measure AMPH preference in *Drosophila,* we built custom vials to measure liquid food consumption from volumetric capillaries. Each vial contained two volumetric capillaries: capillary A (100 mM sucrose) and capillary B (100 mM sucrose; 500 μM blue dye). Food consumption was measured every 24 h when capillaries were replaced and refilled. Adult male flies were individually transferred to vials and acclimated to liquid food for 24 h. Baseline preference for capillary A and capillary B was assayed at 48 h. To determine AMPH preference, in experimental groups, capillary B was supplemented with AMPH (1 or 10 mM) and measured at 72 h. In control groups, capillary B was supplemented with vehicle (water) and measured at 72 h. Preference was determined as consumption of capillary B over total consumption (capillary A and capillary B) at 48 h (baseline) versus 72 h (preference).

Molecular dynamics (MD) simulations: The full length hDAT was taken from previous study (207). Four simulation systems were constructed: hDAT WT, hDAT R443A, hDAT S/D (Ser 2, 4, 7, 12 and 13 mutated to Asp), and hDAT S/D R443A. Transporters were embedded into neuronal membrane/lipids composed of 1-palmitoyl-2-oleoyl-sn-glycero-3-phosphoethanolamine (POPE) and -phosphocholine (POPC), cholesterol (CHOL), palmitoyl-oleoyl-phosphatidylinositol (POPI), and phosphatidylinositol 4,5-bisphosphate (PIP_2) using CHARMM-GUI Membrane Builder module (267). The lipid composition accounted for the asymmetric lipid distribution of neuronal membranes, as done previously (303). Fully equilibrated TIP3P waters were added to build a simulation box of ~102 ×102 ×140 Å, Na^+ and Cl^- ions were added to obtain a 0.15 M neutral solution. Each simulation system contained ~ 134,000 atoms, ~290 lipid molecules, and 30,000 water molecules. All simulations were performed using the MD NAMD package (268) as previously (303). For each system, two or three independent runs of up to 200 ns were performed. The probability of PIP_2 binding was evaluated as the frequency of PIP_2/DAT contacts; mainly, the fraction of 0.2 ns snapshots where PIP_2 was located within 4.0 Å from any DAT atom.

N-terminus/IL4 binding assay: The hDAT WT or hDAT S/D (Ser 2,4,7,12,13 mutated to Asp) N-terminus were cloned into pAT109 with a N-terminus GST and C-terminus His-tag. Proteins were expressed in Bl21(DE3) *E. coli.* Bacteria were induced with 0.5 mM isopropylβ-d-1thiogalactopyranoside, pelleted, and lysed with lysozyme and 1% Triton-X100. Supernatants were isolated and bound to HisPur Cobalt Resin (ThermoFisher Scientific), eluted with 0.5 M imidazole, dialyzed and applied to a glutathione column (GE Healthcare Life Sciences, Chicago, IL). Protein was eluted with 10 mM glutathione, dialyzed, centrifuged and protein quantified. Soluble, fluorescent IL4 (RHodamine-(PEGx3)-IDEFQLLHRHRE) was synthesized by the peptide synthesis core at University of Texas Southwestern. N-terminus of hDAT (WT and S/D) (2 μM) and IL4 (3 μM) were incubated for 2 h at RT in 25 mM HEPES (pH 7.2), 2 mM DTT and 15 mM NaCl. Magnetic cobalt loaded beads were applied, incubated for 30 min, and washed three times

in binding buffer. Beads were eluted with 0.3 M imidazole and assayed for fluorescence using TECAN Infinite 200 Pro microplate (ex 546 / em 579 ± 9 nm)

Statistical methods: Both animal and cell studies were designed using statistical power calculations considering means and standard errors from preliminary data. For example, our calculation rendered a minimum sample size of n = 6 for *ex vivo* animal studies (power=80%, α=0.05). We estimated a maximum attrition of 33%; thus, we needed 10 animals per group. Shapiro-Wilk normality tests were performed to evaluate sample distributions. Appropriate nonparametric tests were performed to compare samples with unequal variances. Otherwise parametric tests were used to compare data. Experiments were performed at random, except when indicated. In such cases, experiments were performed paired. Appropriate statistical analyses were conducted to reflect the paradigm used. Preference assays were performed blinded to genotype. All other animal studies were performed unblinded.

Chapter IV

ATYPICAL DOPAMINE EFFLUX CAUSED BY 3,4-METHYLENEDIOXYPYROVALERONE VIA THE HUMAN DOPAMINE TRANSPORTER

The work described in this chapter is part of, and adapted from the published manuscript "Shekar A*, Aguilar JI*, *et al*. Atypical dopamine efflux caused by 3,4-methylenedioxypyrovalerone (MDPV) via the human dopamine transporter. *J Chem Neuroanat*. 2017"

* denotes equal contribution

Abstract

Recently synthetic cathinone drugs or "bath salts" have become a major health concern, as use and abuse of these drugs continues to rise. Use of these designer drugs can result in severe cardiovascular and psychiatric symptoms, including tachycardia, delusions, hallucinations, seizures and even death. MDPV, the principal constituent in bath salts is associated with many of these deleterious stimulant and hallucinogenic effects. Similar to other psychostimulants, including cocaine and amphetamine, MPDV exerts its physiological effects through its action on the dopamine transporter (DAT). Previous studies have shown that MDPV acts as a high affinity blocker of the DAT at micromolar-range concentrations and elicits amphetamine-like behavioral effects. In this study, we demonstrate for the first time, a new mode of action of MDPV, namely its ability to promote DAT-mediated DA efflux. Using single cell amperometric assays, we determined that nanomolar-range concentrations of MDPV can cause reverse transport of DA via DAT. Notably, administration of MDPV leads to hyperlocomotion in *Drosophila* melanogaster. By uncovering a new mode of action for MPDV, these findings reveal a new area of research these designer drugs, and potentially new therapeutic strategies to treat the individuals that abuse them.

Introduction

The neurotransmitter dopamine (DA) mediates behaviors relating to reward, motivation, attention, and cognition (205, 304). Important to dopamine neurotransmission is the dopamine transporter (DAT). DAT is a presynaptic membrane protein responsible for the reuptake and recycling of DA following vesicular release (43). Dysfunctions in DAT can lead to dopamine-associated neuropsychiatric disorders including ADHD, autism spectrum disorders, schizophrenia, and bipolar disorder(305). DAT is also the target of commonly abused psychostimulants and controlled substances, namely cocaine and amphetamine (AMPH). Cocaine acts as a high-affinity antagonist of the transporter and blocks DA uptake, whereas AMPH acts as a substrate of the transporter and, through a series of intracellular mechanisms, causes DAT to reverse transport or "efflux" DA into the extracellular space(306). The actions of cocaine and AMPH on the DAT are well-known to play a role in their rewarding properties and abuse potential. Thus, determining the effects of psychostimulants on DAT function is important for understanding the neural and molecular mechanisms underlying psychostimulant drug action.

In recent years, the abuse of synthetic cathinones or "bath salts" has grown to become a major world-wide health concern (307). These substances are synthetic derivatives of the naturally-occurring stimulant, cathinone, found in the flowering plant *Catha edulis* (308). The psychoactive effects of synthetic cathinones vary from the cocaine-like stimulant effects seen with 3,4-methylenedioxypyrovalerone (MDPV) (309) to the MDMA-like empathogenic effects of methylone (3,4-methylenedioxymethcathinone) (310). Among a number of identified biological sites, cathinones are known to target proteins that modulate dopamine neurotransmission, increasing dopaminergic signaling and associated behaviors (311-316), including drug-seeking(317, 318). When consumed in small doses, cathinones can lead to euphoria, alertness, increased libido, and elevated blood pressure. When consumed at higher doses, tremors, seizures, paranoia, violent behavior, psychoses, tachycardia (319), delusions/hallucinations (320), and death(321) can occur. A recent report released by the Substance Abuse and Mental

Health Services Administration (SAMHSA) showed that nearly 23,000 emergency room visits in 2011 were a result of cathinone abuse (322). Due to the high risk associated with the use and the abuse potential of these compounds, the Drug Enforcement Administration (DEA) designated mephedrone (4-methylmethcathinone), methylone and MDPV as Schedule 1 substances under the Controlled Substances Act (323). Nonetheless, illegal manufacturers continue to circumvent this ban by synthesizing "designer" substances with novel chemical structures but which produce similar psychostimulant effects (324). These compounds are readily available; sold with fraudulent labels such as “plant food”, “research chemicals”, or “bath salts” at gas stations, tobacco stores, and over the Internet with a warning that the contents are not intended for human consumption. Their continued production and availability make it nearly impossible to control the exponentially rising sales and consumption of synthetic cathinones.

Despite increased data regarding the use and abuse of cathinones(325), little is known about their mechanism of action. To address this issue, several research groups have begun to study the chemistry, pharmacology, and behavioral effects of various synthetic cathinones. Of these, MDPV is most commonly implicated in high-risk use (319, 321, 324, 326-330). First synthesized in 1969, MDPV gained popularity much later in 2010 (331). As a highly lipophilic analogue of the synthetic cathinone pyrovalerone (332), MDPV readily crosses the blood-brain barrier. Importantly, MDPV, when administered to animals exhibits striatal distribution, a brain region enriched in DA projections (314). MDPV also shows high abuse potential in animal behavioral tasks (313-315, 333).

Early research on MDPV demonstrated that this drug acts similarly to cocaine (a known DAT blocker), but with a 10- to 50-fold higher potency (309, 334). However, increasing data suggests that there may be more to MDPV action. Work from Bauman *et al.* showed that after intravenous administration of MDPV, DA levels remain elevated for far longer than after cocaine administration(309). In addition, MDPV administration results in long lasting cross-sensitization in mice, similar to the effects of methamphetamine (317). These results suggest that MDPV, in

addition to acting as a DAT blocker, may also display other modes of action. To examine further the molecular mechanisms of MDPV on the DAT, we performed amperometric studies. Specifically, to obtain greater temporal resolution, we studied MDPV action on human DAT (hDAT) by employing single cell amperometry. This assay has been previously used to discriminate AMPH versus cocaine actions in a single cell and these results have been reproduced in different model systems (52). Further, we assessed MDPV-induced behaviors in *Drosophila melanogaster*, specifically focusing on known DAT-associated behaviors. *Drosophila* is a powerful genetic model for studying behaviors that are associated with DA as well as promoted by psychostimulants (51, 52, 63), as several genes that regulate DA transport, synthesis, and signaling are conserved between flies and humans (178).

Results

1 nM MDPV alone does not produce an amperometric signal

As a first control experiment, we demonstrated that hDAT cells pre-loaded with DA (see methods section) did not release DA upon application of vehicle (**Fig. 40**, Vehicle). Next, we tested whether MDPV alone does not react at the carbon fiber electrode. At concentrations as low as 1 nM, MDPV did not elicit any amperometric current when applied to a bath chamber in the absence of hDAT cells (**Fig. 40**, MDPV). Finally, to demonstrate that we can record DA efflux with our amperometric electrode, we show that bath application of 10 μM AMPH causes a robust DA efflux in the presence of hDAT cells (**Fig. 40**, AMPH). We have previously shown that this AMPH-induced DA efflux is mediated by the hDAT and is cocaine-sensitive (156). These control experiments were conducted to ensure that amperometry is a fitting technique to elucidate the actions of MDPV in terms of DA efflux and that MDPV at a concentration of 1 nM does not produce a non-specific amperometric signal.

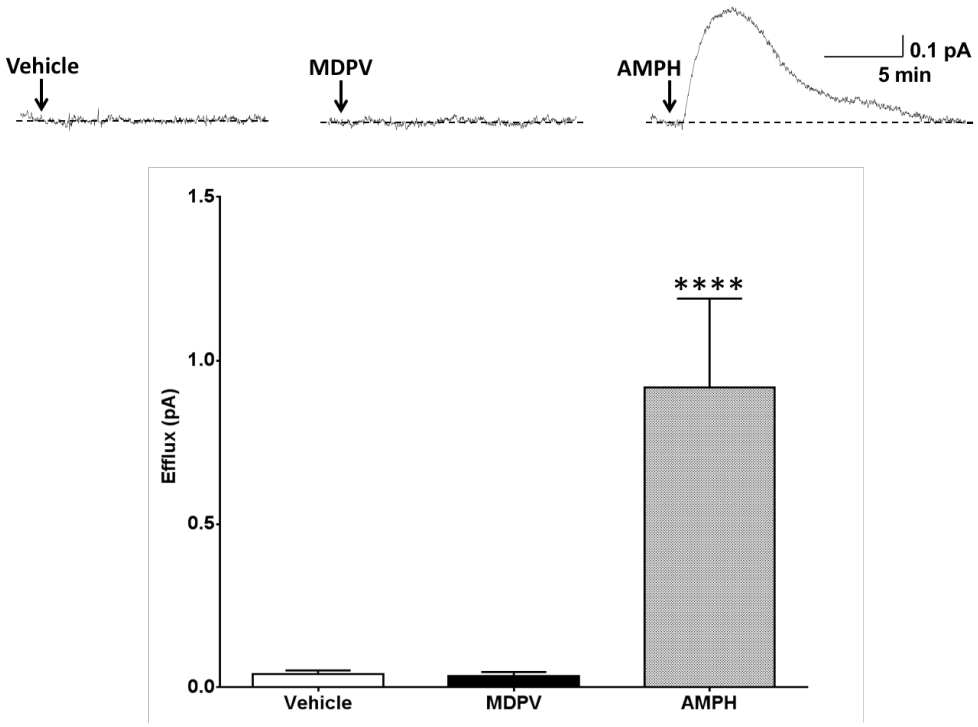

Figure 40: 1 nM MDPV does not elicit an amperometric current in the absence of hDAT cells

Top: Representative amperometric traces recorded from hDAT cells in response to application of vehicle to (Vehicle), application of 1 nM MDPV to bath in the absence of hDAT cells (MDPV), or application of 10 μM AMPH in the presence of hDAT cells. Bottom: Quantitation of the peak amperometric current amplitude measured after vehicle or drug treatment (**** = $p < 0.0001$ by One-way ANOVA with Dunnett's multiple comparisons post-hoc analysis; n = 5–6).

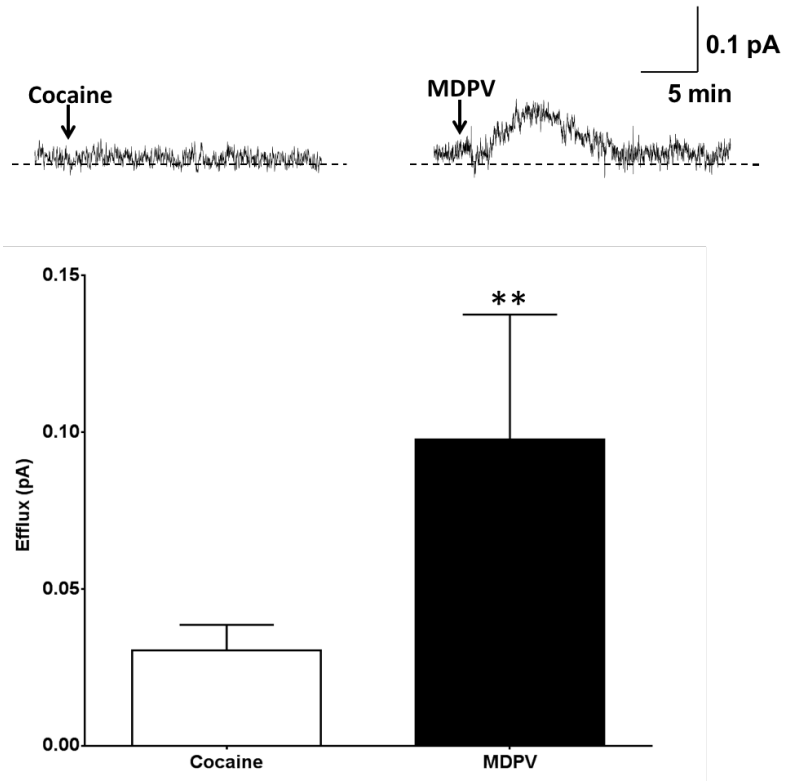

Figure 41: MDPV, but not cocaine, induces reverse transport of DA via hDAT in cells

Top: Representative amperometric traces recorded in response to 10 μM cocaine or 1 nM MDPV from hDAT cells. Bottom: Quantitation of DA efflux measured as peak amplitude of the amperometric current after drug or vehicle treatment (** = $p < 0.01$ by Student's t-test; n = 5–8).

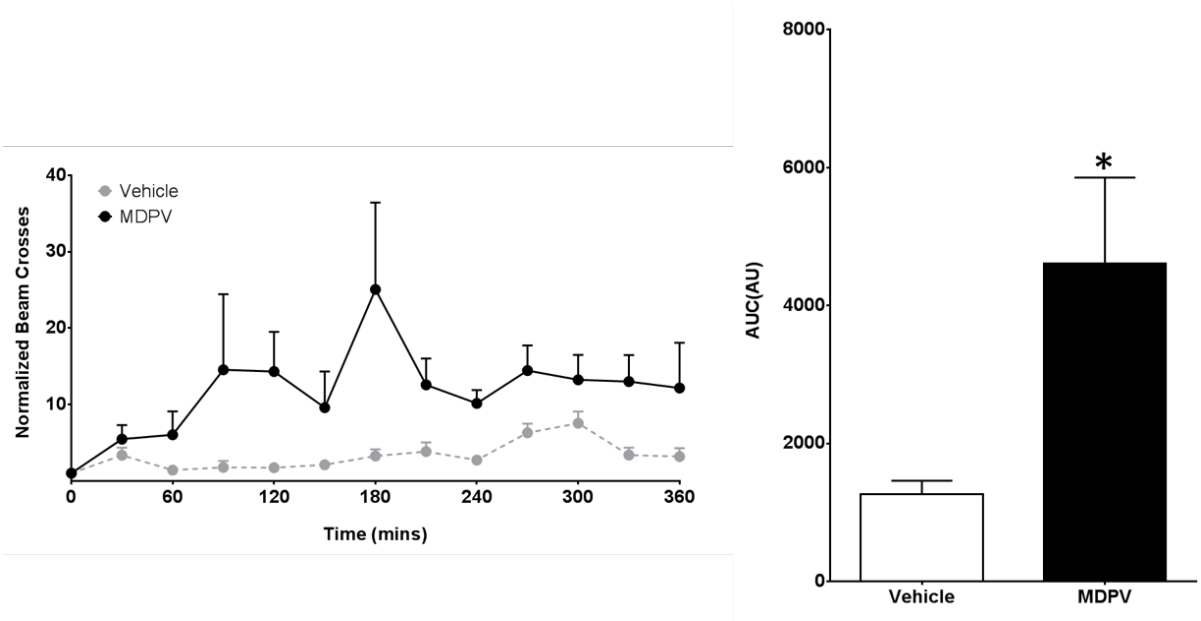

Figure 42: MDPV induces hyperlocomotion in flies

Left: Locomotion was measured by average beam crosses following 20 μM MDPV (n = 16) or vehicle (n = 15) administration. Beam crosses were normalized to pre-treatment conditions for each fly. Right: Cumulative beam breaks were quantified for up to six hours post drug or vehicle administration. Flies exposed to MDPV displayed an increase in cumulative bream breaks compared with vehicle-controls (* = $p < 0.05$ by Student's t-test; n = 15–16).

New mode of action of MDPV

24 hours after plating, hDAT cells were preloaded with DA (see methods). Amperometric measurements were taken from individual hDAT cells after application of a low concentration of MDPV (1 nM) or cocaine (10 μM). As expected, 10 μM cocaine did not cause DA efflux as reflected by a lack of an upward deflection of the amperometric trace. These data are in agreement with previously published studies (51, 156) and also establishes that there is no anomalous dopamine efflux or "leak" associated with the transporter in this *in vitro* system as previously shown (156). Surprisingly, and in contrast to the effects of cocaine, amperometric traces recorded in response to 1 nM MDPV show a clear upward deflection of the amperometric current. This upward deflection reflects DAT-mediated DA efflux (**Fig. 41**, MDPV). To note, hDAT cells the peak amperometric responses for MDPV were smaller than those recorded for AMPH (positive controls; compare **Fig. 40** (AMPH) to **Fig. 41** (MDPV).

MDPV causes hyperlocomotion in flies

Building on our *in vitro* findings, we examined MDPV's role in modifying DA-associated behaviors in *Drosophila melanogaster*. Wildtype flies were placed in locomotion chambers and acclimated for a period of five days. 20 μM MDPV or vehicle was administered orally via voluntary consumption. Locomotion was quantified as average beam crosses per 30 minutes normalized to pre-treatment conditions. Flies administered MDPV (n = 16) show an elevated rate of locomotion compared with those administered vehicle (n = 15) (**Fig. 42**). Cumulative beam breaks over a period of 6 hours show a greater than two-fold increase in locomotion in flies administered MDPV compared with vehicle (**Fig. 42**).

Discussion

DA homeostasis in the central nervous system is essential to regulating important brain functions, including reward. Synthetic cathinones disrupt normal dopaminergic neurotransmission and thus affect DA-associated behaviors. These drugs elicit behaviors indicative of enhanced

dopaminergic signaling. The past ten years of research on MDPV and other synthetic cathinones demonstrate that the rewarding properties of synthetic cathinones are derived, in part, from their actions on monoamine transporters (335, 336). Understanding how MDPV disrupts normal DA neurotransmission *via* its actions on the DAT is essential to the development of novel treatment options that can restore normal DA homeostasis in individuals that abuse MDPV and other synthetic cathinones. In this study, we aimed to reveal new modes by which low concentrations of MDPV cause an elevation in extracellular DA levels, and the behavioral consequences of its actions on DAT.

Using single cell amperometry we reveal that low concentrations of MDPV (1 nM) cause reverse transport of DA *via* DAT. Amperometry is a well-established paradigm that has been used by our group and others in several studies to determine different aspects of monoamine release mediated by catecholamine transporters (i.e. vesicular release or membrane diffusion)(51, 52, 63, 167). We first established that this assay is suitable for studying reverse transport of DA mediated by MDPV. We conducted an initial characterization of MDPV to demonstrate that at low concentrations, MDPV does not interact with the carbon fiber electrode to produce an artificial signal. Next, we demonstrate that in hDAT cells MDPV (1 nM) causes reverse transport of DA mediated by hDAT. To note is that high concentrations of MDPV, such as 100 nM, cause a non-specific amperometric signal (i.e. an amperometric current is recorded with MDPV in the absence of hDAT cells). These data describe for the first time a novel mode of action of MDPV at the DAT. Interestingly and importantly, previous work with hDAT has shown that higher concentrations of MDPV can block DAT function (20-30 nM) (309). Taken together, these data suggest that MDPV might have multiple modes of action that are concentration-dependent, where at low concentrations MDPV works to cause DAT reverse transport, and at high concentrations MDPV primarily causes DAT blockade.

Drosophila melanogaster has been used in the past as a model organism to study the behavioral consequences of newly discovered molecular mechanisms of AMPH and

cocaine(122),(19). In *Drosophila*, locomotion requires functional DA neurotransmission. Therefore, to understand the significance of the actions of MDPV *in vivo*, in terms of changes in extracellular DA levels, we use flies as a behavioral model. Here, we show that MDPV administration leads to hyperlocomotion in *Drosophila melanogaster*. These data point to *Drosophila melanogaster* as a good animal model to further characterize *in vivo* the multiple actions of MDPV at the hDAT. This increase in locomotor activity has been previously documented to be associated with an increased in extracellular DA promoted by DAT blockers (e.g. cocaine) as well as DA effluxers (e.g. AMPH).

In this study, we did not determine whether the increase in *Drosophila* locomotion is driven by either the MDPV ability to block the hDAT, to cause DA efflux, or both. In the near future, we aim to explore these different possibilities by generating flies that are insensitive to the ability of MDPV to cause DA efflux, as we have done for AMPH (data not shown).

Further studying the different mode of actions of MDPV and other synthetic cathinone drugs as well as their specific behavioral consequences will not only lead to better treatment strategies for those who abuse them, but will also lead to better recognition/prediction of the dangers posed by novel designer cathinones that are emerging in the market today.

Materials and Methods

Drugs: (±)-3,4-Methylenedioxypyrovalerone HCl (MDPV), was synthesized in racemic form in our laboratories. Chemical and structural analysis included proton nuclear magnetic resonance, gas chromatography/mass spectrometry, thin layer chromatography, and melting point determination. All data were consistent with the expected structures. All other drugs used in this study including their salt and enantiomeric forms were as follows and purchased from Sigma-Aldrich (St. Louis, MO): Dopamine (i.e., 3-hydroxytyramine hydrochloride), D-amphetamine hemisulphate salt and Cocaine hydrochloride.

Amperometry: Chinese hamster ovary (CHO) cells stably expressing hDAT (here defined as hDAT cells) were plated at a density of ~20,000 per 35-mm culture dish. To preload cells with DA, dishes were washed with KRH assay buffer (130 mM NaCl, 4.8 mM KCl, 1.2 mM KH_2PO_4, 25 mM HEPES, 1.1mM $MgSO_4$ 2.2 mM $CaCl_2$, pH 7.4) supplemented with 10 mM dextrose, 100 μM pargyline, 1 mM tropolone, and 100 μM ascorbic acid, and incubated with 1 μM DA in KRH assay buffer for 20 minutes at 37°C. To record DA efflux, a carbon fiber electrode (ProCFE; fiber diameter of 5 μm; obtained from Dagan Corporation) juxtaposed to the plasma membrane and held at +700 mV (a potential greater than the oxidation potential of DA) was used to measure DA flux through oxidation reactions. Amperometric currents in response to the addition of 1 nM MDPV were recorded using an Axopatch 200B amplifier (Molecular Devices, Union City, CA) with a low-pass Bessel filter set at 1 kHz; traces were digitally filtered offline at 1 Hz using Clampex9 software (Molecular Devices, Union City, CA). DA efflux was quantified as the peak value of the amperometric current.

***Drosophila melanogaster* Behavior:** To measure the locomotor response to MDPV we used the TriKinetics *Drosophila* Activity Monitoring (DAM) system as described in earlier studies (337, 338). Wild-type Oregon-R male flies were entrained for seven days in 12:12 h light:dark (LD) cycles at 25°C on standard cornmeal-molasses medium. On day two, flies were transferred individually to activity tubes and acclimated for a period of five days. On day seven, flies were transferred into identical activity tubes containing 20 μM MDPV or vehicle (water) in standard medium. Activity was continuously measured as the number of times a fly crossed the infrared beam (beam crosses) per 30 minutes. Activity data was recorded for six hours after drug administration. Change in activity in response to drug treatment was reported as beam crosses normalized to average beam crosses 30 minutes prior to drug administration.

CHAPTER V

FUTURE DIRECTIONS

The DAT regulates the spatial and temporal dynamics of extracellular DA levels, maintaining DA homeostasis. Multiple neuropsychiatric and neurological disorders (47, 48) (49-52) are associated with abnormal DA tone. Recent studies have identified rare variants in the DAT in patients with DTDS (162, 163), early-onset PD (164), ASD (50-52, 165-167), ADHD (164, 168) among others (169); directly implicating DAT dysfunction in many of these disorders. The DAT is also the target for various pharmacological agents that are used to treat these disorders as well as drugs of abuse and neurotoxins. Studies focusing on DAT structure, function and regulation have provided significant insight into DAT trafficking, binding partners and transport; however, much remains unclear about the mechanisms that underlie psychostimulant action as well as how DAT dysfunction underlies disease pathology. To this end, the studies outlined in this dissertation focus on defining (1) the structural and functional mechanisms that underlie DAT dysfunction and how DAT dysfunction contributes to specific behaviors associated with DTDS pathology and (2) molecular mechanisms that underlie DA efflux induced by AMPH and MDPV.

Chapter II provided valuable structural, dynamic, and behavioral insights into a DTDS-associated hDAT variant, R445C. Substitutions at R445C disrupted an IC network of interactions, which conferred a channel-like intermediate in the hDAT and impaired hDAT function and expression. *Drosophila* expressing hDAT R445C exhibited motor deficits, characterized by lack of movement vigor and coordination that is typically associated with DTDS and PD phenotypes. These behaviors were linked with altered DAergic signaling that stemmed from a loss of DA neurons and reduced DA availability. Together these studies shed light on how a DTDS-linked DAT underlies phenotypes observed in DTDS and PD, more broadly.

Chapter II also unveiled that specific substitutions at R445 have differential effects on DAT function. Although MD simulations suggested that Arg, Asp or Ala substitutions at R445 in the hDAT confer a channel-like mode, electrophysiological studies measured DA leak (ADE) only in hDAT R445A. This dichotomy poses an interesting question: Is persistent DA leak (ADE) necessitated by a channel-like mode? ADE has been measured in two other DAT variants A559V, identified in patients with ASD, ADHD and bipolar disorder and T356M identified in a patient with ASD. Whether T356M supports channel-like activity has not been tested. On the contrary, hDAT A559V was found to support a channel-like mode in the DAT, where D2R antagonism and CAMKII-inhibition damped channel-like activity and ADE (86). Together, these data suggest that ADE is supported by channel-like activity in hDAT A559V likely through a common signaling pathway. Future studies will use electrophysiological methods to determine whether ADE in hDAT R445A is necessitated by a channel-like mode and whether ADE occurs through similar mechanisms observed in hDAT A559V. Specifically, we will assess D2R antagonism and CAMKII-inhibition in suppressing channel-like activity or ADE. In addition, we will use phosphodeficient variants (hDAT S/A R445A) to define the role of N-terminal phosphorylation in supporting channel-like activity in hDAT R445A. Additional studies will evaluate whether channel-like activity conferred by hDAT variants (R445A, T356M, A559V) is sufficient to depolarize DA neurons, resulting in D2R/ CAMKII activation. Together, these findings will determine whether ADE in hDAT R445A occurs through a channel-like mode and whether a common mechanism promotes channel-like activity across DAT variants.

Future studies will also focus on understanding disease progression in this *Drosophila* model of DTDS. DA dysfunction and motor deficits were not observed early in the life-span of hDAT R445C *Drosophila* (data not shown), suggesting that these phenotypes are progressive in nature. Foremost, we will use more sophisticated behavioral analyses, such as those available through DeepLabCut to determine if subtle changes in gait or in movement fluidity precede more noticeable deficits in movement vigor or coordination. In addition, it is possible that non-motor

phenotypes which in humans usually precede full PD prognosis are present earlier in this model. To this end, we will determine if there are disruptions in circadian rhythms, increased anxiety-like behaviors or hyposmia (inability to smell) in hDAT R445C *Drosophila*. The identification of early symptoms will allow us to test whether early pharmacological interventions (i.e. CQ) are more effective in preventing or delaying deficits in movement coordination.

Chapter III established that DAT/PIP_2 interactions are necessary for AMPH-induced DAT phosphorylation, a modification required for DA efflux. Previous work from the Galli Lab demonstrated that PIP_2 directly interacts with the DAT N-terminus to regulate DA efflux (63). N-terminal Lys 3 and 5 were found to mediate this interaction, where neutralizing substitutions at these sites (hDAT K/A) weakened DAT/PIP_2 interactions and decreased AMPH-induced DA efflux and behaviors. Chapter III showed that the association between DAT/PIP_2 specifically regulates AMPH-induced DA efflux by promoting N-terminal phosphorylation. Notably, we found that PIP_2 was not essential in coordinating the interaction of the phosphorylated N-terminus with IL4, as shown through pharmacological depletion and peptide-mediated "sequestration" of PIP_2 levels. Disrupting N-terminus/IL4 interactions by a neutralizing substitution at a key residue, R443 (hDAT R443A) impaired AMPH-induced DA efflux in *Drosophila* brains and inhibited AMPH's psychomotor and rewarding effects in *Drosophila*. Interestingly, AMPH avoidance at high concentrations was maintained suggesting that this behavior is likely mediated by mechanisms that are independent of DA efflux and/or are DAT independent.

Although Chapter III clarified the role of DAT/PIP_2 interactions in DA efflux, PIP_2 has been shown to modulate the interaction of the DAT with other binding partners, including STX1 (71, 72, 155). Thus, future studies are necessary to determine if and how these protein-protein and protein-lipid interactions work in concert to promote DA efflux. Recent studies showed that STX1 binds the DAT N-terminus to promote DA efflux (52, 69). STX1 phosphorylation increases DAT/STX1 association and is required for DA efflux (52). PIP_2 is thought to coordinate STX1 phosphorylation, DAT/STX1 associations and DA efflux; however, the details of this mechanism

remain unclear. Unaddressed is whether (1) STX1 N-terminus and DAT N-terminus compete for PIP_2 binding, (2) the phosphorylated state of the DAT N-terminus regulates STX1 association, (3) STX1 binding regulates DAT phosphorylation and/or (4) phosphorylated versions of these proteins interact with PIP_2. To address these questions, I suggest a multipronged approach that utilizes MD simulations, biochemistry and FRET. These approaches will be used to determine whether DAT/PIP_2/STX1 form a single complex or whether DAT has a higher affinity for STX1 or PIP_2. The use of pseudophosphorylated or phospho-deficient mutants of hDAT and STX1 will also clarify whether the phosphorylation state of each protein modulates their interactions. Finally, the use of pharmacological PIP_2 depletion or peptide-mediated PIP_2 sequestration in combination with these mutants will clarify the role of PIP_2 in regulating the association of the DAT/STX1 in various phosphorylation states. Finally, to determine whether DAT phosphorylation is altered in these conditions we will quantify DAT phosphorylation by metabolic labeling ($^{32}PO_4$). Together, these findings will elucidate how DAT/PIP_2/STX1 interact to promote DAT phosphorylation and AMPH-induced DA efflux.

Chapter III also developed two critical tools: (1) a *Drosophila* model to specifically study the contribution of AMPH-induced DA efflux to behaviors and (2) a two-choice administration paradigm that can be employed in future studies to define the mechanisms that underlie reward motivation, and perseverance. *Drosophila* brains expressing hDAT R443A uptake DA normally, but have impaired AMPH-induced DA efflux. Thus, in this animal model the known physiological function of the DAT (DA uptake) is uncoupled from AMPH-induced reverse transport. Future studies will utilize this *Drosophila* model to define the contribution of DA efflux to various AMPH-associated behaviors. For, example AMPHs increase attention and as such are effectively and commonly used to treat ADHD. To date, the contribution of DA efflux to changes in attention-like behavior has not been explored. Using our existing *Drosophila* model, in combination with paradigms to measure visual attention, including flight paradigms, future studies will assess the contribution of AMPH-induced DA efflux to attention-like behaviors. Further, common side effects

of AMPHs use include anorexia, loss-of-appetite and anxiety, among others. Our *Drosophila* model will be used to study the contribution of AMPH-induced DA efflux to these behaviors. Notably, through the use of various genetic and pharmacological tools we will also begin to disentangle the contribution of the serotonergic system to these AMPH-associated behaviors.

The two-choice administration paradigm developed here will be employed to understand the rewarding properties of various stimulants, including cocaine, and MPDV as well as food. Various modifications to this paradigm can be made to measure other aspects of drug use. For example, motivation can be measured by placing rewarding stimuli at farther and farther distances away from flight-deficient animals. Thus, allowing us to determine the maximum distance an animal will travel for a rewarding stimulus. We can also measure persistence using this paradigm. We can fill a single capillary with both aversive (quinine) and rewarding (cocaine) stimuli, to determine the concentrations of aversive stimulus through which an animal will continue to pursue a rewarding stimulus. In this way, the experimental paradigms developed in this Chapter will assess various aspects of drug use as well as the contribution of DA efflux to AMPH behaviors.

Chapter IV showed that a major constituent of bath salts, MDPV has actions similar to that of AMPH at low concentrations, promoting DA efflux and similar to that of cocaine at high concentrations, inhibiting DA uptake. Future studies will explore the molecular mechanisms regulating MPDV-stimulated DA efflux. These studies will test the requirement for DAT N-terminus phosphorylation, involvement of various DAT interacting partners and activation of downstream signaling pathways. Studies will also focus on understating specific behaviors associated with MPDV administration. Together, these studies will assess whether MDPV and AMPH cause DAT reverse transport via independent versus overlapping mechanisms.

REFERENCES

1. Hornykiewicz O. Dopamine miracle: from brain homogenate to dopamine replacement. Mov Disord. 2002;17(3):501-8.
2. Marsden CA. Dopamine: the rewarding years. Br J Pharmacol. 2006;147 Suppl 1:S136-44.
3. Montagu KA. Catechol compounds in rat tissues and in brains of different animals. Nature. 1957;180(4579):244-5.
4. Carlsson A, Lindqvist M, Magnusson T, Waldeck B. On the presence of 3-hydroxytyramine in brain. Science. 1958;127(3296):471.
5. Shippenberg TS, Thompson AC. Overview of microdialysis. Curr Protoc Neurosci. 2001;Chapter 7:Unit7 1.
6. Rubi B, Maechler P. Minireview: new roles for peripheral dopamine on metabolic control and tumor growth: let's seek the balance. Endocrinology. 2010;151(12):5570-81.
7. Murphy MB. Dopamine: a role in the pathogenesis and treatment of hypertension. J Hum Hypertens. 2000;14 Suppl 1:S47-50.
8. Ciarka A, Vincent JL, van de Borne P. The effects of dopamine on the respiratory system: friend or foe? Pulm Pharmacol Ther. 2007;20(6):607-15.
9. McDonald RH, Jr., Goldberg LI, McNay JL, Tuttle EP, Jr. Effect of Dopamine in Man: Augmentation of Sodium Excretion, Glomerular Filtration Rate, and Renal Plasma Flow. J Clin Invest. 1964;43:1116-24.
10. Li ZS, Schmauss C, Cuenca A, Ratcliffe E, Gershon MD. Physiological modulation of intestinal motility by enteric dopaminergic neurons and the D2 receptor: analysis of dopamine receptor expression, location, development, and function in wild-type and knock-out mice. J Neurosci. 2006;26(10):2798-807.

11. Dunkley PR, Bobrovskaya L, Graham ME, von Nagy-Felsobuki EI, Dickson PW. Tyrosine hydroxylase phosphorylation: regulation and consequences. Journal of neurochemistry. 2004;91(5):1025-43.
12. Meiser J, Weindl D, Hiller K. Complexity of dopamine metabolism. Cell Commun Signal. 2013;11(1):34.
13. Ford CP. The role of D2-autoreceptors in regulating dopamine neuron activity and transmission. Neuroscience. 2014;282:13-22.
14. Pothos EN, Mosharov E, Liu KP, Setlik W, Haburcak M, Baldini G, et al. Stimulation-dependent regulation of the pH, volume and quantal size of bovine and rodent secretory vesicles. J Physiol. 2002;542(Pt 2):453-76.
15. Pothos EN, Larsen KE, Krantz DE, Liu Y, Haycock JW, Setlik W, et al. Synaptic vesicle transporter expression regulates vesicle phenotype and quantal size. Journal of Neuroscience. 2000;20(19):7297-306.
16. Blakely RD, Edwards RH. Vesicular and plasma membrane transporters for neurotransmitters. Cold Spring Harb Perspect Biol. 2012;4(2).
17. Sulzer D, Pothos EN. Regulation of quantal size by presynaptic mechanisms. Rev Neurosci. 2000;11(2-3):159-212.
18. Edwards RH. The neurotransmitter cycle and quantal size. Neuron. 2007;55(6):835-58.
19. Freyberg Z, Sonders MS, Aguilar JI, Hiranita T, Karam CS, Flores J, et al. Mechanisms of amphetamine action illuminated through optical monitoring of dopamine synaptic vesicles in Drosophila brain. Nature communications. 2016;7:10652.
20. Goh GY, Huang H, Ullman J, Borre L, Hnasko TS, Trussell LO, et al. Presynaptic regulation of quantal size: K+/H+ exchange stimulates vesicular glutamate transport. Nat Neurosci. 2011;14(10):1285-92.
21. Hnasko TS, Edwards RH. Neurotransmitter corelease: mechanism and physiological role. Annual review of physiology. 2012;74:225-43.

22. Aguilar JI, Dunn M, Mingote S, Karam CS, Farino ZJ, Sonders MS, et al. Neuronal Depolarization Drives Increased Dopamine Synaptic Vesicle Loading via VGLUT. Neuron. 2017;95(5):1074-88 e7.
23. Fon EA, Pothos EN, Sun BC, Killeen N, Sulzer D, Edwards RH. Vesicular transport regulates monoamine storage and release but is not essential for amphetamine action. Neuron. 1997;19(6):1271-83.
24. Wang YM, Gainetdinov RR, Fumagalli F, Xu F, Jones SR, Bock CB, et al. Knockout of the vesicular monoamine transporter 2 gene results in neonatal death and supersensitivity to cocaine and amphetamine. Neuron. 1997;19(6):1285-96.
25. Segura-Aguilar J, Paris I, Munoz P, Ferrari E, Zecca L, Zucca FA. Protective and toxic roles of dopamine in Parkinson's disease. Journal of neurochemistry. 2014;129(6):898-915.
26. Graves SM, Xie Z, Stout KA, Zampese E, Burbulla LF, Shih JC, et al. Dopamine metabolism by a monoamine oxidase mitochondrial shuttle activates the electron transport chain. Nat Neurosci. 2020;23(1):15-20.
27. Goto Y, Otani S, Grace AA. The Yin and Yang of dopamine release: a new perspective. Neuropharmacology. 2007;53(5):583-7.
28. Baik JH. Dopamine signaling in reward-related behaviors. Front Neural Circuits. 2013;7:152.
29. Berke JD. What does dopamine mean? Nat Neurosci. 2018;21(6):787-93.
30. Zhang L, Doyon WM, Clark JJ, Phillips PE, Dani JA. Controls of tonic and phasic dopamine transmission in the dorsal and ventral striatum. Molecular pharmacology. 2009;76(2):396-404.
31. Sulzer D. How addictive drugs disrupt presynaptic dopamine neurotransmission. Neuron. 2011;69(4):628-49.
32. Beaulieu JM, Gainetdinov RR. The physiology, signaling, and pharmacology of dopamine receptors. Pharmacol Rev. 2011;63(1):182-217.

33. Savica R, Benarroch EE. Dopamine receptor signaling in the forebrain: recent insights and clinical implications. Neurology. 2014;83(8):758-67.
34. Tritsch NX, Sabatini BL. Dopaminergic modulation of synaptic transmission in cortex and striatum. Neuron. 2012;76(1):33-50.
35. Lebowitz JJ, Khoshbouei H. Heterogeneity of dopamine release sites in health and degeneration. Neurobiol Dis. 2020;134:104633.
36. Starke K, Gothert M, Kilbinger H. Modulation of neurotransmitter release by presynaptic autoreceptors. Physiol Rev. 1989;69(3):864-989.
37. Benoit-Marand M, Ballion B, Borrelli E, Boraud T, Gonon F. Inhibition of dopamine uptake by D2 antagonists: an in vivo study. Journal of neurochemistry. 2011;116(3):449-58.
38. Perreault ML, Hasbi A, O'Dowd BF, George SR. Heteromeric dopamine receptor signaling complexes: emerging neurobiology and disease relevance. Neuropsychopharmacology. 2014;39(1):156-68.
39. Carli M, Kolachalam S, Aringhieri S, Rossi M, Giovannini L, Maggio R, et al. Dopamine D2 Receptors Dimers: How can we Pharmacologically Target Them? Curr Neuropharmacol. 2018;16(2):222-30.
40. Klein MO, Battagello DS, Cardoso AR, Hauser DN, Bittencourt JC, Correa RG. Dopamine: Functions, Signaling, and Association with Neurological Diseases. Cell Mol Neurobiol. 2019;39(1):31-59.
41. Bortolato M, Chen K, Shih JC. Monoamine oxidase inactivation: from pathophysiology to therapeutics. Adv Drug Deliv Rev. 2008;60(13-14):1527-33.
42. Schendzielorz N, Oinas JP, Myohanen TT, Reenila I, Raasmaja A, Mannisto PT. Catechol-O-methyltransferase (COMT) protein expression and activity after dopaminergic and noradrenergic lesions of the rat brain. PloS one. 2013;8(4):e61392.
43. Giros B, Caron MG. Molecular characterization of the dopamine transporter. Trends in pharmacological sciences. 1993;14(2):43-9.

44. Sulzer D, Cragg SJ, Rice ME. Striatal dopamine neurotransmission: regulation of release and uptake. Basal Ganglia. 2016;6(3):123-48.
45. Collaborators GBDPsD. Global, regional, and national burden of Parkinson's disease, 1990-2016: a systematic analysis for the Global Burden of Disease Study 2016. Lancet Neurol. 2018;17(11):939-53.
46. Trinh J, Farrer M. Advances in the genetics of Parkinson disease. Nat Rev Neurol. 2013;9(8):445-54.
47. Swanson JM, Kinsbourne M, Nigg J, Lanphear B, Stefanatos GA, Volkow N, et al. Etiologic subtypes of attention-deficit/hyperactivity disorder: brain imaging, molecular genetic and environmental factors and the dopamine hypothesis. Neuropsychol Rev. 2007;17(1):39-59.
48. Russo SJ, Nestler EJ. The brain reward circuitry in mood disorders. Nat Rev Neurosci. 2013;14(9):609-25.
49. Meisenzahl EM, Schmitt GJ, Scheuerecker J, Moller HJ. The role of dopamine for the pathophysiology of schizophrenia. Int Rev Psychiatry. 2007;19(4):337-45.
50. Bowton E, Saunders C, Reddy IA, Campbell NG, Hamilton PJ, Henry LK, et al. SLC6A3 coding variant Ala559Val found in two autism probands alters dopamine transporter function and trafficking. Translational psychiatry. 2014;4:e464.
51. Hamilton PJ, Campbell NG, Sharma S, Erreger K, Herborg Hansen F, Saunders C, et al. De novo mutation in the dopamine transporter gene associates dopamine dysfunction with autism spectrum disorder. Molecular psychiatry. 2013;18(12):1315-23.
52. Cartier E, Hamilton PJ, Belovich AN, Shekar A, Campbell NG, Saunders C, et al. Rare autism-associated variants implicate syntaxin 1 (STX1 R26Q) phosphorylation and the dopamine transporter (hDAT R51W) in dopamine neurotransmission and behaviors. EBioMedicine. 2015;2(2):135-46.
53. Vaughan RA, Foster JD. Mechanisms of dopamine transporter regulation in normal and disease states. Trends in pharmacological sciences. 2013;34(9):489-96.

54. Giros B, el Mestikawy S, Godinot N, Zheng K, Han H, Yang-Feng T, et al. Cloning, pharmacological characterization, and chromosome assignment of the human dopamine transporter. Molecular pharmacology. 1992;42(3):383-90.
55. Sonders MS, Zhu SJ, Zahniser NR, Kavanaugh MP, Amara SG. Multiple ionic conductances of the human dopamine transporter: the actions of dopamine and psychostimulants. Journal of Neuroscience. 1997;17(3):960-74.
56. Sitte HH, Huck S, Reither H, Boehm S, Singer EA, Pifl C. Carrier-mediated release, transport rates, and charge transfer induced by amphetamine, tyramine, and dopamine in mammalian cells transfected with the human dopamine transporter. Journal of neurochemistry. 1998;71(3):1289-97.
57. Khoshbouei H, Wang H, Lechleiter JD, Javitch JA, Galli A. Amphetamine-induced dopamine efflux. A voltage-sensitive and intracellular Na+-dependent mechanism. The Journal of biological chemistry. 2003;278(14):12070-7.
58. Penmatsa A, Wang KH, Gouaux E. X-ray structure of dopamine transporter elucidates antidepressant mechanism. Nature. 2013;503(7474):85-90.
59. Wang KH, Penmatsa A, Gouaux E. Neurotransmitter and psychostimulant recognition by the dopamine transporter. Nature. 2015;521(7552):322-7.
60. Coleman JA, Green EM, Gouaux E. X-ray structures and mechanism of the human serotonin transporter. Nature. 2016;532(7599):334-9.
61. Yamashita A, Singh SK, Kawate T, Jin Y, Gouaux E. Crystal structure of a bacterial homologue of Na+/Cl--dependent neurotransmitter transporters. Nature. 2005;437(7056):215-23.
62. Shan J, Javitch JA, Shi L, Weinstein H. The substrate-driven transition to an inward-facing conformation in the functional mechanism of the dopamine transporter. PloS one. 2011;6(1):e16350.

63. Hamilton PJ, Belovich AN, Khelashvili G, Saunders C, Erreger K, Javitch JA, et al. PIP2 regulates psychostimulant behaviors through its interaction with a membrane protein. Nat Chem Biol. 2014;10(7):582-9.
64. Belovich AN, Aguilar JI, Mabry SJ, Cheng MH, Zanella D, Hamilton PJ, et al. A network of phosphatidylinositol (4,5)-bisphosphate (PIP2) binding sites on the dopamine transporter regulates amphetamine behavior in Drosophila Melanogaster. Molecular psychiatry. 2019.
65. Khelashvili G, Weinstein H. Functional mechanisms of neurotransmitter transporters regulated by lipid-protein interactions of their terminal loops. Biochimica et biophysica acta. 2015;1848(9):1765-74.
66. Khelashvili G, Stanley N, Sahai MA, Medina J, LeVine MV, Shi L, et al. Spontaneous inward opening of the dopamine transporter is triggered by PIP2-regulated dynamics of the N-terminus. ACS Chem Neurosci. 2015;6(11):1825-37.
67. Khelashvili G, Doktorova M, Sahai MA, Johner N, Shi L, Weinstein H. Computational modeling of the N-terminus of the human dopamine transporter and its interaction with PIP2 -containing membranes. Proteins. 2015;83(5):952-69.
68. Fog JU, Khoshbouei H, Holy M, Owens WA, Vaegter CB, Sen N, et al. Calmodulin Kinase II Interacts with the Dopamine Transporter C Terminus to Regulate Amphetamine-Induced Reverse Transport. Neuron. 2006;51(4):417-29.
69. Binda F, Dipace C, Bowton E, Robertson SD, Lute BJ, Fog JU, et al. Syntaxin 1A interaction with the dopamine transporter promotes amphetamine-induced dopamine efflux. Molecular pharmacology. 2008;74(4):1101-8.
70. Johnson LA, Guptaroy B, Lund D, Shamban S, Gnegy ME. Regulation of amphetamine-stimulated dopamine efflux by protein kinase C beta. The Journal of biological chemistry. 2005;280(12):10914-9.

71. Garcia-Olivares J, Baust T, Harris S, Hamilton P, Galli A, Amara SG, et al. Gbetagamma subunit activation promotes dopamine efflux through the dopamine transporter. Molecular psychiatry. 2017;22(12):1673-9.
72. Mauna JC, Harris SS, Pino JA, Edwards CM, DeChellis-Marks MR, Bassi CD, et al. G protein betagamma subunits play a critical role in the actions of amphetamine. Translational psychiatry. 2019;9(1):81.
73. Mayfield RD, Zahniser NR. Dopamine D2 receptor regulation of the dopamine transporter expressed in Xenopus laevis oocytes is voltage-independent. Molecular pharmacology. 2001;59(1):113-21.
74. Lee FJ, Pei L, Moszczynska A, Vukusic B, Fletcher PJ, Liu F. Dopamine transporter cell surface localization facilitated by a direct interaction with the dopamine D2 receptor. The EMBO journal. 2007;26(8):2127-36.
75. Binda F, Lute BJ, Dipace C, Blakely RD, Galli A. The N-terminus of the norepinephrine transporter regulates the magnitude and selectivity of the transporter-associated leak current. Neuropharmacology. 2006;50(3):354-61.
76. Wei Y, Williams JM, Dipace C, Sung U, Javitch JA, Galli A, et al. Dopamine transporter activity mediates amphetamine-induced inhibition of Akt through a Ca2+/calmodulin-dependent kinase II-dependent mechanism. Molecular pharmacology. 2007;71(3):835-42.
77. Navaroli DM, Stevens ZH, Uzelac Z, Gabriel L, King MJ, Lifshitz LM, et al. The plasma membrane-associated GTPase Rin interacts with the dopamine transporter and is required for protein kinase C-regulated dopamine transporter trafficking. J Neurosci. 2011;31(39):13758-70.
78. Garcia-Olivares J, Torres-Salazar D, Owens WA, Baust T, Siderovski DP, Amara SG, et al. Inhibition of dopamine transporter activity by G protein betagamma subunits. PloS one. 2013;8(3):e59788.

79. Krishnamurthy H, Gouaux E. X-ray structures of LeuT in substrate-free outward-open and apo inward-open states. Nature. 2012;481(7382):469-74.
80. Forrest LR, Zhang YW, Jacobs MT, Gesmonde J, Xie L, Honig BH, et al. Mechanism for alternating access in neurotransmitter transporters. Proc Natl Acad Sci U S A. 2008;105(30):10338-43.
81. Kazmier K, Sharma S, Quick M, Islam SM, Roux B, Weinstein H, et al. Conformational dynamics of ligand-dependent alternating access in LeuT. Nat Struct Mol Biol. 2014;21(5):472-9.
82. Kniazeff J, Shi L, Loland CJ, Javitch JA, Weinstein H, Gether U. An intracellular interaction network regulates conformational transitions in the dopamine transporter. The Journal of biological chemistry. 2008;283(25):17691-701.
83. Pedersen AV, Andreassen TF, Loland CJ. A conserved salt bridge between transmembrane segments 1 and 10 constitutes an extracellular gate in the dopamine transporter. The Journal of biological chemistry. 2014;289(50):35003-14.
84. Nielsen AK, Moller IR, Wang Y, Rasmussen SGF, Lindorff-Larsen K, Rand KD, et al. Substrate-induced conformational dynamics of the dopamine transporter. Nature communications. 2019;10(1):2714.
85. Kahlig KM, Binda F, Khoshbouei H, Blakely RD, McMahon DG, Javitch JA, et al. Amphetamine induces dopamine efflux through a dopamine transporter channel. Proc Natl Acad Sci U S A. 2005;102(9):3495-500.
86. Bowton E, Saunders C, Erreger K, Sakrikar D, Matthies HJ, Sen N, et al. Dysregulation of dopamine transporters via dopamine D2 autoreceptors triggers anomalous dopamine efflux associated with attention-deficit hyperactivity disorder. J Neurosci. 2010;30(17):6048-57.
87. Carvelli L, McDonald PW, Blakely RD, Defelice LJ. Dopamine transporters depolarize neurons by a channel mechanism. Proc Natl Acad Sci U S A. 2004;101(45):16046-51.

88. Ingram SL, Prasad BM, Amara SG. Dopamine transporter-mediated conductances increase excitability of midbrain dopamine neurons. Nat Neurosci. 2002;5(10):971-8.
89. German CL, Baladi MG, McFadden LM, Hanson GR, Fleckenstein AE. Regulation of the Dopamine and Vesicular Monoamine Transporters: Pharmacological Targets and Implications for Disease. Pharmacol Rev. 2015;67(4):1005-24.
90. Foster JD, Vaughan RA. Phosphorylation mechanisms in dopamine transporter regulation. Journal of chemical neuroanatomy. 2017;83-84:10-8.
91. Moritz AE, Rastedt DE, Stanislowski DJ, Shetty M, Smith MA, Vaughan RA, et al. Reciprocal Phosphorylation and Palmitoylation Control Dopamine Transporter Kinetics. The Journal of biological chemistry. 2015;290(48):29095-105.
92. Melikian HE, Buckley KM. Membrane trafficking regulates the activity of the human dopamine transporter. Journal of Neuroscience. 1999;19(18):7699-710.
93. Hong WC, Amara SG. Differential targeting of the dopamine transporter to recycling or degradative pathways during amphetamine- or PKC-regulated endocytosis in dopamine neurons. FASEB J. 2013;27(8):2995-3007.
94. Foster JD, Adkins SD, Lever JR, Vaughan RA. Phorbol ester induced trafficking-independent regulation and enhanced phosphorylation of the dopamine transporter associated with membrane rafts and cholesterol. Journal of neurochemistry. 2008;105(5):1683-99.
95. Foster JD, Cervinski MA, Gorentla BK, Vaughan RA. Regulation of the dopamine transporter by phosphorylation. Handb Exp Pharmacol. 2006(175):197-214.
96. Foster JD, Pananusorn B, Vaughan RA. Dopamine transporters are phosphorylated on N-terminal serines in rat striatum. The Journal of biological chemistry. 2002;277(28):25178-86.
97. Granas C, Ferrer J, Loland CJ, Javitch JA, Gether U. N-terminal truncation of the dopamine transporter abolishes phorbol ester- and substance P receptor-stimulated phosphorylation without impairing transporter internalization. The Journal of biological chemistry. 2003;278(7):4990-5000.

98. Rastedt DE, Vaughan RA, Foster JD. Palmitoylation mechanisms in dopamine transporter regulation. Journal of chemical neuroanatomy. 2017;83-84:3-9.
99. Foster JD, Vaughan RA. Palmitoylation controls dopamine transporter kinetics, degradation, and protein kinase C-dependent regulation. The Journal of biological chemistry. 2011;286(7):5175-86.
100. Miranda M, Dionne KR, Sorkina T, Sorkin A. Three ubiquitin conjugation sites in the amino terminus of the dopamine transporter mediate protein kinase C-dependent endocytosis of the transporter. Mol Biol Cell. 2007;18(1):313-23.
101. Vina-Vilaseca A, Sorkin A. Lysine 63-linked polyubiquitination of the dopamine transporter requires WW3 and WW4 domains of Nedd4-2 and UBE2D ubiquitin-conjugating enzymes. The Journal of biological chemistry. 2010;285(10):7645-56.
102. Miklya I, Goltl P, Hafenscher F, Pencz N. [The role of parkin in Parkinson's disease]. Neuropsychopharmacol Hung. 2014;16(2):67-76.
103. Li LB, Chen N, Ramamoorthy S, Chi L, Cui XN, Wang LC, et al. The role of N-glycosylation in function and surface trafficking of the human dopamine transporter. The Journal of biological chemistry. 2004;279(20):21012-20.
104. Torres GE, Carneiro A, Seamans K, Fiorentini C, Sweeney A, Yao WD, et al. Oligomerization and trafficking of the human dopamine transporter. Mutational analysis identifies critical domains important for the functional expression of the transporter. The Journal of biological chemistry. 2003;278(4):2731-9.
105. Lew R, Vaughan R, Simantov R, Wilson A, Kuhar MJ. Dopamine transporters in the nucleus accumbens and the striatum have different apparent molecular weights. Synapse. 1991;8(2):152-3.
106. Afonso-Oramas D, Cruz-Muros I, Alvarez de la Rosa D, Abreu P, Giraldez T, Castro-Hernandez J, et al. Dopamine transporter glycosylation correlates with the vulnerability of midbrain dopaminergic cells in Parkinson's disease. Neurobiol Dis. 2009;36(3):494-508.

107. Torres GE, Yao WD, Mohn AR, Quan H, Kim KM, Levey AI, et al. Functional interaction between monoamine plasma membrane transporters and the synaptic PDZ domain-containing protein PICK1. Neuron. 2001;30(1):121-34.

108. Rickhag M, Hansen FH, Sorensen G, Strandfelt KN, Andresen B, Gotfryd K, et al. A C-terminal PDZ domain-binding sequence is required for striatal distribution of the dopamine transporter. Nature communications. 2013;4:1580.

109. Bjerggaard C, Fog JU, Hastrup H, Madsen K, Loland CJ, Javitch JA, et al. Surface targeting of the dopamine transporter involves discrete epitopes in the distal C terminus but does not require canonical PDZ domain interactions. J Neurosci. 2004;24(31):7024-36.

110. Jensen KL, Sorensen G, Dencker D, Owens WA, Rahbek-Clemmensen T, Brett Lever M, et al. PICK1-Deficient Mice Exhibit Impaired Response to Cocaine and Dysregulated Dopamine Homeostasis. eNeuro. 2018;5(3).

111. Butler B, Saha K, Rana T, Becker JP, Sambo D, Davari P, et al. Dopamine Transporter Activity Is Modulated by alpha-Synuclein. The Journal of biological chemistry. 2015;290(49):29542-54.

112. Moszczynska A, Saleh J, Zhang H, Vukusic B, Lee FJ, Liu F. Parkin disrupts the alpha-synuclein/dopamine transporter interaction: consequences toward dopamine-induced toxicity. J Mol Neurosci. 2007;32(3):217-27.

113. Barone MC, Sykiotis GP, Bohmann D. Genetic activation of Nrf2 signaling is sufficient to ameliorate neurodegenerative phenotypes in a Drosophila model of Parkinson's disease. Dis Model Mech. 2011;4(5):701-7.

114. Bertolino A, Fazio L, Di Giorgio A, Blasi G, Romano R, Taurisano P, et al. Genetically determined interaction between the dopamine transporter and the D2 receptor on prefronto-striatal activity and volume in humans. J Neurosci. 2009;29(4):1224-34.

115. Hastrup H, Sen N, Javitch JA. The human dopamine transporter forms a tetramer in the plasma membrane: cross-linking of a cysteine in the fourth transmembrane segment is sensitive to cocaine analogs. The Journal of biological chemistry. 2003;278(46):45045-8.
116. Sorkina T, Doolen S, Galperin E, Zahniser NR, Sorkin A. Oligomerization of dopamine transporters visualized in living cells by fluorescence resonance energy transfer microscopy. The Journal of biological chemistry. 2003;278(30):28274-83.
117. Li Y, Cheng SY, Chen N, Reith ME. Interrelation of dopamine transporter oligomerization and surface presence as studied with mutant transporter proteins and amphetamine. Journal of neurochemistry. 2010;114(3):873-85.
118. Hadlock GC, Chu PW, Walters ET, Hanson GR, Fleckenstein AE. Methamphetamine-induced dopamine transporter complex formation and dopaminergic deficits: the role of D2 receptor activation. The Journal of pharmacology and experimental therapeutics. 2010;335(1):207-12.
119. Hong WC, Amara SG. Membrane cholesterol modulates the outward facing conformation of the dopamine transporter and alters cocaine binding. The Journal of biological chemistry. 2010;285(42):32616-26.
120. Jones KT, Zhen J, Reith ME. Importance of cholesterol in dopamine transporter function. Journal of neurochemistry. 2012;123(5):700-15.
121. Cremona ML, Matthies HJ, Pau K, Bowton E, Speed N, Lute BJ, et al. Flotillin-1 is essential for PKC-triggered endocytosis and membrane microdomain localization of DAT. Nat Neurosci. 2011;14(4):469-77.
122. Pizzo AB, Karam CS, Zhang Y, Yano H, Freyberg RJ, Karam DS, et al. The membrane raft protein Flotillin-1 is essential in dopamine neurons for amphetamine-induced behavior in Drosophila. Molecular psychiatry. 2013;18(7):824-33.

123. Fong WM, Erreger K, Choi SJ, Reddy I, Johnson CW, Mosharov EV, et al. Membrane composition influences the conformation and function of the dopamine transporter *in vivo*. bioRxiv. 2019:755819.

124. Buchmayer F, Schicker K, Steinkellner T, Geier P, Stubiger G, Hamilton PJ, et al. Amphetamine actions at the serotonin transporter rely on the availability of phosphatidylinositol-4,5-bisphosphate. Proc Natl Acad Sci U S A. 2013;110(28):11642-7.

125. Darracq L, Blanc G, Glowinski J, Tassin JP. Importance of the noradrenaline-dopamine coupling in the locomotor activating effects of D-amphetamine. Journal of Neuroscience. 1998;18(7):2729-39.

126. Davis WM, Smith SG, Khalsa JH. Noradrenergic role in the self-administration of morphine or amphetamine. Pharmacol Biochem Behav. 1975;3(3):477-84.

127. Pifl C, Agneter E, Drobny H, Sitte HH, Singer EA. Amphetamine reverses or blocks the operation of the human noradrenaline transporter depending on its concentration: superfusion studies on transfected cells. Neuropharmacology. 1999;38(1):157-65.

128. Sulzer D, Sonders MS, Poulsen NW, Galli A. Mechanisms of neurotransmitter release by amphetamines: a review. Prog Neurobiol. 2005;75(6):406-33.

129. Sulzer D, Maidment NT, Rayport S. Amphetamine and other weak bases act to promote reverse transport of dopamine in ventral midbrain neurons. Journal of neurochemistry. 1993;60(2):527-35.

130. Wall SC, Gu H, Rudnick G. Biogenic amine flux mediated by cloned transporters stably expressed in cultured cell lines: amphetamine specificity for inhibition and efflux. Molecular pharmacology. 1995;47(3):544-50.

131. Pifl C, Drobny H, Reither H, Hornykiewicz O, Singer EA. Mechanism of the dopamine-releasing actions of amphetamine and cocaine: plasmalemmal dopamine transporter versus vesicular monoamine transporter. Molecular pharmacology. 1995;47(2):368-73.

132. Fleckenstein AE, Volz TJ, Riddle EL, Gibb JW, Hanson GR. New insights into the mechanism of action of amphetamines. Annu Rev Pharmacol Toxicol. 2007;47(1):681-98.
133. Sulzer D, Rayport S. Amphetamine and other psychostimulants reduce pH gradients in midbrain dopaminergic neurons and chromaffin granules: a mechanism of action. Neuron. 1990;5(6):797-808.
134. Liang NY, Rutledge CO. Comparison of the release of [3H]dopamine from isolated corpus striatum by amphetamine, fenfluramine and unlabelled dopamine. Biochem Pharmacol. 1982;31(6):983-92.
135. Zaczek R, Culp S, De Souza EB. Interactions of [3H]amphetamine with rat brain synaptosomes. II. Active transport. Journal of Pharmacology & Experimental Therapeutics. 1991;257(2):830-5.
136. Fischer JF, Cho AK. Chemical release of dopamine from striatal homogenates: evidence for an exchange diffusion model. The Journal of pharmacology and experimental therapeutics. 1979;208(2):203-9.
137. Robertson SD, Matthies HJ, Galli A. A closer look at amphetamine-induced reverse transport and trafficking of the dopamine and norepinephrine transporters. Mol Neurobiol. 2009;39(2):73-80.
138. Pifl C, Agneter E, Drobny H, Reither H, Singer EA. Induction by low Na+ or Cl- of cocaine sensitive carrier-mediated efflux of amines from cells transfected with the cloned human catecholamine transporters. Br J Pharmacol. 1997;121(2):205-12.
139. Pifl C, Singer EA. Ion dependence of carrier-mediated release in dopamine or norepinephrine transporter-transfected cells questions the hypothesis of facilitated exchange diffusion. Molecular pharmacology. 1999;56(5):1047-54.
140. Cervinski MA, Foster JD, Vaughan RA. Psychoactive substrates stimulate dopamine transporter phosphorylation and down regulation by cocaine sensitive and protein kinase C dependent mechanisms. The Journal of biological chemistry. 2005;280(49):40442-9.

141. Khoshbouei H, Sen N, Guptaroy B, Johnson L, Lund D, Gnegy ME, et al. N-terminal phosphorylation of the dopamine transporter is required for amphetamine-induced efflux. PLoS Biol. 2004;2(3):E78.

142. Pizzo AB, Karam CS, Zhang Y, Ma CL, McCabe BD, Javitch JA. Amphetamine-induced behavior requires CaMKII-dependent dopamine transporter phosphorylation. Molecular psychiatry. 2014;19(3):279-81.

143. Giambalvo CT. Protein kinase C and dopamine transport--1. Effects of amphetamine in vivo. Neuropharmacology. 1992;31(12):1201-10.

144. Giambalvo CT. Protein kinase C and dopamine transport--2. Effects of amphetamine in vitro. Neuropharmacology. 1992;31(12):1211-22.

145. Giambalvo CT. Differential effects of amphetamine transport vs. dopamine reverse transport on particulate PKC activity in striatal synaptoneurosomes. Synapse. 2003;49(2):125-33.

146. Cowell RM, Kantor L, Hewlett GH, Frey KA, Gnegy ME. Dopamine transporter antagonists block phorbol ester-induced dopamine release and dopamine transporter phosphorylation in striatal synaptosomes. European journal of pharmacology. 2000;389(1):59-65.

147. Kantor L, Gnegy ME. Protein kinase C inhibitors block amphetamine-mediated dopamine release in rat striatal slices. The Journal of pharmacology and experimental therapeutics. 1998;284(2):592-8.

148. Browman KE, Kantor L, Richardson S, Badiani A, Robinson TE, Gnegy ME. Injection of the protein kinase C inhibitor Ro31-8220 into the nucleus accumbens attenuates the acute response to amphetamine: tissue and behavioral studies. Brain Res. 1998;814(1-2):112-9.

149. Chen R, Furman CA, Zhang M, Kim MN, Gereau RWt, Leitges M, et al. Protein kinase Cbeta is a critical regulator of dopamine transporter trafficking and regulates the behavioral response to amphetamine in mice. The Journal of pharmacology and experimental therapeutics. 2009;328(3):912-20.

150. Steinkellner T, Mus L, Eisenrauch B, Constantinescu A, Leo D, Konrad L, et al. In vivo amphetamine action is contingent on alphaCaMKII. Neuropsychopharmacology. 2014;39(11):2681-93.
151. Gnegy ME, Khoshbouei H, Berg KA, Javitch JA, Clarke WP, Zhang M, et al. Intracellular Ca2+ regulates amphetamine-induced dopamine efflux and currents mediated by the human dopamine transporter. Molecular pharmacology. 2004;66(1):137-43.
152. Cameron KN, Solis E, Jr., Ruchala I, De Felice LJ, Eltit JM. Amphetamine activates calcium channels through dopamine transporter-mediated depolarization. Cell Calcium. 2015;58(5):457-66.
153. Cervinski MA, Foster JD, Vaughan RA. Syntaxin 1A regulates dopamine transporter activity, phosphorylation and surface expression. Neuroscience. 2010;170(2):408-16.
154. Foletti DL, Lin R, Finley MA, Scheller RH. Phosphorylated syntaxin 1 is localized to discrete domains along a subset of axons. J Neurosci. 2000;20(12):4535-44.
155. Khelashvili G, Galli A, Weinstein H. Phosphatidylinositol 4,5-biphosphate (PIP(2)) lipids regulate the phosphorylation of syntaxin N-terminus by modulating both its position and local structure. Biochemistry. 2012;51(39):7685-98.
156. Mazei-Robison MS, Bowton E, Holy M, Schmudermaier M, Freissmuth M, Sitte HH, et al. Anomalous dopamine release associated with a human dopamine transporter coding variant. J Neurosci. 2008;28(28):7040-6.
157. Fleckenstein AE, Metzger RR, Wilkins DG, Gibb JW, Hanson GR. Rapid and reversible effects of methamphetamine on dopamine transporters. The Journal of pharmacology and experimental therapeutics. 1997;282(2):834-8.
158. Saunders C, Ferrer JV, Shi L, Chen J, Merrill G, Lamb ME, et al. Amphetamine-induced loss of human dopamine transporter activity: An internalization-dependent and cocaine-sensitive mechanism. Proceedings of the National Academy of Sciences. 2000;97(12):6850-5.

159. Nemoda Z, Szekely A, Sasvari-Szekely M. Psychopathological aspects of dopaminergic gene polymorphisms in adolescence and young adulthood. Neuroscience and biobehavioral reviews. 2011;35(8):1665-86.
160. Zhai D, Li S, Zhao Y, Lin Z. SLC6A3 is a risk factor for Parkinson's disease: a meta-analysis of sixteen years' studies. Neuroscience letters. 2014;564:99-104.
161. Rylaarsdam L, Guemez-Gamboa A. Genetic Causes and Modifiers of Autism Spectrum Disorder. Front Cell Neurosci. 2019;13:385.
162. Ng J, Zhen J, Meyer E, Erreger K, Li Y, Kakar N, et al. Dopamine transporter deficiency syndrome: phenotypic spectrum from infancy to adulthood. Brain. 2014;137(Pt 4):1107-19.
163. Kurian MA, Li Y, Zhen J, Meyer E, Hai N, Christen HJ, et al. Clinical and molecular characterisation of hereditary dopamine transporter deficiency syndrome: an observational cohort and experimental study. Lancet Neurol. 2011;10(1):54-62.
164. Hansen FH, Skjorringe T, Yasmeen S, Arends NV, Sahai MA, Erreger K, et al. Missense dopamine transporter mutations associate with adult parkinsonism and ADHD. J Clin Invest. 2014;124(7):3107-20.
165. Campbell NG, Shekar A, Aguilar JI, Peng D, Navratna V, Yang D, et al. Structural, functional, and behavioral insights of dopamine dysfunction revealed by a deletion in SLC6A3. Proc Natl Acad Sci U S A. 2019;116(9):3853-62.
166. DiCarlo GE, Aguilar JI, Matthies HJ, Harrison FE, Bundschuh KE, West A, et al. Autism-linked dopamine transporter mutation alters striatal dopamine neurotransmission and dopamine-dependent behaviors. J Clin Invest. 2019;129(8):3407-19.
167. Hamilton PJ, Shekar A, Belovich AN, Christianson NB, Campbell NG, Sutcliffe JS, et al. Zn(2+) reverses functional deficits in a de novo dopamine transporter variant associated with autism spectrum disorder. Mol Autism. 2015;6:8.

168. Mazei-Robison MS, Blakely RD. Expression studies of naturally occurring human dopamine transporter variants identifies a novel state of transporter inactivation associated with Val382Ala. Neuropharmacology. 2005;49(6):737-49.
169. Grunhage F, Schulze TG, Muller DJ, Lanczik M, Franzek E, Albus M, et al. Systematic screening for DNA sequence variation in the coding region of the human dopamine transporter gene (DAT1). Molecular psychiatry. 2000;5(3):275-82.
170. Ronald A, Hoekstra RA. Autism spectrum disorders and autistic traits: a decade of new twin studies. American journal of medical genetics Part B, Neuropsychiatric genetics : the official publication of the International Society of Psychiatric Genetics. 2011;156B(3):255-74.
171. Mazei-Robison MS, Couch RS, Shelton RC, Stein MA, Blakely RD. Sequence variation in the human dopamine transporter gene in children with attention deficit hyperactivity disorder. Neuropharmacology. 2005;49(6):724-36.
172. Mergy MA, Gowrishankar R, Gresch PJ, Gantz SC, Williams J, Davis GL, et al. The rare DAT coding variant Val559 perturbs DA neuron function, changes behavior, and alters in vivo responses to psychostimulants. Proc Natl Acad Sci U S A. 2014;111(44):E4779-88.
173. Kurian MA. SLC6A3-Related Dopamine Transporter Deficiency Syndrome. In: Adam MP, Ardinger HH, Pagon RA, Wallace SE, Bean LJH, Stephens K, et al., editors. GeneReviews((R)). Seattle (WA)1993.
174. Kurian MA, Zhen J, Cheng SY, Li Y, Mordekar SR, Jardine P, et al. Homozygous loss-of-function mutations in the gene encoding the dopamine transporter are associated with infantile parkinsonism-dystonia. J Clin Invest. 2009;119(6):1595-603.
175. Martin CA, Krantz DE. Drosophila melanogaster as a genetic model system to study neurotransmitter transporters. Neurochemistry international. 2014;73:71-88.
176. Tian Y, Zhang ZC, Han J. Drosophila Studies on Autism Spectrum Disorders. Neurosci Bull. 2017;33(6):737-46.
177. Nagoshi E. Drosophila Models of Sporadic Parkinson's Disease. Int J Mol Sci. 2018;19(11).

178. Yamamoto S, Seto ES. Dopamine dynamics and signaling in Drosophila: an overview of genes, drugs and behavioral paradigms. Experimental animals. 2014;63(2):107-19.
179. Mao Z, Davis RL. Eight different types of dopaminergic neurons innervate the Drosophila mushroom body neuropil: anatomical and physiological heterogeneity. Front Neural Circuits. 2009;3:5.
180. Chang HY, Grygoruk A, Brooks ES, Ackerson LC, Maidment NT, Bainton RJ, et al. Overexpression of the Drosophila vesicular monoamine transporter increases motor activity and courtship but decreases the behavioral response to cocaine. Molecular psychiatry. 2006;11(1):99-113.
181. Wicker-Thomas C, Hamann M. Interaction of dopamine, female pheromones, locomotion and sex behavior in Drosophila melanogaster. Journal of insect physiology. 2008;54(10-11):1423-31.
182. Liu T, Dartevelle L, Yuan C, Wei H, Wang Y, Ferveur JF, et al. Reduction of dopamine level enhances the attractiveness of male Drosophila to other males. PloS one. 2009;4(2):e4574.
183. Keleman K, Vrontou E, Kruttner S, Yu JY, Kurtovic-Kozaric A, Dickson BJ. Dopamine neurons modulate pheromone responses in Drosophila courtship learning. Nature. 2012;489(7414):145-9.
184. Sadaf S, Reddy OV, Sane SP, Hasan G. Neural control of wing coordination in flies. Curr Biol. 2015;25(1):80-6.
185. Zhang SX, Rogulja D, Crickmore MA. Dopaminergic Circuitry Underlying Mating Drive. Neuron. 2016;91(1):168-81.
186. Riemensperger T, Isabel G, Coulom H, Neuser K, Seugnet L, Kume K, et al. Behavioral consequences of dopamine deficiency in the Drosophila central nervous system. Proc Natl Acad Sci U S A. 2011;108(2):834-9.
187. Kume K, Kume S, Park SK, Hirsh J, Jackson FR. Dopamine is a regulator of arousal in the fruit fly. J Neurosci. 2005;25(32):7377-84.

188. Ueno T, Kume K. Functional characterization of dopamine transporter in vivo using Drosophila melanogaster behavioral assays. Front Behav Neurosci. 2014;8:303.

189. Berry JA, Cervantes-Sandoval I, Nicholas EP, Davis RL. Dopamine is required for learning and forgetting in Drosophila. Neuron. 2012;74(3):530-42.

190. Kirkhart C, Scott K. Gustatory learning and processing in the Drosophila mushroom bodies. J Neurosci. 2015;35(15):5950-8.

191. van Swinderen B. Attention in Drosophila. Int Rev Neurobiol. 2011;99:51-85.

192. McClung C, Hirsh J. Stereotypic behavioral responses to free-base cocaine and the development of behavioral sensitization in Drosophila. Curr Biol. 1998;8(2):109-12.

193. Highfill CA, Baker BM, Stevens SD, Anholt RRH, Mackay TFC. Genetics of cocaine and methamphetamine consumption and preference in Drosophila melanogaster. PLoS genetics. 2019;15(5):e1007834.

194. Xiong Y, Yu J. Modeling Parkinson's Disease in Drosophila: What Have We Learned for Dominant Traits? Front Neurol. 2018;9:228.

195. Cackovic J, Gutierrez-Luke S, Call GB, Juba A, O'Brien S, Jun CH, et al. Vulnerable Parkin Loss-of-Function Drosophila Dopaminergic Neurons Have Advanced Mitochondrial Aging, Mitochondrial Network Loss and Transiently Reduced Autophagosome Recruitment. Front Cell Neurosci. 2018;12:39.

196. Asjad HMM, Kasture A, El-Kasaby A, Sackel M, Hummel T, Freissmuth M, et al. Pharmacochaperoning in a Drosophila model system rescues human dopamine transporter variants associated with infantile/juvenile parkinsonism. The Journal of biological chemistry. 2017;292(47):19250-65.

197. Feany MB, Bender WW. A Drosophila model of Parkinson's disease. Nature. 2000;404(6776):394-8.

198. Zhang YQ, Friedman DB, Wang Z, Woodruff E, 3rd, Pan L, O'Donnell J, et al. Protein expression profiling of the drosophila fragile X mutant brain reveals up-regulation of monoamine synthesis. Mol Cell Proteomics. 2005;4(3):278-90.
199. Chai C, Lim KL. Genetic insights into sporadic Parkinson's disease pathogenesis. Curr Genomics. 2013;14(8):486-501.
200. Ingelsson M. Alpha-Synuclein Oligomers-Neurotoxic Molecules in Parkinson's Disease and Other Lewy Body Disorders. Frontiers in neuroscience. 2016;10:408.
201. Stefanis L. alpha-Synuclein in Parkinson's disease. Cold Spring Harbor perspectives in medicine. 2012;2(2):a009399.
202. Lill CM. Genetics of Parkinson's disease. Mol Cell Probes. 2016;30(6):386-96.
203. Beerepoot P, Lam VM, Salahpour A. Pharmacological Chaperones of the Dopamine Transporter Rescue Dopamine Transporter Deficiency Syndrome Mutations in Heterologous Cells. The Journal of biological chemistry. 2016;291(42):22053-62.
204. Borre L, Andreassen TF, Shi L, Weinstein H, Gether U. The second sodium site in the dopamine transporter controls cation permeation and is regulated by chloride. The Journal of biological chemistry. 2014;289(37):25764-73.
205. Bjorklund A, Dunnett SB. Fifty years of dopamine research. Trends in neurosciences. 2007;30(5):185-7.
206. Palmiter RD. Dopamine signaling in the dorsal striatum is essential for motivated behaviors: lessons from dopamine-deficient mice. Ann N Y Acad Sci. 2008;1129(1):35-46.
207. Cheng MH, Block E, Hu F, Cobanoglu MC, Sorkin A, Bahar I. Insights into the Modulation of Dopamine Transporter Function by Amphetamine, Orphenadrine, and Cocaine Binding. Front Neurol. 2015;6:134.
208. Loland CJ, Granas C, Javitch JA, Gether U. Identification of intracellular residues in the dopamine transporter critical for regulation of transporter conformation and cocaine binding. The Journal of biological chemistry. 2004;279(5):3228-38.

209. Reith MEA, Jones KT, Zhen J, Topiol S. Latch and trigger role for R445 in DAT transport explains molecular basis of DTDS. Bioorg Med Chem Lett. 2018;28(3):470-5.
210. Razavi AM, Khelashvili G, Weinstein H. How structural elements evolving from bacterial to human SLC6 transporters enabled new functional properties. BMC Biol. 2018;16(1):31.
211. Brand AH, Perrimon N. Targeted gene expression as a means of altering cell fates and generating dominant phenotypes. Development. 1993;118(2):401-15.
212. van den Berg C, Beek PJ, Wagenaar RC, van Wieringen PC. Coordination disorders in patients with Parkinson's disease: a study of paced rhythmic forearm movements. Exp Brain Res. 2000;134(2):174-86.
213. Zabalax FA, Card GM, Fontaine EI, Murray RM, Dickinson MH, editors. Dynamics of escaping flight initiations of Drosophila melanogaster. 2008 2nd IEEE RAS & EMBS International Conference on Biomedical Robotics and Biomechatronics; 2008 19-22 Oct. 2008.
214. Pitmon E, Stephens G, Parkhurst SJ, Wolf FW, Kehne G, Taylor M, et al. The D1 family dopamine receptor, DopR, potentiates hind leg grooming behavior in Drosophila. Genes, brain, and behavior. 2016;15(3):327-34.
215. Panigrahi B, Martin KA, Li Y, Graves AR, Vollmer A, Olson L, et al. Dopamine Is Required for the Neural Representation and Control of Movement Vigor. Cell. 2015;162(6):1418-30.
216. Turner RS, Desmurget M. Basal ganglia contributions to motor control: a vigorous tutor. Curr Opin Neurobiol. 2010;20(6):704-16.
217. Politis M, Niccolini F. Serotonin in Parkinson's disease. Behav Brain Res. 2015;277:136-45.
218. Trinh K, Moore K, Wes PD, Muchowski PJ, Dey J, Andrews L, et al. Induction of the phase II detoxification pathway suppresses neuron loss in Drosophila models of Parkinson's disease. J Neurosci. 2008;28(2):465-72.

219. Whitworth AJ, Theodore DA, Greene JC, Benes H, Wes PD, Pallanck LJ. Increased glutathione S-transferase activity rescues dopaminergic neuron loss in a Drosophila model of Parkinson's disease. Proc Natl Acad Sci U S A. 2005;102(22):8024-9.

220. Claridge-Chang A, Roorda RD, Vrontou E, Sjulson L, Li H, Hirsh J, et al. Writing memories with light-addressable reinforcement circuitry. Cell. 2009;139(2):405-15.

221. Aso Y, Herb A, Ogueta M, Siwanowicz I, Templier T, Friedrich AB, et al. Three dopamine pathways induce aversive odor memories with different stability. PLoS genetics. 2012;8(7):e1002768.

222. Shekar A, Aguilar JI, Galli G, Cozzi NV, Brandt SD, Ruoho AE, et al. Atypical dopamine efflux caused by 3,4-methylenedioxypyrovalerone (MDPV) via the human dopamine transporter. Journal of chemical neuroanatomy. 2017;83-84:69-74.

223. Beuming T, Shi L, Javitch JA, Weinstein H. A comprehensive structure-based alignment of prokaryotic and eukaryotic neurotransmitter/Na+ symporters (NSS) aids in the use of the LeuT structure to probe NSS structure and function. Molecular pharmacology. 2006;70(5):1630-42.

224. Claxton DP, Quick M, Shi L, de Carvalho FD, Weinstein H, Javitch JA, et al. Ion/substrate-dependent conformational dynamics of a bacterial homolog of neurotransmitter:sodium symporters. Nat Struct Mol Biol. 2010;17:822.

225. Cheng MH, Bahar I. Complete mapping of substrate translocation highlights the role of LeuT N-terminal segment in regulating transport cycle. PLoS computational biology. 2014;10(10):e1003879.

226. McHaourab HS, Steed PR, Kazmier K. Toward the fourth dimension of membrane protein structure: insight into dynamics from spin-labeling EPR spectroscopy. Structure. 2011;19(11):1549-61.

227. Cheng MH, Bahar I. Molecular mechanism of dopamine transport by human dopamine transporter. Structure. 2015;23(11):2171-81.

228. Coleman JA, Yang D, Zhao Z, Wen P-C, Yoshioka C, Tajkhorshid E, et al. Serotonin transporter–ibogaine complexes illuminate mechanisms of inhibition and transport. Nature. 2019;569(7754):141.

229. Cheng MH, Bahar I. Monoamine transporters: structure, intrinsic dynamics and allosteric regulation. Nat Struct Mol Biol. 2019;26(7):545-56.

230. Cheng MH, Kaya C, Bahar I. Quantitative Assessment of the Energetics of Dopamine Translocation by Human Dopamine Transporter. J Phys Chem B. 2018;122(21):5336-46.

231. Daniels GM, Amara SG. Regulated trafficking of the human dopamine transporter. Clathrin-mediated internalization and lysosomal degradation in response to phorbol esters. The Journal of biological chemistry. 1999;274(50):35794-801.

232. Loder MK, Melikian HE. The dopamine transporter constitutively internalizes and recycles in a protein kinase C-regulated manner in stably transfected PC12 cell lines. The Journal of biological chemistry. 2003;278(24):22168-74.

233. Wu S, Bellve KD, Fogarty KE, Melikian HE. Ack1 is a dopamine transporter endocytic brake that rescues a trafficking-dysregulated ADHD coding variant. Proc Natl Acad Sci U S A. 2015;112(50):15480-5.

234. Cartier E, Garcia-Olivares J, Janezic E, Viana J, Moore M, Lin ML, et al. The SUMO-Conjugase Ubc9 Prevents the Degradation of the Dopamine Transporter, Enhancing Its Cell Surface Level and Dopamine Uptake. Front Cell Neurosci. 2019;13:35.

235. Faivre F, Joshi A, Bezard E, Barrot M. The hidden side of Parkinson's disease: Studying pain, anxiety and depression in animal models. Neuroscience and biobehavioral reviews. 2019;96:335-52.

236. McGregor MM, Nelson AB. Circuit Mechanisms of Parkinson's Disease. Neuron. 2019;101(6):1042-56.

237. Jenner P. Treatment of the later stages of Parkinson's disease - pharmacological approaches now and in the future. Transl Neurodegener. 2015;4:3.

238. Weintraub D, Koester J, Potenza MN, Siderowf AD, Stacy M, Voon V, et al. Impulse control disorders in Parkinson disease: a cross-sectional study of 3090 patients. Arch Neurol. 2010;67(5):589-95.

239. Giovannoni G, O'Sullivan JD, Turner K, Manson AJ, Lees AJ. Hedonistic homeostatic dysregulation in patients with Parkinson's disease on dopamine replacement therapies. J Neurol Neurosurg Psychiatry. 2000;68(4):423-8.

240. Mou L, Ding W, Fernandez-Funez P. Open questions on the nature of Parkinson's disease: from triggers to spreading pathology. J Med Genet. 2019;57(2):73-81.

241. Stolzenberg S, Quick M, Zhao C, Gotfryd K, Khelashvili G, Gether U, et al. Mechanism of the Association between Na+ Binding and Conformations at the Intracellular Gate in Neurotransmitter:Sodium Symporters. The Journal of biological chemistry. 2015;290(22):13992-4003.

242. Hartenstein V, Stollewerk A. The evolution of early neurogenesis. Dev Cell. 2015;32(4):390-407.

243. Anderson DJ, Adolphs R. A framework for studying emotions across species. Cell. 2014;157(1):187-200.

244. Kaiser M. Neuroanatomy: connectome connects fly and mammalian brain networks. Curr Biol. 2015;25(10):R416-8.

245. Taylor TN, Greene JG, Miller GW. Behavioral phenotyping of mouse models of Parkinson's disease. Behav Brain Res. 2010;211(1):1-10.

246. Card G, Dickinson M. Performance trade-offs in the flight initiation of Drosophila. The Journal of experimental biology. 2008;211(Pt 3):341-53.

247. Salvatore MF, Calipari ES, Jones SR. Regulation of Tyrosine Hydroxylase Expression and Phosphorylation in Dopamine Transporter-Deficient Mice. ACS Chem Neurosci. 2016;7(7):941-51.

248. Jones SR, Gainetdinov RR, Hu XT, Cooper DC, Wightman RM, White FJ, et al. Loss of autoreceptor functions in mice lacking the dopamine transporter. Nat Neurosci. 1999;2(7):649-55.

249. Achan J, Talisuna AO, Erhart A, Yeka A, Tibenderana JK, Baliraine FN, et al. Quinine, an old anti-malarial drug in a modern world: role in the treatment of malaria. Malar J. 2011;10:144.

250. Weyerhauser P, Kantelhardt SR, Kim EL. Re-purposing Chloroquine for Glioblastoma: Potential Merits and Confounding Variables. Front Oncol. 2018;8:335.

251. Friggi-Grelin F, Coulom H, Meller M, Gomez D, Hirsh J, Birman S. Targeted gene expression in Drosophila dopaminergic cells using regulatory sequences from tyrosine hydroxylase. J Neurobiol. 2003;54(4):618-27.

252. Wang JW, Beck ES, McCabe BD. A modular toolset for recombination transgenesis and neurogenetic analysis of Drosophila. PloS one. 2012;7(7):e42102.

253. Barlow KA, Ó Conchúir S, Thompson S, Suresh P, Lucas JE, Heinonen M, et al. Flex ddG: Rosetta Ensemble-Based Estimation of Changes in Protein–Protein Binding Affinity upon Mutation. J Phys Chem B. 2018;122(21):5389-99.

254. Kuenze G, Duran AM, Woods H, Brewer KR, McDonald EF, Vanoye CG, et al. Upgraded molecular models of the human KCNQ1 potassium channel. PloS one. 2019;14(9):e0220415.

255. Alford RF, Koehler Leman J, Weitzner BD, Duran AM, Tilley DC, Elazar A, et al. An Integrated Framework Advancing Membrane Protein Modeling and Design. PLoS computational biology. 2015;11(9):e1004398.

256. Aragao D, Aishima J, Cherukuvada H, Clarken R, Clift M, Cowieson NP, et al. MX2: a high-flux undulator microfocus beamline serving both the chemical and macromolecular crystallography communities at the Australian Synchrotron. J Synchrotron Radiat. 2018;25(Pt 3):885-91.

257. Kabsch W. Xds. Acta Crystallogr D Biol Crystallogr. 2010;66(Pt 2):125-32.
258. McCoy AJ, Grosse-Kunstleve RW, Adams PD, Winn MD, Storoni LC, Read RJ. Phaser crystallographic software. J Appl Crystallogr. 2007;40(Pt 4):658-74.
259. Emsley P, Lohkamp B, Scott WG, Cowtan K. Features and development of Coot. Acta Crystallogr D Biol Crystallogr. 2010;66(Pt 4):486-501.
260. Murshudov GN, Skubak P, Lebedev AA, Pannu NS, Steiner RA, Nicholls RA, et al. REFMAC5 for the refinement of macromolecular crystal structures. Acta Crystallogr D Biol Crystallogr. 2011;67(Pt 4):355-67.
261. Winn MD, Isupov MN, Murshudov GN. Use of TLS parameters to model anisotropic displacements in macromolecular refinement. Acta Crystallogr D Biol Crystallogr. 2001;57(Pt 1):122-33.
262. Chen VB, Arendall WB, 3rd, Headd JJ, Keedy DA, Immormino RM, Kapral GJ, et al. MolProbity: all-atom structure validation for macromolecular crystallography. Acta Crystallogr D Biol Crystallogr. 2010;66(Pt 1):12-21.
263. Pettersen EF, Goddard TD, Huang CC, Couch GS, Greenblatt DM, Meng EC, et al. UCSF Chimera--a visualization system for exploratory research and analysis. Journal of computational chemistry. 2004;25(13):1605-12.
264. Jeschke G, Polyhach Y. Distance measurements on spin-labelled biomacromolecules by pulsed electron paramagnetic resonance. Physical chemistry chemical physics : PCCP. 2007;9(16):1895-910.
265. Zou P, McHaourab HS. Increased sensitivity and extended range of distance measurements in spin-labeled membrane proteins: Q-band double electron-electron resonance and nanoscale bilayers. Biophysical journal. 2010;98(6):L18-20.
266. Jeschke G, Koch A, Jonas U, Godt A. Direct conversion of EPR dipolar time evolution data to distance distributions. Journal of magnetic resonance. 2002;155(1):72-82.

267. Wu EL, Cheng X, Jo S, Rui H, Song KC, Dávila-Contreras EM, et al. CHARMM-GUI membrane builder toward realistic biological membrane simulations. Journal of computational chemistry. 2014;35(27):1997-2004.
268. Phillips JC, Braun R, Wang W, Gumbart J, Tajkhorshid E, Villa E, et al. Scalable molecular dynamics with NAMD. Journal of computational chemistry. 2005;26(16):1781-802.
269. Humphrey W, Dalke A, Schulten K. VMD: visual molecular dynamics. Journal of molecular graphics. 1996;14(1):33-8, 27-8.
270. Winkelman TNA, Admon LK, Jennings L, Shippee ND, Richardson CR, Bart G. Evaluation of Amphetamine-Related Hospitalizations and Associated Clinical Outcomes and Costs in the United States. JAMA Netw Open. 2018;1(6):e183758.
271. Berman S, O'Neill J, Fears S, Bartzokis G, London ED. Abuse of amphetamines and structural abnormalities in the brain. Ann N Y Acad Sci. 2008;1141:195-220.
272. UN Office DaC. World Drug Report 2017. United Nations Publication; 2017. Report No.: 978-92-1-148291-1.
273. Suh BC, Hille B. PIP2 is a necessary cofactor for ion channel function: how and why? Annu Rev Biophys. 2008;37:175-95.
274. McLaughlin S, Murray D. Plasma membrane phosphoinositide organization by protein electrostatics. Nature. 2005;438(7068):605-11.
275. Kadamur G, Ross EM. Mammalian phospholipase C. Annual review of physiology. 2013;75:127-54.
276. Czech MP. PIP2 and PIP3: complex roles at the cell surface. Cell. 2000;100(6):603-6.
277. Ben-Aissa K, Patino-Lopez G, Belkina NV, Maniti O, Rosales T, Hao JJ, et al. Activation of moesin, a protein that links actin cytoskeleton to the plasma membrane, occurs by phosphatidylinositol 4,5-bisphosphate (PIP2) binding sequentially to two sites and releasing an autoinhibitory linker. The Journal of biological chemistry. 2012;287(20):16311-23.

278. Whorton MR, MacKinnon R. Crystal structure of the mammalian GIRK2 K+ channel and gating regulation by G proteins, PIP2, and sodium. Cell. 2011;147(1):199-208.
279. Thapa N, Anderson RA. PIP2 signaling, an integrator of cell polarity and vesicle trafficking in directionally migrating cells. Cell Adh Migr. 2012;6(5):409-12.
280. Robbins J, Marsh SJ, Brown DA. Probing the regulation of M (Kv7) potassium channels in intact neurons with membrane-targeted peptides. J Neurosci. 2006;26(30):7950-61.
281. Yu K, Jiang T, Cui Y, Tajkhorshid E, Hartzell HC. A Network of Phosphatidylinositol 4,5-bisphosphate Binding Sites Regulate Gating of the Ca2+ activated Cl- Channel ANO1 (TMEM16A). bioRxiv. 2019:625897.
282. Kaun KR, Azanchi R, Maung Z, Hirsh J, Heberlein U. A Drosophila model for alcohol reward. Nat Neurosci. 2011;14(5):612-9.
283. Arias-Carrion O, Stamelou M, Murillo-Rodriguez E, Menendez-Gonzalez M, Poppel E. Dopaminergic reward system: a short integrative review. Int Arch Med. 2010;3:24.
284. Scaplen KM, Kaun KR. Reward from bugs to bipeds: a comparative approach to understanding how reward circuits function. J Neurogenet. 2016;30(2):133-48.
285. Dubol M, Trichard C, Leroy C, Sandu AL, Rahim M, Granger B, et al. Dopamine Transporter and Reward Anticipation in a Dimensional Perspective: A Multimodal Brain Imaging Study. Neuropsychopharmacology. 2018;43(4):820-7.
286. Schott BH, Minuzzi L, Krebs RM, Elmenhorst D, Lang M, Winz OH, et al. Mesolimbic functional magnetic resonance imaging activations during reward anticipation correlate with reward-related ventral striatal dopamine release. J Neurosci. 2008;28(52):14311-9.
287. Ja WW, Carvalho GB, Mak EM, de la Rosa NN, Fang AY, Liong JC, et al. Prandiology of Drosophila and the CAFE assay. Proc Natl Acad Sci U S A. 2007;104(20):8253-6.
288. Diegelmann S, Jansen A, Jois S, Kastenholz K, Velo Escarcena L, Strudthoff N, et al. The CApillary FEeder Assay Measures Food Intake in Drosophila melanogaster. J Vis Exp. 2017(121):e55024.

289. Devineni AV, Heberlein U. Preferential ethanol consumption in Drosophila models features of addiction. Curr Biol. 2009;19(24):2126-32.
290. Foltin RW. The behavioral pharmacology of anorexigenic drugs in nonhuman primates: 30 years of progress. Behav Pharmacol. 2012;23(5-6):461-77.
291. Cummings BS, Pati S, Sahin S, Scholpa NE, Monian P, Trinquero PM, et al. Differential effects of cocaine exposure on the abundance of phospholipid species in rat brain and blood. Drug and alcohol dependence. 2015;152:147-56.
292. Ross BM, Turenne SD. Chronic cocaine administration reduces phospholipase A(2) activity in rat brain striatum. Prostaglandins Leukot Essent Fatty Acids. 2002;66(5-6):479-83.
293. Leussen DC, Rong. Psychostimulants, Brain Membrane Lipids and Dopamine Transmission. Journal of Biomolecular Research & Therapeutics. 2016;5(2):1000143.
294. Marchant NJ, Kaganovsky K, Shaham Y, Bossert JM. Role of corticostriatal circuits in context-induced reinstatement of drug seeking. Brain Res. 2015;1628(Pt A):219-32.
295. Ross BM, Moszczynska A, Peretti FJ, Adams V, Schmunk GA, Kalasinsky KS, et al. Decreased activity of brain phospholipid metabolic enzymes in human users of cocaine and methamphetamine. Drug and alcohol dependence. 2002;67(1):73-9.
296. Lee KH, Kim MY, Kim DH, Lee YS. Syntaxin 1A and receptor for activated C kinase interact with the N-terminal region of human dopamine transporter. Neurochem Res. 2004;29(7):1405-9.
297. Amara SG, Kuhar MJ. Neurotransmitter transporters: recent progress. Annual review of neuroscience. 1993;16:73-93.
298. Volkow ND, Fowler JS, Wang GJ. The addicted human brain viewed in the light of imaging studies: brain circuits and treatment strategies. Neuropharmacology. 2004;47 Suppl 1:3-13.
299. Cabib S, Orsini C, Le Moal M, Piazza PV. Abolition and reversal of strain differences in behavioral responses to drugs of abuse after a brief experience. Science. 2000;289(5478):463-5.

300. O'Neill MF, Shaw G. Comparison of dopamine receptor antagonists on hyperlocomotion induced by cocaine, amphetamine, MK-801 and the dopamine D1 agonist C-APB in mice. Psychopharmacology. 1999;145(3):237-50.
301. Pignatelli M, Bonci A. Role of Dopamine Neurons in Reward and Aversion: A Synaptic Plasticity Perspective. Neuron. 2015;86(5):1145-57.
302. Hu H. Reward and Aversion. Annual review of neuroscience. 2016;39(1):297-324.
303. Cheng MH, Ponzoni L, Sorkina T, Lee JY, Zhang S, Sorkin A, et al. Trimerization of dopamine transporter triggered by AIM-100 binding: Molecular mechanism and effect of mutations. Neuropharmacology. 2019;161:107676.
304. Iversen SD, Iversen LL. Dopamine: 50 years in perspective. Trends in neurosciences. 2007;30(5):188-93.
305. Gowrishankar R, Hahn MK, Blakely RD. Good riddance to dopamine: roles for the dopamine transporter in synaptic function and dopamine-associated brain disorders. Neurochemistry international. 2014;73:42-8.
306. Schmitt KC, Reith ME. Regulation of the dopamine transporter: aspects relevant to psychostimulant drugs of abuse. Ann N Y Acad Sci. 2010;1187:316-40.
307. German CL, Fleckenstein AE, Hanson GR. Bath salts and synthetic cathinones: an emerging designer drug phenomenon. Life Sci. 2014;97(1):2-8.
308. Brenneisen R, Fisch HU, Koelbing U, Geisshusler S, Kalix P. Amphetamine-like effects in humans of the khat alkaloid cathinone. Br J Clin Pharmacol. 1990;30(6):825-8.
309. Baumann MH, Partilla JS, Lehner KR, Thorndike EB, Hoffman AF, Holy M, et al. Powerful cocaine-like actions of 3,4-methylenedioxypyrovalerone (MDPV), a principal constituent of psychoactive 'bath salts' products. Neuropsychopharmacology. 2013;38(4):552-62.
310. Liechti M. Novel psychoactive substances (designer drugs): overview and pharmacology of modulators of monoamine signaling. Swiss Med Wkly. 2015;145:w14043.

311. Glennon RA, Yousif M, Naiman N, Kalix P. Methcathinone: a new and potent amphetamine-like agent. Pharmacol Biochem Behav. 1987;26(3):547-51.
312. Nguyen JD, Aarde SM, Cole M, Vandewater SA, Grant Y, Taffe MA. Locomotor Stimulant and Rewarding Effects of Inhaling Methamphetamine, MDPV, and Mephedrone via Electronic Cigarette-Type Technology. Neuropsychopharmacology. 2016;41(11):2759-71.
313. King HE, Wetzell B, Rice KC, Riley AL. An assessment of MDPV-induced place preference in adult Sprague-Dawley rats. Drug and alcohol dependence. 2015;146:116-9.
314. Novellas J, Lopez-Arnau R, Carbo ML, Pubill D, Camarasa J, Escubedo E. Concentrations of MDPV in rat striatum correlate with the psychostimulant effect. Journal of psychopharmacology. 2015;29(11):1209-18.
315. Kehr J, Ichinose F, Yoshitake S, Goiny M, Sievertsson T, Nyberg F, et al. Mephedrone, compared with MDMA (ecstasy) and amphetamine, rapidly increases both dopamine and 5-HT levels in nucleus accumbens of awake rats. Br J Pharmacol. 2011;164(8):1949-58.
316. Bonano JS, Glennon RA, De Felice LJ, Banks ML, Negus SS. Abuse-related and abuse-limiting effects of methcathinone and the synthetic "bath salts" cathinone analogs methylenedioxypyrovalerone (MDPV), methylone and mephedrone on intracranial self-stimulation in rats. Psychopharmacology. 2014;231(1):199-207.
317. Watterson LR, Watterson E, Olive MF. Abuse liability of novel 'legal high' designer stimulants: evidence from animal models. Behav Pharmacol. 2013;24(5-6):341-55.
318. Lisek R, Xu W, Yuvasheva E, Chiu YT, Reitz AB, Liu-Chen LY, et al. Mephedrone ('bath salt') elicits conditioned place preference and dopamine-sensitive motor activation. Drug and alcohol dependence. 2012;126(1-2):257-62.
319. Borek HA, Holstege CP. Hyperthermia and multiorgan failure after abuse of "bath salts" containing 3,4-methylenedioxypyrovalerone. Annals of emergency medicine. 2012;60(1):103-5.

320. Penders TM, Gestring R. Hallucinatory delirium following use of MDPV: "Bath Salts". Gen Hosp Psychiatry. 2011;33(5):525-6.
321. Wyman JF, Lavins ES, Engelhart D, Armstrong EJ, Snell KD, Boggs PD, et al. Postmortem tissue distribution of MDPV following lethal intoxication by "bath salts". J Anal Toxicol. 2013;37(3):182-5.
322. Services USDoHaH. Drug Abuse Warning Network (DAWN) Report. Administration SAaMH; 2013.
323. Administration UDoJDE. Drugs of Abuse: A DEA RESOURCE GUIDE. 2017.
324. Marusich JA, Antonazzo KR, Wiley JL, Blough BE, Partilla JS, Baumann MH. Pharmacology of novel synthetic stimulants structurally related to the "bath salts" constituent 3,4-methylenedioxypyrovalerone (MDPV). Neuropharmacology. 2014;87:206-13.
325. Zawilska JB, Wojcieszak J. Designer cathinones--an emerging class of novel recreational drugs. Forensic Sci Int. 2013;231(1-3):42-53.
326. Coppola M, Mondola R. Synthetic cathinones: chemistry, pharmacology and toxicology of a new class of designer drugs of abuse marketed as "bath salts" or "plant food". Toxicol Lett. 2012;211(2):144-9.
327. Ross EA, Reisfield GM, Watson MC, Chronister CW, Goldberger BA. Psychoactive "bath salts" intoxication with methylenedioxypyrovalerone. The American journal of medicine. 2012;125(9):854-8.
328. Wright TH, Cline-Parhamovich K, Lajoie D, Parsons L, Dunn M, Ferslew KE. Deaths involving methylenedioxypyrovalerone (MDPV) in Upper East Tennessee. J Forensic Sci. 2013;58(6):1558-62.
329. Murray BL, Murphy CM, Beuhler MC. Death following recreational use of designer drug "bath salts" containing 3,4-Methylenedioxypyrovalerone (MDPV). J Med Toxicol. 2012;8(1):69-75.

330. Kriikku P, Wilhelm L, Schwarz O, Rintatalo J. New designer drug of abuse: 3,4-Methylenedioxypyrovalerone (MDPV). Findings from apprehended drivers in Finland. Forensic Sci Int. 2011;210(1-3):195-200.
331. Organization WH. 3,4-Methylenedioxypyrovalerone (MDPV) Critical Review Report. 2014.
332. Coppola M, Mondola R. 3,4-methylenedioxypyrovalerone (MDPV): chemistry, pharmacology and toxicology of a new designer drug of abuse marketed online. Toxicol Lett. 2012;208(1):12-5.
333. Watterson LR, Kufahl PR, Nemirovsky NE, Sewalia K, Grabenauer M, Thomas BF, et al. Potent rewarding and reinforcing effects of the synthetic cathinone 3,4-methylenedioxypyrovalerone (MDPV). Addict Biol. 2014;19(2):165-74.
334. Cameron KN, Kolanos R, Solis E, Jr., Glennon RA, De Felice LJ. Bath salts components mephedrone and methylenedioxypyrovalerone (MDPV) act synergistically at the human dopamine transporter. Br J Pharmacol. 2013;168(7):1750-7.
335. Eshleman AJ, Wolfrum KM, Hatfield MG, Johnson RA, Murphy KV, Janowsky A. Substituted methcathinones differ in transporter and receptor interactions. Biochem Pharmacol. 2013;85(12):1803-15.
336. Kolanos R, Solis E, Jr., Sakloth F, De Felice LJ, Glennon RA. "Deconstruction" of the abused synthetic cathinone methylenedioxypyrovalerone (MDPV) and an examination of effects at the human dopamine transporter. ACS Chem Neurosci. 2013;4(12):1524-9.
337. Pfeiffenberger C, Lear BC, Keegan KP, Allada R. Locomotor activity level monitoring using the Drosophila Activity Monitoring (DAM) System. Cold Spring Harbor protocols. 2010;2010(11):pdb.prot5518.
338. Andretic R, van Swinderen B, Greenspan RJ. Dopaminergic modulation of arousal in Drosophila. Curr Biol. 2005;15(13):1165-75.